ISOTOPIC LABELLING OF ALAMETHICIN WITH ^{15}N AND ITS CONFORMATION IN METHANOL BY ^{1}H AND ^{15}N NMR

BY

ADELINDA A. YEE

A Thesis
Submitted to the Faculty of Graduate Studies
in Partial Fulfillment of the Requirements
for the degree of

MASTER OF SCIENCE

Department of Chemistry
University of Manitoba
Winnipeg, Manitoba

ISBN 0-315-77810-5

ISOTOPIC LABELLING OF ALAMETHICIN WITH ^{15}N AND ITS CONFORMATION IN METHANOL BY ^{1}H AND ^{15}N NMR

BY

ADELINDA A. YEE

A thesis submitted to the Faculty of Graduate Studies of the University of Manitoba in partial fulfillment of the requirements of the degree of

MASTER OF SCIENCE

Acknowledgements

I would like to extend my gratitude to my research advisor, Dr. J. D. J. O'Neil, for his financial assistance, advice, helpful comments and discussions during the course of this study. And also for introducing me to the very interesting world of nmr.

I would like to thank the members of my examining committee, Dr. F. E. Hruska and Dr. J. Peeling. And also to Mr. K. Marat and T. Woloweic for helping me run and process some of my nmr spectra, to F. Yeh for the invaluable comments on aseptic techniques, to A. Belkhiri of the Department of Microbiology for showing me how to isolate single spores of *T. viride*, to Dr. H. Duckworth and Dr. L. Donald for allowing us to use their HPLC and centrifuge, to Dr. Hruska for lending us the freeze dryer, and to the Department of Microbiology and Dr. A. Secco for lending us the autoclave.

I would also like to thank all the members of Dr. O'neil's laboratory and the other chemistry graduate students, past and present, for their friendship. And also to Darry and Nancy for their friendship and for those wonderful summer barbeques and sumptuous christmas dinners.

Finally, I would like to thank my family, especially Paning, Aday and Benny, for their love, support, encouragement, and phone calls that kept me going even at the coldest Winnipeg winter.

ABSTRACT

Alamethicin is a 20 amino acid peptide excreted by the fungus *T. viride*. The peptide was uniformly labelled with ^{15}N by growing *T. viride* in a semi-basal medium containing dextrin and sucrose as the carbon source and $K^{15}NO_3$ as the sole nitrogen source. The percentage of isotopic labelling was determined using spin echo difference spectroscopy, and was found to vary from 85% to 92% with the glutamine sidechains having the highest percentage labelling. The alamethicin fraction studied here has a glutamine in the 18th residue instead of a glutamic acid. The ^1H nmr resonances of alamethicin in methanol were assigned using DQF-COSY, TOCSY, and ROESY. The ^1H noe data suggest the presence of a helix from residues 2 to 12. Residues 4 to 11 have $^3J_{NH-\alpha CH} < 6$ Hz, suggesting that the backbone of residues 4 to 11 adopts an α-helical conformation. Residues 12, 15, and 18 have 6 Hz $< {}^3J_{NH-\alpha CH} < 9$ Hz, suggesting that these residues' conformation is neither α helix nor β sheet; the terminal phenylalaninol residue has $^3J_{NH-\alpha CH} > 9$ Hz, suggesting that it adopts an extended conformation. The ^{15}N resonance assignments were done using a heteronuclear $^{15}N-^1H$ correlation spectrum. Heteronuclear $^{15}N\{^1H\}$ noe data suggest that the glutamine sidechains have more conformational freedom than the rest of the backbone.

Table of contents: Page

Lists of Symbols and Abbreviations

γ_I : magnetogyric ratio of nuclei I

δ : chemical shift

μ_o : permeability constant in a vacuum

ρ_I : dipolar relaxation of nucleus I

σ_{IS}: cross relaxation between nucleus I and S

τ_c : rotational correlation time

ω : resonance frequency

χ, ψ : dihedral angles in the peptide bonds. Refer to page 44 for nomenclature.

A : alanine

Ac: acetyl

Aib : α-aminoisobutyric acid

Ala : alanine

B : α-aminoisobutyric acid

COSY : two dimensional Correlation Spectroscopy

d_{NN}, $d_{\alpha N}$, $d_{\beta N}$: Noe connectivity between the NH, αH and βH, respectively of the i^{th} residue to the NH of the $(i+1)^{th}$ residue

DQF-COSY : two dimensional Double Quantum Filtered Correlation Spectroscopy

DSS : 2,2-dimethyl-2-silapentane-5-sulfonate

Gln : glutamine

Glu : glutamic acid

Gly : glycine

$\hbar$: Planck's constant

HMQC : two dimensional Heteronuclear Multiple Quantum Coherence Spectroscopy

HPLC : High performance liquid chromatography

HOHAHA : Homonuclear Hartmann Hahn Coherence Transfer

I_o, S_o : equilibrium magnetization of spins I and S, respectively

$\langle I_z \rangle$, $\langle S_z \rangle$: instantaneous spin magnetization of I and S, respectively

J : spin-spin coupling constant

L : leucine

Leu : leucine

NMR : nuclear magnetic resonance

Noe : nuclear Overhauser effect

NOESY : two dimensional Nuclear Overhauser Effect Spectroscopy

P : proline

Phol : phenylalaninol

Pro : proline

Q : glutamine

r_{IS} : distance between the nuclei I and S

ROESY : two dimensional Rotating Frame Overhauser Effect Spectroscopy

SEDS : Spin Echo Difference Spectroscopy

SDS : sodium dodecyl sulfate

T : Tesla

TOCSY : two dimensional Total Coherence Transfer Spectroscopy

TPPI : time proportional phase incrementation

V : valine

Val : valine

List of Figures: Page

List of Tables: Page

Chapter 1
INTRODUCTION

Alamethicins are natural peptides secreted by the fungus *Trichoderma viride* [15,63]. At high concentrations, the peptides exhibit antimicrobial activity [15,45,63] and cause haemolysis of red blood cells [43,76]. Both of these properties are attributed to the strong hydrophobicity of the peptides which penetrate the membrane, changing the permeability of the membranes to ions [65] and small molecules [76]; this leads to swelling of the cell and its eventual rupture. At low concentrations, alamethicin induces voltage-dependent conductances similar to those observed in nerve cell membranes [24]. The propagation of action potentials in nerves results from a transient increase in membrane permeability to sodium followed by an increase in potassium permeability. Electrical conductance studies have shown that the increase in K^+ and Na^+ permeability are a function of voltage and are a result of the opening of numerous small pores in the membrane [24].

Other effects of alamethicin include an influence on glandular secretion which resembles that of the nicotine-evoked secretion [1]. Alamethicin has also been shown to produce holes in black lipid films [46]. The number of Ca^{2+} binding sites in membranes containing alamethicin is found to be twice that in its absence [50]. Alamethicin forms organic solvent-soluble complexes with alkali metal ions although the

complexation does not alter the nmr spectrum of alamethicin in organic solvents [38]. ^{13}C nmr lanthanide-induced shift studies indicate that the cation binding sites are at the amide carbonyls of glutamines [46].

To explain the molecular mechanism of the several actions of alamethicin on membranes it is important to know the structure and conformation of the alamethicin molecule.

1.1 Primary Sequence.

Natural alamethicin is a mixture of closely related compounds [2,15,32,43]. The primary structure was first thought of as cyclic [74,77] but was later found to be an open chain [2,32,80,81,94]. Alamethicin belongs to a class of peptide antibiotics called peptaibols. Peptides of this class have been found to have several α-aminoisobutyric acid residues, an acetyl-protected amino terminal and a phenylalaninol-protected carboxyl terminal group in common. The major component of natural alamethicin was synthesized [2,32,49,80,81,94] and the suggested primary sequence is: Ac-aib-pro-aib-ala-aib-(ala or aib)-gln-aib-val-aib-gly-leu-aib-pro-val-aib-aib-glu-gln-phol, where ac is acetyl, aib is α-aminoisobutyric acid, phol is phenylalaninol.

1.2 Secondary Structure:

The crystal structure of alamethicin was determined by Fox and Richards [29] at 1.5Å resolution and the result showed that alamethicin exists in a helical conformation over

the entire length of the molecule. The helix axis is bent slightly near the pro 14 residue. The accommodation of the pro 14 into the helical backbone is accomplished by introduction of a 4-to-1 hydrogen bond characteristic of a 3_{10} helix (N-15 to O-12) which shifts the proline imino ring from a position directly above the carbonyl of aib 10 to one between the carbonyls of aib 10 and gly 11. The carbonyls of aib 10 and gly 11 do not participate in backbone hydrogen bonds. The carbonyl of gly 11 in one of the molecules is hydrogen bonded to the amide side chain of gln 7 of another molecule in the crystal.

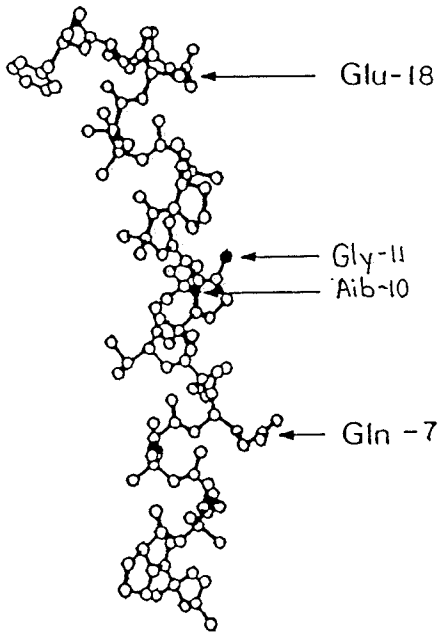

Figure 1: Crystal structure of alamethicin , crystallized from acetonitrile-methanol solution. (From Fox and Richards [29])

Circular dichroism studies of alamethicin in organic solvents and in aqueous solutions, however, suggested that the helical content of the peptide in methanol is only 40% and the percentage of α-helix in aqueous phosphate buffer decreases with increasing pH [26]. Two nmr studies of alamethicin in methanol [3,4,26] reported conflicting conformations of the molecule in solution.

Banerjee *et al.* [3,4] proposed a structure for alamethicin in methanol that is partly extended and partly helical, and a dimer. This was based on the coupling constants between amide protons and αCH ($^3J_{NH-\alpha CH}$). Amino acids at the C-terminal end generally have higher $^3J_{NH-\alpha CH}$ values, which suggested to those authors a β-pleated sheet structure, while the N-terminal end has $^3J_{NH-\alpha CH}$ consistent with an α-helix. Since alamethicin is a linear peptide, an extended β-sheet structure in a part of the molecule could only be stabilized by intermolecular hydrogen bonding. Banerjee *et al.* proposed that the amide protons of residues 15 to 20 are intermolecularly hydrogen bonded with the opposing molecule to create a rigid, extended parallel β-sheet structure for the C-terminal end of the molecule. Pro 14 breaks the continuity of the structure and amino acids 10 to 14 are forced into an open non-hydrogen bonded conformation. Amino acids 3 to 9 are folded into an α-helix with gln 7 sidechains from the two strands in the right juxtaposition to facilitate hydrogen bonding between them. The dimeric structure was supported by a study of the

relaxation times of the N-terminal acetyl [3]. The decay of the acetyl resonance was non-exponential and the relaxation data fitted to a sum of two exponentials. In the presence of urea, the decay of the acetyl resonance became mono exponential, indicating that the multiple exponential decay in methanol was a consequence of the structure of the molecule.

Esposito *et al.* [26], on the other hand, proposed a conformation of alamethicin in methanol at -5°C that is very similar to the crystal structure. The structure deduced from the NOESY spectrum following Wuthrich's method [93]. The conformation was described as follows: ala 4 to aib 10 and aib 16 to glu 18 form regular helical structures. The aib 1-to-pro 2 peptide bond is *trans* and so is the pro 14-to-aib 13 peptide bond. Both of these prolyl residues appear to be in the helical regions. Gly 11 to aib 13 shows "tightening" of the helix in this region and the axis of the entire molecule might be tilted with a slight bend around these three residues. Aib 16 to glu 18 is a regular continuation of the helix. The aib 1 N-terminus is not in a helical conformation and the C-terminal dipeptide (19-20) exists in a somewhat extended structure. No evidence of a head-to-head dimer was found.

However, restrained molecular dynamics simulations were done using both the x-ray diffraction data and the noe constraints from Esposito *et al.* [26] and showed the following: Aib 1 to val 9 behaves like a rigid rod with an

almost fixed helical conformation; aib 10 and gly 11 represent a hinge region characterized by a large amplitude motion and leu 12 to phol 20 is the most flexible region with an ill-defined structure [30].

Hall *et al.* [35] suggested a structure that would satisfy the electrical conductance properties of alamethicin. It should be noted, however, that the electrical conductance data were interpreted that the net movement of charge from one side of the membrane to the other associated with the gating event is a consequence of monomer(s) "flip". Similar deductions were arrived at from conductance studies using small polypeptides [62]. The suggested structure is bent with gly 11 to pro 14 forming a β-bend, residues aib 1 to aib 10 forming a helix, and the C terminus from val 15 to phol 20 forming an extended β-sheet.

1.3 Pore Channel Models

The electrical potential across a membrane is due to the ionic gradients and selective permeability of the membrane. The electrical properties of the membrane can be studied by the voltage clamp technique [38]. In this experiment, the process is reversed, *i.e.*, a constant voltage is applied across the membrane and the conductance per unit time, or current, is measured. The permeability of the membrane is proportional to the conductance measured. Alamethicin induces several remarkable electrical conductance

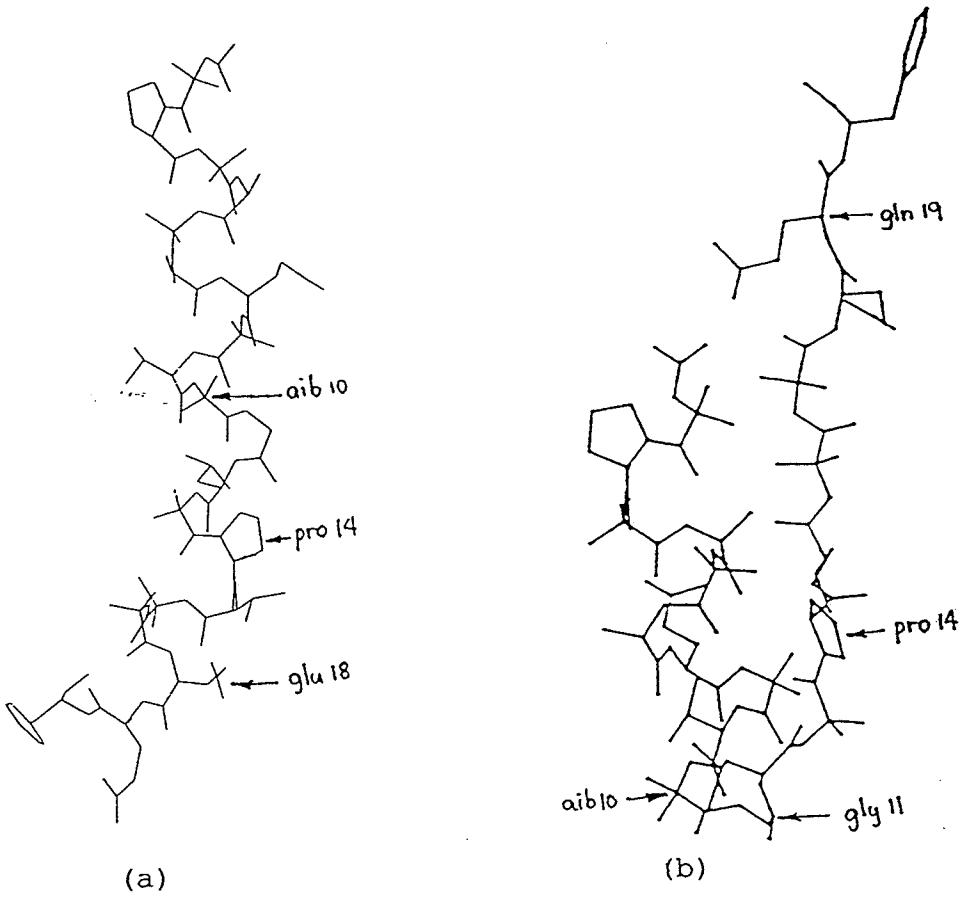

Figure 2: Suggested alamethicin monomer structure (a) in methanol.(from Esposito *et al.* [26]) (b) in the lipid bilayer to satisfy the electrical conductance data, see text. (from Hall *et. al.* [35])

properties in the membrane and a pore channel model must be consistent with the electrical properties observed.

The permeability of lipid monolayers to cations is increased by alamethicin [65]. The macroscopic conductance induced by alamethicin fluctuates between different levels which are independent of the voltage and alamethicin concentration. These were interpreted to suggest that the pores fluctuate between several distinct states of conformation (substates) [24]. When alamethicin is added to one side of the membrane, an asymmetric current-voltage curve is obtained, i.e., a positive voltage elevates the conductance more than the negative voltage of the same magnitude. The sign of the asymmetry depends on the peptide structure. When the negative charge of the carboxyl side chain of glu 18 is blocked by esterification or by lowering the pH, the current-voltage curve becomes more symmetric compared to unmodified alamethicin [21]. Kinetic studies show that the average number of pores at any given time is governed by their rates of formation and disappearance; both rates depend on the applied voltage and a positive charge is displaced when a pore is formed [24]. The alamethicin pores do not show strong selectivity for Na^+, K^+ or Ca^{2+} [24], although they are less permeable to negative ions than to positive ions [65].

In the absence of applied voltage, alamethicin was found to insert itself, whether as a monomer or as aggregates, into the lipid bilayer. This was shown by the

photolytic cross-linking of alamethicin to a phosphatidylcholine analogue containing a carbene precursor at the fatty acyl chain [52]. It was also shown, using freeze-fracture and negative stain experiments [60] that, in the absence of applied voltage, there is an increase in the bilayer width suggesting that alamethicin somehow modifies the hydrocarbon chain packing in the bilayer and that at least part of the alamethicin molecule resides at the surface of the bilayer hence modifying the hydrophilic part of the bilayer. Molecular models were used to explain these pore structures [12,29,35,57].

Fox and Richards [29] proposed a channel model consisting of 8 to 12 molecules based on the crystal structure of the alamethicin molecule. The alamethicin molecule is divided into two segments by pro 14 (see crystal structure description, page 2). The channel has a funnel-like appearance with a flair at the C-terminal because sidechains of the residues at this end are bulky. One εH of each gln 7 sidechain is hydrogen bonded with another gln 7 sidechain's carbonyl oxygen (εO) of the neighboring molecule forming a hydrogen bonded annulus within the channel. The other εH is hydrogen bonded with a solvent molecule. One possible arrangement of the solvent in the annulus is shown in Figure 4b. The glu 18 sidechains of individual chains do not make direct contact with one another. The two amide protons of the gln 19 sidechain are hydrogen bonded to the oxygen atom of the hydroxyl of phol 20 whereas the phol 20 carbonyl is

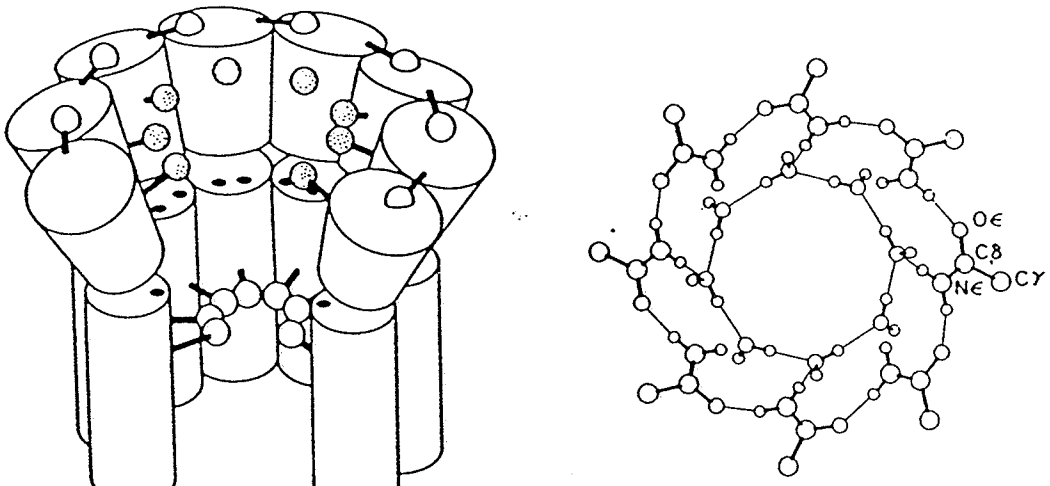

(a) (b)

Figure 3: (a) Schematic representation of the pore. Each alamethicin monomer is represented by two cylindrical segments. The open circles at the center represent the hydrogen bonded gln 7 annulus, the stippled circles are the glu 18 side chains, and the open circles at the top are the hydrogen bonded gln 19 residues. The black dots on the face of each cylinder are the solvent-accessible carbonyl groups of aib 10 and gly 11. (b) Top view of the gln 7 annulus. The inner ring shows the hydrogen bonded water molecules. (from Fox and Richards [29]).

directed towards the oligomer axis. The hydroxyl of phol 20 is in turn hydrogen bonded to the carbonyl oxygens of aib 17 and glu 18. This hydrogen bonding system stabilizes the C-terminal domain. The exterior of the channel is highly hydrophobic containing only small alkyl sidechains with no polar groups. The conductance substates observed in the alamethicin channels are ascribed to the alteration of the stability of the gln 7 annulus by the applied voltage. The dipole moment of each gln 7 sidechain amide is oriented almost perpendicular to the electric field in the channel. At sufficient voltage, the amide group would reorient such that the carbonyl is directed towards the C-terminus of the channel. This reorientation would result in an enlargement of the channel diameter. Since different gln 7 sidechain amide groups are involved, there would be fluctuating conductance substates. A spin label study of alamethicin in thylakoids supports the notion that the gating event involves changes in the conformation of the membrane-bound peptide assembly rather than the redistribution of peptide between aqueous solution and membrane [93].

The channel structure proposed by Hall *et al.* [35] was based on the electrical conductance data obtained with alamethicin and its analogues. The channel is composed of parallel monomers forming a two-layered barrel with β-sheet on the inside and α-helix on the outside since the monomer structure they suggested is bent (see structure page 7). The bent structure would stabilize the channel by partially

neutralizing the electrostatic repulsion of the parallel dipole moments of the α-helices. An applied voltage across the membrane would cause the rotation of the helix dipole so that the N-terminus crosses the membrane and the helix rotates across the membrane by forcing the β-bend to become helical.

Another hypothesis, the helix dipole model suggested by Mathew and Balaram [57], is that the interstitial channel is formed by the aggregation of alamethicin helices. The lifetime of the conducting channel would depend on the monomer-monomer interactions that stabilize the aggregate in the membrane phase, i.e., interchain hydrogen bonding and dipole-dipole interactions.(see Figure 5). The aqueous-phase aggregates with their polar surfaces on the exterior would insert into the membrane, rotating about the helix axis to present a hydrophobic exterior and facilitate hydrogen bonding, forming a closed pore. When voltage is applied, the "core piece" (see Figure 5), which is not hydrogen bonded to its neighbors, would be ejected creating an open channel. In this model, the voltage dependence of the alamethicin conductance has been ascribed to an increase in the number of open channels with increasing voltage. The conductance substates observed in a single channel have been ascribed to the variations in the dipole states of the channel due to changes in the number of monomers making up the channel.

Yet another hypothesis, suggested by Boheim *et al.* [12], is called the helix flip-flop model. Membrane

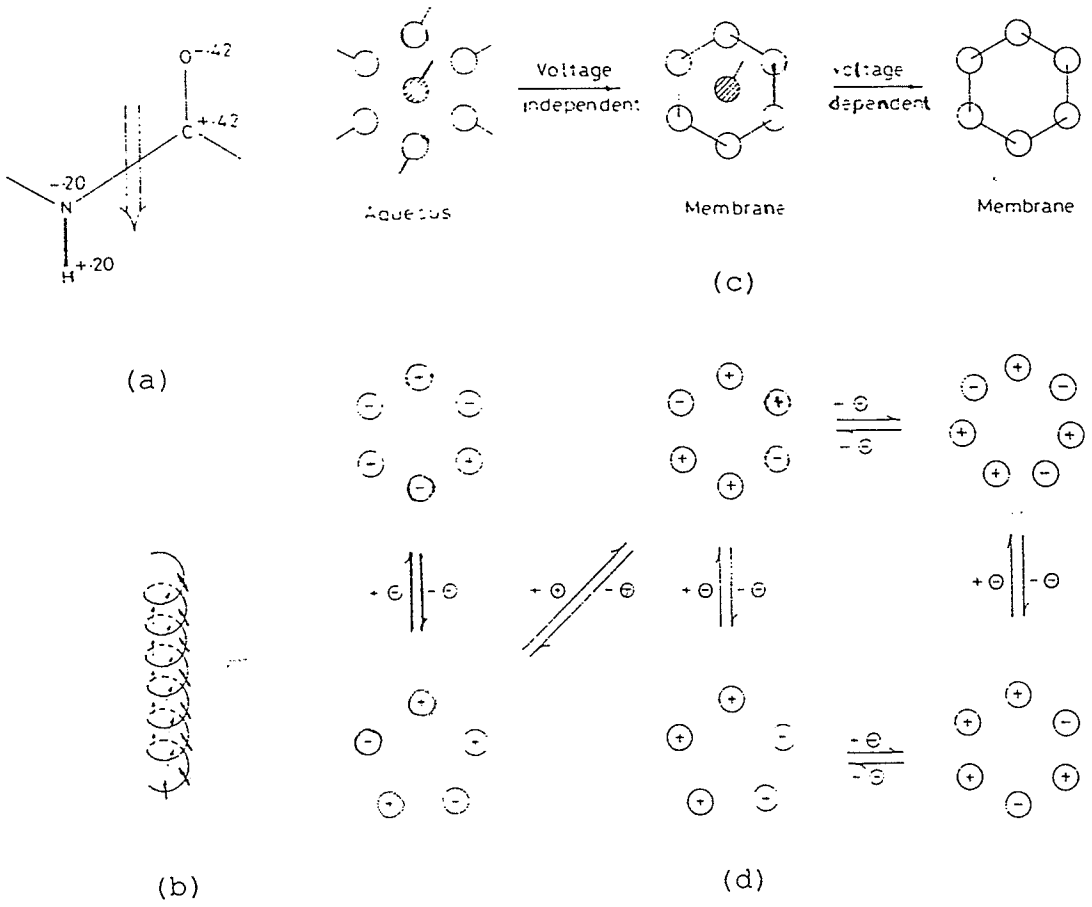

Figure 4: (a) Charge distribution in a peptide unit showing the resultant dipole moment. (b) Schematic representation of the near parallel orientations of the peptide dipoles in a helix. (c) Schematic representation of the helix dipole model. The shaded monomer at the center is the "core piece". (d) Schematic representation of the conductance substate transitions in a single channel. The peptide helices are viewed in cross-section; + and - refer to opposite orientations of the helix dipoles. (from Mathew and Balaram [57])

aggregates are built up of alamethicin molecules arranged in an antiparallel fashion. When voltage is applied, the monomers would rotate to a parallel configuration such that the negatively charged C-terminal poles are directed towards the side of the positive applied voltage. Within an aggregate, neighboring dipoles would repel each other, thus creating an open pore. The conductance substates were ascribed to the continual uptake and release of monomers resulting in changes of the dipole states of the channel, similar to the helix dipole model. Conductance studies on small polypeptides further support this model [38].

1.4 Structure determination by Nmr

Nmr has become a valuable method for elucidating the three dimensional structure of small proteins in solution. The procedure involved is outlined by K. Wuthrich [96] and also reviewed by Kaptein *et al.* [47] and Clore and Gronenborn [19].

1.4.1 Sequence Specific Assignment

The first step is to assign the proton resonances. The spin systems of the protons in individual amino acid residues are first identified using as far as possible through bond ^{1}H-^{1}H connectivities. For this, COSY [7,44], or other modified versions of it, or more recently TOCSY [6], are usually used. The cross peaks in a COSY spectrum result from coherence transfer between two coupled spins only. For extended

coupling networks, coherence can be transferred throughout the network by the relayed-COSY sequence. The TOCSY spectrum, obtained at sufficiently long mixing time is similar to that of a relayed-COSY spectrum. However, in TOCSY, unlike relayed-COSY, the coherence is transferred *via* HOHAHA transfer and the efficiency of this transfer is essentially independent of the magnitude of scalar coupling in the network [40]. The through-bond connectivities used to identify the ^1H spin systems of the individual residues are unambiguous in the sense that no connectivities between protons located in different residues are possible. The sequentially neighboring amino acid ^1H spin systems are identified from observation of the sequential noe connectivities d_{NN}, $d_{\alpha N}$, and $d_{\beta N}$. These sequential connectivities are obtained from the analysis of the regions containing NH-αH, NH-NH and NH-βH cross peaks in a NOESY or ROESY [5,13] spectrum. Sequence-specific assignments are then obtained by matching the peptide segments identified by nmr with the corresponding segments in the amino acid sequence. The amino acid sequence must be obtained independently (i.e., chemically sequenced and not by nmr) so as to eliminate erroneous assignment pathways which may have resulted because of chemical shift degeneracies or because nonsequential noe connectivities were interpreted as sequential ones. Observation of more than one connectivity, (i.e., d_{NN}, $d_{\alpha N}$, $d_{\beta N}$) increases the reliability of the resonance assignments.

1.4.2 Secondary Structure

Once sequence-specific assignment has been done, other nmr parameters are measured such as non-sequential noes, spin-spin coupling constants and amide-proton exchange rates, and these can be attributed to a specified location within the sequence. Certain patterns of these nmr parameters along the peptide indicate the presence of regular secondary structure. The presence of an noe is a good indication of a short distance between two protons, since it can only be observed between protons whose distance is less than 5Å. The spin-spin coupling constant between two vicinal protons can be related to the dihedral angle *via* a Karplus-type equation. The Karplus relationships between protons in the peptide backbone and the side chains were derived by plotting the coupling constants observed from nmr with the dihedral angles determined by x-ray crystallography of several analogous proteins with only one or two amino acid residue differences [21]. The points are then fitted to a Karplus-type equation of the form : $^3J(\theta)=A\cos^2\theta-B\cos\theta+C$. For the backbone amide proton to the α proton, the following equations were reported: $^3J(\theta)=6.4\cos^2(\theta)-1.4\cos(\theta)+1.9$ [96] (equation 1) and $^3J(\theta)=5.4\cos^2(\theta)-1.3\cos(\theta)+2.2$ [71] (equation 2), where $\theta = |\phi-60|$.

Using the equations 1 and 2 on a standard α-helix with ϕ of -57°, the coupling constant can be calculated as 3.9 Hz and 3.8 Hz, respectively. For a standard β-sheet, the ϕ angle is -139°, which would give a coupling constant of 8.9 Hz and

8.3 Hz, respectively. The following values are used as a boundary between the helix conformation and the β-sheet: a series of residues having a $^3J_{NH\alpha}$ of less than 6 Hz, corresponding to ϕ range of -10° to -80° [19], is considered to be in an α-helix conformation and those with $^3J_{NH\alpha}$ greater than 9 Hz, corresponding to -100° to -130° [19], is said to be in the β-sheet conformation. Other papers give different ranges for the β-sheet conformation, e.g., Wuthrich [96] suggested $^3J_{NH\alpha} > 7$ and Kaptein [47] suggested $^3J_{NH\alpha} > 8$ for the β-sheet. J coupling values intermediate between a helix and extended β-sheet may be a result of an unusual conformation or motional averaging. Hence, care should be taken in interpreting values of $6 < {}^3J_{NH\alpha} < 9$ Hz. In some large proteins, the amide region of the proton spectrum is not well resolved in the one dimensional spectrum so that the $^3J_{NH\alpha}$ values are obtained from the minimum distance between the antiphase components of a phase-sensitive COSY (or COSY-like) spectrum. Clore and Gronenborn [19] and Kaptein *et al.* [47] warned the use of $^3J_{NH\alpha}$ of less than 5 Hz measured in this manner since the value is not very reliable due to cancellation effects in antiphase multiplets.

Regular secondary structure in polypeptides involves hydrogen bonding between backbone amide protons and backbone carbonyl oxygens. These hydrogen bonds are manifested in the individual amide-proton exchange rates. Individual proton-amide exchange rates, therefore, can provide fully independent evidence for regular secondary structures.

The conformation of the sidechain in some residues may also be determined from a Karplus equation [21,27]. The Karplus equation defining the torsion angle (χ^1) dependence of the coupling between the sidechain α and β protons ($^3J_{\alpha\beta}$) was derived as $^3J_{\alpha\beta}=9.4\cos^2(\chi^1)-1.4\cos(\chi^1)+1.6$ [21]. The conformations of the sidechain CH_2 were divided into three classes corresponding to the three minimum energy staggered conformations [90]. Classification of the sidechain conformation requires both the coupling constants and the noe information as shown on Figure 6.

The three dimensional structure determination of a protein is based primarily on the distance constraints derived from noe measurements. A 3D molecular model is constructed using a distance geometry (DG) program. In this program, an embedding algorithm finds 3D structures that are an approximate fit to the conformational constraints imposed by the nmr noe data, coupling constants and the covalent structure. The fit is then further improved by numerical optimization. The quality of the protein structures based on geometric constraints can be improved by taking energy considerations into account (e.g., restrained energy minimization and restrained molecular dynamics calculations) [90].

1.5 Nuclear Overhauser Effect [70,71]

The nuclear Overhauser effect is a change in integrated nmr absorption intensity of a nuclear spin when

Case	1	2	3
χ^1	60°	180°	-60°

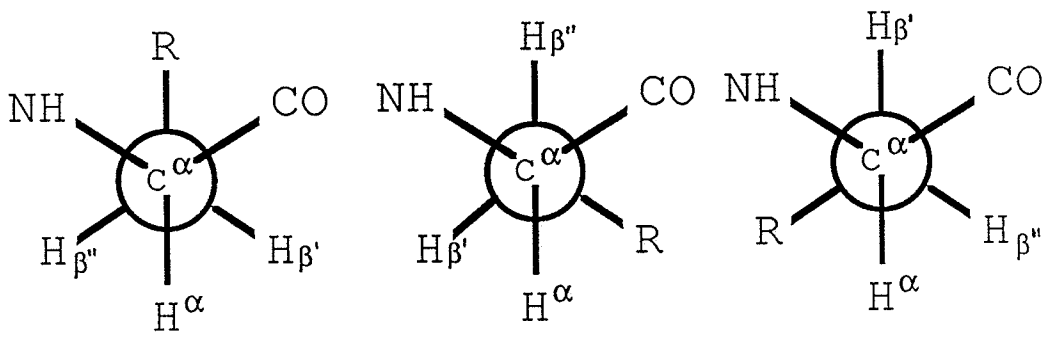

$^3J\alpha\beta'$ (Hz)	3.4	3.4	12.9
$^3J\alpha\beta''$ (Hz)	3.4	12.9	3.4
noe(α,β')	strong	strong	weak
noe(α,β")	strong	weak	strong
noe(NH,β')	weak	strong	strong
noe(NH,β")	strong	strong	weak

Figure 5 : Minimum energy staggered conformations of a residue sidechain.

the nmr absorption of another spin is saturated. The theory discussed in this section was taken from references 70 and 71. Consider two nuclear spins 1/2 (I and S) that are chemically shifted but not J-coupled. The energy levels will be :

level 1 : spin I is α, spin S is α -- $\alpha\alpha$

level 2 : spin I is α, spin S is β -- $\alpha\beta$

level 3 : spin I is β, spin S is α -- $\beta\alpha$

level 4 : spin I is β, spin S is β -- $\beta\beta$

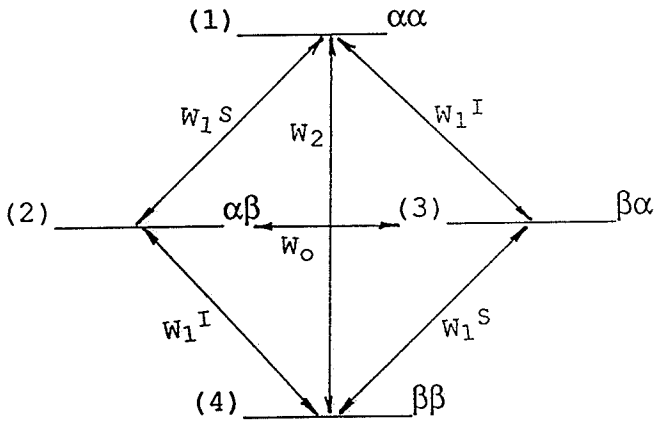

Fig 6 : Energy level diagram for a two-spin system.

The spin-lattice relaxation requires four transition probabilities:

W_1^I : the single quantum transition probability that spin I will go from α to β (or β to α) while the state of spin S remains unchanged.

W_1^S : the single quantum transition probability for spin S when spin I remains unchanged.

W_2 : the two quantum transition probability for the two spins to relax simultaneously in the same direction.

W_o : the zero quantum transition probability for a mutual spin flip

The rate of change of magnetization of spin I and S are given by Solomon's equations:

$$d\langle I_z\rangle/dt = -\rho_I(\langle I_z\rangle - I_o) - \sigma_{IS}(\langle S_z\rangle - S_o)$$

$$d\langle S_z\rangle/dt = -\rho_S(\langle S_z\rangle - S_o) - \sigma_{IS}(\langle I_z\rangle - I_o)$$

Where: $\rho_I = 2W_1^I + W_o + W_2$

$\sigma_{IS} = W_2 - W_o$

The transition probability for a first order two-spin system for the intermolecular dipole-dipole mechanism of relaxation is:

$$W_1^I = (3/40)K^2\ [2\tau_c/(1+\omega_I\tau_c^2)]$$

$$W_o = (K^2/20)\{2\tau_c/[1+(\omega_I-\omega_S)^2\tau_c^2]\}$$

$$W_2 = (3K^2/10)\{2\tau_c/[1+(\omega_I+\omega_S)2\tau_c^2]\}$$

where $K = (\mu_o/4\pi)\hbar\gamma_I\gamma_S r_{IS}^{-3}$

τ_c is the rotational correlation time, that is the time required for the molecule to rotate by one radian about any axis.

ω_I and ω_S are the resonance frequencies of spins I and S, respectively.

In a steady state experiment, spin S is irradiated with strong radiofrequency field, and the fractional enhancement of the integrated intensity of I compared to its equilibrium intensity can be solved from Solomon's equation using the following boundary conditions: $\langle S_z\rangle = 0$ and $d\langle I_z\rangle/dt = 0$. The fractional enhancement is $f_I\{S\} = (\langle I_z\rangle - I_o)/I_o = \sigma_{IS}S_o/\rho_I I_o$

But S_o is proportional to $S(S+1)\gamma_S$; likewise I_o is proportional to $I(I+1)\gamma_I$. Therefore:

$$f_I\{S\} = \sigma_{IS}S(S+1)\gamma_S/[\rho_I I(I+1)\gamma_I] \text{ ---- (equation 3).}$$

Equation 3 only considers dipole-dipole relaxation between the two nuclei. Other relaxation pathways contribute only to W_1^I and not to W_o or W_2. This equation can be extended to include other relaxation pathways by simply introducing a total direct relaxation rate (R_I) in place of ρ_I, where $R_I=\Sigma\rho_{IS}+\rho_I^*$, where ρ_{IS} is the direct dipole-dipole relaxation between I and S, and ρ_I^* is the direct relaxation of spin I due to other relaxation pathways [69]. The effect of internal motion can be included in the equation by considering the rate of internal motion [69].

The noe enhancement as given in equation 3 is a function of the ratio of the magnetogyric ratios of the two nuclei. Since ^{15}N has a negative γ and protons have a positive γ, the $f_N\{H\}$ is negative, therefore, the signal $(1+f_N\{H\})$ may disappear when $f_N\{H\}$ is -1.

1.6 Heteronuclear 2D Correlation Spectroscopy

Since proteins have nitrogen atoms along their backbone, ^{15}N nmr offers independent information on the backbone conformation of proteins. The three-bond scalar coupling between ^{15}N and the α proton of the preceding residue may provide information on the torsion angle (ψ) of the peptide bond [11]. In spite of this biological relevance, ^{15}N nmr has been limited in its applications because of

sensitivity. ^{15}N has only 0.36% isotopic abundance and a magnetogyric ratio of -2.7126×10^7 $s^{-1}T^{-1}$ [56]. It can also have a long longitudinal relaxation time.

Heteronuclear two dimensional correlation transfer can enhance the sensitivity of insensitive nuclei like ^{15}N [8,9,10,58]. The experiment can be started with excitation of either the proton spins or the ^{15}N spins and may end with the observation of either proton or ^{15}N magnetizations. The sensitivity of these experiments is determined by different factors [25]: (1) The available polarization is determined by the equilibrium polarization which is proportional to the magnetogyric ratio (γ_{exc}) of the nuclear species excited at the beginning of the sequence, and by the extent of recovery through T_1 relaxation mechanisms between subsequent scans separated by an interval time t. This may be expressed by a saturation factor : $\{1-\exp(-t/T_1^{exc})\}$. The available polarization therefore is proportional to $\gamma_{exc}\{1-\exp(-t/T_1^{exc})\}$ (2) The response of the observed nucleus is proportional to the amplitude and the frequency of the precessing magnetization. Both of these are proportional to the magnetogyric ratio of the observed nucleus (γ_{obs}). The response is therefore proportional to $(\gamma_{obs})^2$. (3) The detector noise is generally proportional to $(\gamma_{obs})^{1/2}$. Hence the overall sensitivity expressed as the signal-to-noise ratio, is therefore proportional to:

$$\gamma_{exc}\{1-\exp(-t/T_1^{exc})\}(\gamma_{obs})^2/(\gamma_{obs})^{1/2}.$$

$$S/N \propto \gamma_{exc}\gamma_{obs}^{3/2}\{1-\exp(-t/T_1^{exc})\}$$

A simple experiment suggested by Bax, Griffey and Hawkins [8,9] utilizes this sensitivity enhancement as applied to ^{1}H to ^{15}N coherence transfer. The pulse sequence is shown in Figure 7. Theoretically, the sensitivity enhancement compared with one dimensional ^{15}N nmr is $\gamma_N{}^{5/2} : \gamma_H{}^{5/2} = 1:300$.

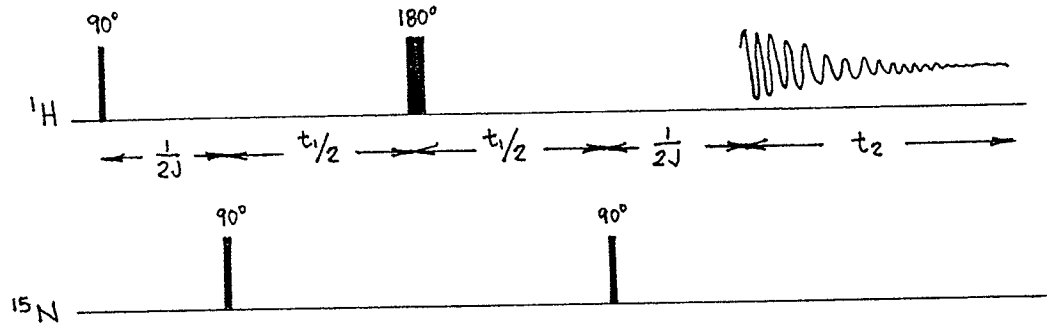

Figure 7: The pulse sequence for ^{15}N-^{1}H heteronuclear correlation spectroscopy as suggested by Bax, Griffey and Hawkins [8,9].

The first 90°(^{1}H) - 1/2J - 90°(^{15}N) pulse sequence converts all longitudinal magnetization of protons directly coupled to ^{15}N into heteronuclear zero and double quantum coherence. ^{15}N chemical shift information is given as $\delta_H+\delta_N$ and $\delta_H-\delta_N$ in the zero and double quantum coherence spectrum, respectively. The 180°(^{1}H) at the middle of the evolution period interchanges the zero and double quantum coherence to eliminate the δ_H information along the ^{15}N chemical shift axis. Combined with phase cycling of the first 90°(^{15}N) and the receiver phase this yields peaks at $(\pm\delta_N, \delta_H \pm J_{NH}/2)$. The

second 90°(^{15}N) pulse converts all the multiple quantum coherence back into observable transverse proton magnetization. The two proton doublet magnetization components are antiphase with each other. For experiments that do not require ^{15}N decoupling, acquisition may start immediately after the second 90°(^{15}N), in which case the doublet would be antiphase. The doublet components will come into phase with each other after a delay of the order 1/2J. For experiments requiring ^{15}N decoupling, the decoupler is turned on and acquisition is started after the 1/2J delay, otherwise, the doublet components would cancel out upon decoupling [8,9].

Heteronuclear 2D correlation experiments not only increase sensitivity by indirect detection of insensitive nuclei but may also unravel overlapping spectra of proton resonances by exploiting the chemical shift dispersion of nitrogen-15. They may also be used to correlate the spectra of different nuclear species for assignment purposes.

1.7 Proposed Experiments

An understanding of the mechanism of alamethicin voltage-gated ion channels in membranes requires a good working model of the channel including knowledge of the conformations of the individual monomers and their association to form a channel. The crystal structure of the alamethicin monomer has been deduced by x-ray crystallography and the solution conformation in methanol has been studied by

two different groups which suggested two different conformations in methanol. ^{15}N nmr offers an independent source of information on the backbone conformation and dynamics of the peptide. The purpose of this thesis is therefore, to label alamethicin with ^{15}N and to characterize the peptide using ^{15}N nmr. In addition, the secondary structure of the peptide in methanol will be determined using ^{1}H nmr with the method outlined by K. Wuthrich [96].

Chapter 2
EXPERIMENTAL

2.1 Materials

An extract of *Trichoderma* growth medium containing alamethicin which was used as standard was kindly provided by Dr. Floyd Kapeki of Upjohn (Kalamazoo, MI). *Trichoderma viride* (NRRL 3199) was purchased from the American Type Culture Collection (USA), catalogue number 38631. Two strains of *Micrococcus luteus* were purchased from ATCC (Rockville, MD), catalogue numbers 5337 and 381, lot number 0487. *M. luteus* was grown in nutrient broth (GIBCO, USA) and maintained on malt agar (DIFCO, USA). *T. viride* was grown on various media containing glucose (Fisher Scientific Co., USA); pharmamedia from cottonseed (Procter and Gamble, USA); molasses (Somerville, Belkin, Canada); and fish meal (Sigma Chemical Co., USA). *T. Viride* was also grown on semi-basal medium containing sucrose (Fisher Scientific Co., USA); dextrin (Matheson, Coleman and Bell, USA); KNO_3 (Fisher Scientific Co., USA). All the vitamins added to the semi-basal medium were purchased from Sigma Chemical Co., USA. The salts and minerals added to the semi-basal medium were NaCl; $CaCl_2$; $ZnSO_4.7H_2O$; NH_4MoO_4 (all obtained from Fisher Scientific Co., USA); $CuSO_4.5H_2O$; $MnSO_4.H_2O$; Boric acid (from Mallinckrodt, Missouri, USA) and $FeSO_4.nH_2O$ (from Science Borealis Ltd., Ontario, Canada).

Buffer used as eluant in HPLC was prepared using glacial acetic acid (Fisher Scientific Co., USA) and deionized water; the pH was adjusted using triethylamine (Fisher Scientific Co.,USA). Other HPLC eluants used were all HPLC-grade solvents from Mallinckrodt, Missouri, USA. Buffer solutions (Fisher Scientific Co., USA) were used to calibrate the pH meter.

$K^{15}NO_3$ (99% atom) purchased from Isotec, Inc., USA was used in the labelling of the peptide. The nmr solvents used were CD_3OD (Aldrich Chemical Co., Wisconsin, USA) and CD_3OH (MSD Isotopes, Ohio, USA). 2,2 Dimethyl-2-silapentane-5 sulfonate (DSS) from Sigma Chemical Co., USA was used as internal reference for proton nmr spectrum. $^{15}NH_4Cl$ (99.5% atom) from Isotec Inc., Ohio, USA was used as external reference for ^{15}N nmr spectra.

2.2 Methods

2.2.1 Thin Layer Chromatography

Thin layer chromatography of Upjohn standard alamethicin was done on a silica gel coated plate with polyester backing (Whatman PE SIL G/UV, 250 μm layer). The solvent system used was chloroform: methanol: glacial acetic acid = 86: 14.5: 4.8. Since the N-terminus of alamethicin is acetylated, ninhydrin can not be used to detect it. The developing method used was the iodine-tolidine method [53]. The plate to be developed was exposed to iodine in a covered tank with iodine crystals in it. After the plate turned

brown, it was exposed to air for a few minutes to remove the excess iodine. The corner of the plate was first tested by spraying with developing solution. It would give a light blue color; gray or black meant that the plate had too much iodine and required more aeration. The developing solution was made of o-tolidine (160 mg), glacial acetic acid (30 mL), 1% potassium iodide solution in water (100 mL) and distilled water to make a total volume of 500 mL. The Upjohn alamethicin standard gave two white spots (R_{f1}=0.26, R_{f2}=0.62) against a bluish background. The spots were visible while the plate was still wet or damp, and disappeared when the plate dried.

2.2.2 Bioassay

The bioassay for alamethicin was the same as that described by Brewer *et al.* [14,15,16] with only slight modification. Nutrient agar (2.3 g dried nutrient agar in 100 mL water) was poured into 10 cm diameter disposable petri dishes. When the agar hardened, a sterile 12.5 mm diameter filter paper (Wattman no. 1) was placed in the center of the dish.

Samples of *T. viride* fermentation broth (see below) were centrifuged in a sterile centrifuge tube for approximately 10 minutes or longer depending on the amount of mycelium in the sample fermentation broth. The centrifuged broth should be clear, otherwise, the bioassay would be

contaminated with the fungus. Samples of 50 to 100 microliters were placed on the filter paper disc.

Micrococcus luteus was grown in nutrient broth (0.8 g dried nutrient broth in 100 mL water) for one day at 25°C with shaking at 170 rpm. A 0.1 mL sample of the one-day-old culture (A_{540}=1.71) was used to inoculate 50 mL of nutrient agar (0.023 g/mL) at 40°C to 50°C. A 5 mL sample of the inoculated agar was poured into the petri dish which was gently swirled on the bench top so that a thin film of inoculated agar would cover both the solidified medium and the paper disc. The petri dishes were then incubated at 35°C for 1 to 2 days until growth of *M. luteus* was visible in the background. The controls, made of standard Upjohn alamethicin (~ 100 µL of 6.4 mg/mL in methanol or less) or alamethicin already extracted from earlier experiments, were run in parallel with the test samples. 50 µL of 6.2 mg/mL standard alamethicin would give an inhibition zone of around 4 cm diameter.

2.2.3 Complex Medium for Culturing *T. viride*

The procedure followed in the growing of *Trichoderma viride* in complex medium was that of Brewer *et al.* [15] with only slight modifications. Primary inoculum was prepared by growing *T. viride* on potato agar slants in 16x125 mm screw-capped culture tubes (Kimax, USA) or petri dishes (10 cm diameter, disposable) at room temperature for at least a week until the agar was covered with green fungus. During the

first two days of growth, white filamentous mycelia of *T. viride* spread across the agar slants or plates, and as the growth becomes dense, it turns green. The agar slants and plates were stored in a freezer (-20°C).

Medium, made of pharmamedia (0.5g) and glucose (0.5g) in water (20mL), was placed in a 125 mL Erlenmeyer flask. A small piece (0.5 cm x 1 cm) of the dense part of the primary inoculum was cut with a sterile blade and used to inoculate the medium. The inoculated cultures (secondary inoculum) were incubated at 25°C for 4 to 5 days in a shaker (Lab-line Orbit Enviro-shaker, USA) running at 100 rpm. The viscosity of the medium was observed to increase.

Finally, 5 mL of the secondary inoculum were used to inoculate 50 mL of the complex medium. The complex medium used was the original medium suggested by Meyer and Reusser [63]. The medium is made up of black strap molasses (20 g/L), dextrin (30 g/L), fish meal (15 g/L), and pharmamedia (15 g/L) in water. The pH of the resulting medium is around 5.8 which is then adjusted to 7 with 2% w/v sodium carbonate solution prior to sterilization. The medium was incubated at 25°C and shaken at 100 rpm. After 7 days, the cultures were sampled daily for alamethicin bioassay. Normally, 9 to 10 days would give satisfactory yields of alamethicin for a 50 mL culture (9.58 mg). Longer incubation periods were required for larger volumes of culture even if the secondary inoculum used to inoculate it was proportionately increased. The pH of the culture would drop to around 5 to 6 during incubation.

2.2.4 Basal Medium

The basal medium suggested by Brewer *et al.* [15] was modified to give a better yield of alamethicin. The modified basal medium (referred to here as semi-basal medium) was composed of sucrose (0.25 g), $K^{15}NO_3$ (0.125 g), dextrin (1.5 g), vitamins and minerals solution (3.57 mL), and water to give a 50 mL total volume. The vitamins and minerals solution was prepared by mixing the vitamins and minerals listed in Tables 1 and 2, and this gives a corresponding final concentration in the semi-basal medium as listed in Table 3.

The pH of the solution was not adjusted since it is already around 7 (6.5 to 7.3) and a very small amount of dilute HCl or Na_2CO_3 solution (2%) would abruptly change the pH since clearly there is no buffer in this medium. The appearance of the solution after sterilization is cloudy because of the suspended dextrin.

50 mL of semi-basal medium were inoculated with 5 mL of 7-day-old complex medium culture instead of the secondary inoculum since better growth and yield was observed by doing so. In the subsequent trials, a much better fungus growth and better yields of alamethicin were observed when mycelia from the fungus already grown on semi-basal medium were used to inoculate a semi-basal medium. Hence, a 50 mL batch, which showed successful growth in the semi-basal medium, was kept in the refrigerator and was used to inoculate the subsequent cultivations.

Table 1: List of vitamins and minerals and the amount added in the semi-basal medium. Water was added to give a final volume of 500 mL.

biotin	77.8 µL of 0.9 mg/mL
thiamine	304.4 µL of 2.3 mg/mL
niacin	538.4 µL of 1.3 mg/mL
calcium pantothenate	318.2 µL of 2.2 mg/mL
riboflavin	875.0 µL of 0.8 mg/mL
pyridoxine	291.7 µL of 2.4 mg/mL
folic acid	437.5 µL of 1.6 mg/mL
4-aminobenzoic acid	140.0 µL of 2.5 mg/mL
vitamin B12	7.4 µL of 3.8 mg/mL
inositol	21 mg
sodium chloride	0.7 g
calcium chloride	0.7 g
mineral salt solution[a]	0.7 mL

[a]composition is listed in table 2

Table 2: Amount of minerals dissolved in 250 mL of water used to make the vitamins and minerals solution.

$ZnSO_4.7H_2O$	22.0 g
$FeSO_4.nH_2O$	2.5 g
$CuSO_4.5H_2O$	1.0 g
$MnSO_4.H_2O$	0.15 g
Boric acid	0.14 g
NH_4MoO_4	0.09 g

Table 3: List of ingredients of the semi-basal medium and their concentration.

Sucrose	5	g/L
KNO_3	2.5	g/L
Dextrin	30.0	g/L
NaCl	0.1	g/L
$CaCl_2$	0.1	g/L
$ZnSO_4.7H_2O$	8.8	mg/L
$FeSO_4.nH_2O$	1.0	mg/L
$CuSO_4.5H_2O$	0.4	mg/L
Boric acid	57.0	µg/L
NH_4MoO_4	36.8	µg/L
$Mn_2SO_4.H_2O$	61.0	µg/L
biotin	10	µg/L
thiamine.HCl (vit. B1)	100	µg/L
niacin	100	µg/L
calcium pantothenate	100	µg/L
riboflavin	100	µg/L
pyridoxine	100	µg/L
folic acid	100	µg/L
4-aminobenzoic acid	50	µg/L
vitamin B12	4	µg/L
inositol	3000	µg/L

The inoculated medium was incubated at 25°C and shaken at 100 rpm. After about 4 days, the fungus mycelium would get coated by the dextrin and it appeared like a white solid mass or "little white balls". In some trials, white flakes appeared on the surface and then the next day were incorporated into the white balls (presumably) because the white flakes disappeared. When all the dextrin had been consumed, the solution turned clear, and after a day or two, it turned to light brown resembling a weak tea. Bioassays showed that at this stage the culture is ready for harvesting. In the subsequent trials, no bioassays were done on the semi-basal medium as the color of the solution is a good indicator of the time for harvesting. The total incubation period is about 9 days, though sometimes up to two weeks are required.

2.2.5 Alamethicin Purification

The procedure described by Brewer *et al.* [15] was followed in the harvesting and extraction of alamethicin with some modifications. The pHs of the media were adjusted to 8 using Na_2CO_3 solution (2% w/v). The culture was then centrifuged (Sorvall Refrigerated Centrifuge), to remove the fungus mycelium and other solid particles, at 2000 rpm for 40 minutes at 4°C. The clear, light to dark brown, supernatant was decanted. The supernatant was then acidified to pH 4.5 using HCl solution to precipitate crude alamethicin; the supernatant turned cloudy upon acidification. A 50 mL

starting medium yielded approximately 40 mL of supernatant. This was then diluted with 100 mL methanol and extracted with 100 mL chloroform. The methanol-chloroform-water mixture was shaken and the phases were allowed to separate. The lower phase was collected and the chloroform-methanol solvent was evaporated in a rotary evaporator (Buchi Rotavapor RE111). Some liquid that had not completely separated was left and this was transferred to a freeze-drying flask. The round bottom flask was then washed with a little *t*-butanol to dissolve all that was left in it and then the *t*-butanol solution was transferred to the same freeze-drying flask.

This extract was then freeze dried (Virtis Lyophilizer, New York) at -56°C and <700 millitorr. The lyophilized solid was light to dark brown in color from the control medium and white to light brown from the semi-basal medium. The lyophilized solid was dissolved in methanol and centrifuged to remove the undissolved particles and then purified by HPLC (Perkin Elmer, USA). A reverse phase column (Beckman Ultrasphere 5μ, 10 mm x 15 cm) was used and the detector was set at 210.6 nm. The eluting solvents were similar to those used by Balasubramanian *et al.* [2]: mobile phase A was 0.05 N acetic acid adjusted to pH 3.5 with triethylamine and mobile phase B was a mixture of tetrahydrofuran (THF), acetonitrile and mobile phase A at a ratio of 8 : 1 : 2, respectively. The HPLC solvent gradient program is shown in Table 4.

Table 4: Solvent program used in the HPLC purification of crude alamethicin.

Step	time (min)	flow (mL/min)	flow* gradient	percentage solvent A	B	methanol	solvent* gradient
equil.	20	1.0	0	60	40	0	0
1	5	2.0	0	60	40	0	0
2	5	1.0	1	51	49	0	1
3	15	1.0	0	51	49	0	0
4	10	1.5	0	0	100	0	0
5	5	2.0	0	0	0	100	0

* Gradient of 0 means no gradient was used while 1 means linear gradient was used.

Samples of 100 µL to 500 µL of crude extract were loaded onto the column. Eluates from about 20 runs were collected. Volatile organic solvents were evaporated from the pooled eluates of each peak by blowing air into the solution. When most of the volatile organic solvents had evaporated, the solution turned cloudy and a white foamy film formed at the surface of the solution. This was then freeze-dried. Lyophilized solid was white to off-white in color. Nmr proton spectra showed that this contained triethylammonium acetate impurities from the mobile phase. To remove these impurities, boiling acetonitrile (~80°C) was used to dissolved the solids which were then pipetted to another vial; the solution was allowed to cool stoppered. The alamethicin would precipitate

at the bottom and some would deposit on the sides of the vial upon cooling. The cooled acetonitrile was then carefully pipetted out of the vial so as not to disturb the alamethicin precipitates at the bottom. The alamethicin precipitate was left to dry in the fume hood overnight. The large proton peaks of the triethylammonium acetate in the nmr spectrum were thereby eliminated.

2.2.6 Nmr Spectroscopy

Nmr samples were made by dissolving a weighed amount of alamethicin in 0.6 mL of CD_3OD or CD_3OH. The solution was centrifuged and then 0.55 mL was pipetted to a 5 mm nmr sample tube (Wilmad number 535 or 537 pp). The phase-sensitive COSY and the DQF-COSY experiments [55] were done on a Bruker AM300 nmr spectrometer equipped with a ^1H-selective probehead optimized for water suppression. Nmr experiments at 11.75 T were done on a Bruker AMX500 nmr spectrometer using either a 5 mm inverse broadband probehead or a triple resonance probehead with the inner coil tuned to ^1H and ^2H (lock), and the outer coil tuned to ^{13}C and ^{15}N. One dimensional ^{15}N observe spectra were acquired with and without WALTZ-16 composite pulse ^1H decoupling during acquisition, or, during acquisition and relaxation delay to maintain the noe. The complete pulse programs for the spin-echo difference experiment [33], TOCSY experiment [6], 2D ROESY experiment [5], and 2D ^1H-^{15}N correlation (HMQC) experiment [8,9] are given in an appendix to this thesis. All 2D experiments were

512 t_1 increments each of 1K data points. All nmr experiments were done at 300 K. Other details are given in appropriate figure legends.

Chapter 3
RESULTS

3.1 Determination of Alamethicin Yield by HPLC

HPLC of crude and Upjohn alamethicin showed several peaks corresponding to retention times 20.18; 21.34; 22.56; 23.33; 24.53; 25.57 min. A chromatogram is shown in Figure 8.

Fungus grown on complex medium yield enough crude alamethicin that purified fractions from the HPLC can be directly weighed. However, the amounts of alamethicin from semi-basal medium after HPLC purification were too small to be accurately weighed. Hence, HPLC was used to measure the amount of alamethicin fraction in the crude sample extracted from semi-basal medium. The standard used for the calibration curve was alamethicin fraction pk21.34 collected from the crude samples from complex medium. A known amount of the standard alamethicin was dissolved in methanol (~0.58 mg/ml). Different volumes (20μL to 85μL) were injected into the HPLC, and the heights of the peaks in the chromatogram were measured. A calibration curve of the peak heights versus the amount of standard injected was plotted. Known amounts of crude alamethicin from the semi-basal medium were dissolved in methanol and injected into the HPLC. The volume injected was adjusted so that it fell within the limits of the calibration curve plotted. The peak heights from the chromatograms were then measured and the amounts of the

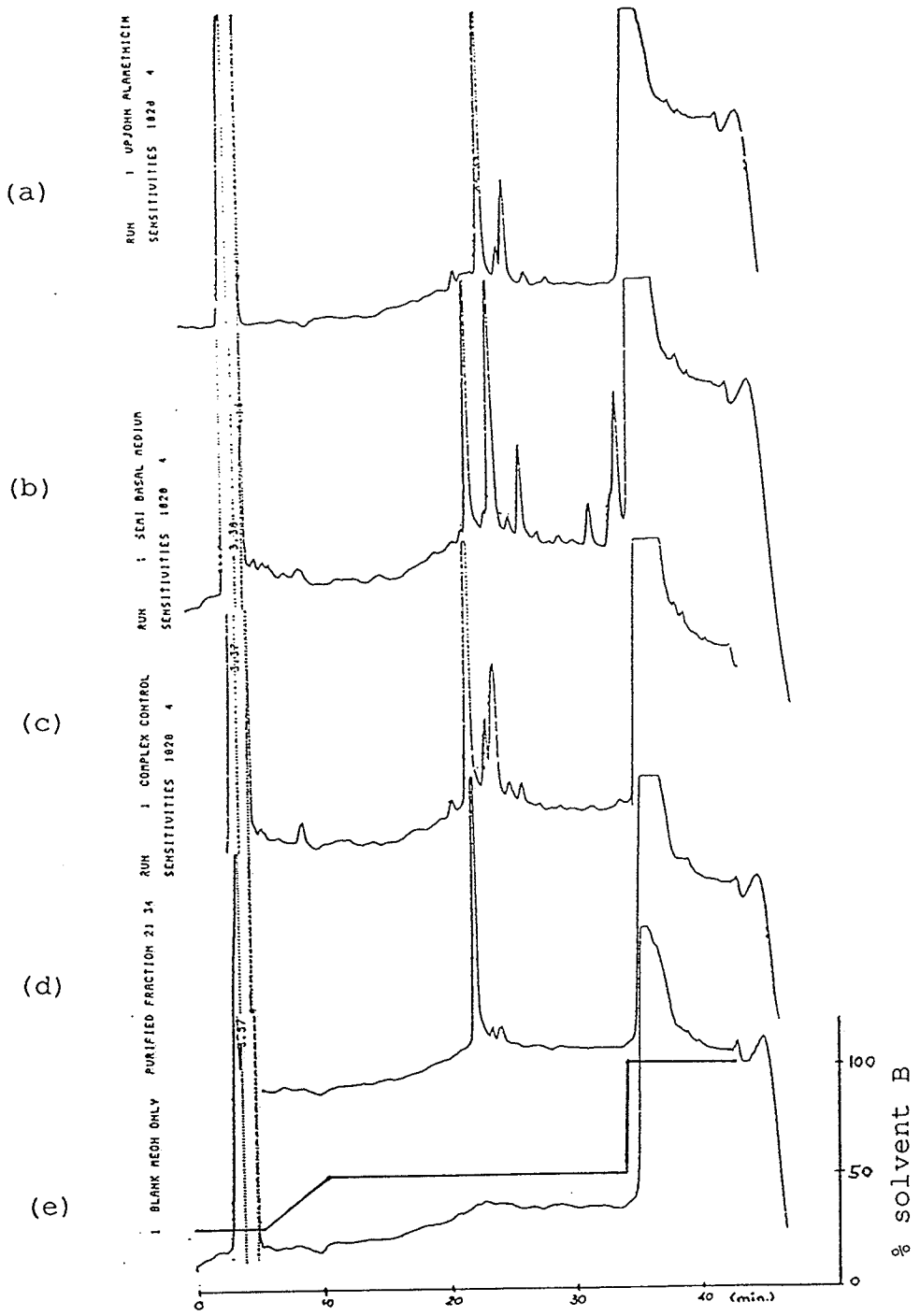

Figure 8: HPLC chromatogram of (a) Upjohn standard alamethicin, (b) crude alamethicin from semi-basal medium, (c) crude alamethicin from complex medium, (d) purified alamethicin pk21.34 fraction, and (e) blank run with the solvent elution gradient shown.

alamethicin fractions were read off the calibration plot. The semi-basal medium gave a yield of 2.5 mg of alamethicin per 50 mL starting medium as compared with 9.6 mg from the complex medium.

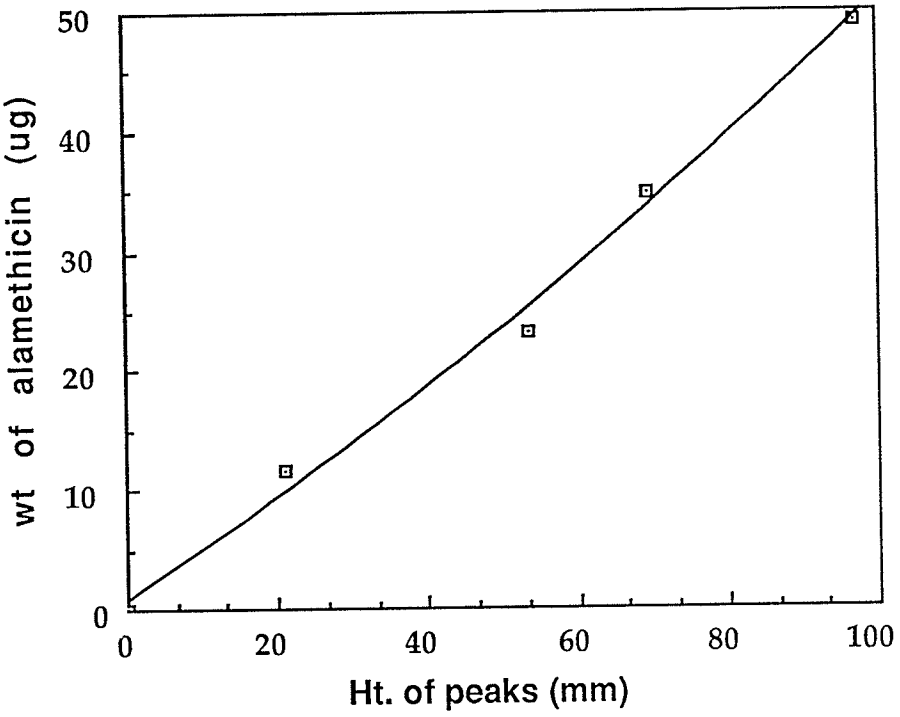

Figure 9 : HPLC calibration curve for alamethicin.

3.2 Spin System Identification in Alamethicin

Identification of the proton spin systems of the individual amino acid residues in a peptide is normally done on a COSY or other J-correlated spectrum. Since there is no scalar coupling observed through a peptide bond, each amino

acid residue can be considered an isolated spin system. Different spin systems give a characteristic geometric pattern in the J-correlated spectra [96]. A table of proton chemical shifts for the common amino acids in water in a random coil is given by Wuthrich [96]. These values are helpful as a starting point in the identification of the spin systems. One should bear in mind that this should only be used as a guide since chemical shift depends on the local environment of the proton [37] and thus chemical shifts could vary significantly.

Identification of the spin systems in alamethicin was first tried using a phase sensitive COSY at 300 MHz. The phase sensitive COSY spectrum of alamethicin in CD_3OH was uninformative because the presence of the intense methyl groups at around 1.5 ppm gave large "tails" which obscure the cross peaks close to the diagonal. To filter out the singlets, arising mainly from the methyl groups of the α-aminoisobutyric acids and alanines, a phase sensitive DQF-COSY experiment was run at 300 MHz. Although this turned out better than the phase-sensitive COSY, not all the spin systems could be identified. For example, in the crowded regions containing crosspeaks between NH and αH/βH, not all the cross peaks are observable. This could be due to some overlapping negative and positive cross peaks of comparable intensity which led to the cancellation of the cross peaks. The spin systems of the amino acid residues in alamethicin were finally identified using a TOCSY spectrum and the one

dimensional proton spectrum acquired at 500 MHz. The DQF-COSY proved very helpful in clearing up the ambiguity in the TOCSY spin system assignments.

Initially it was assumed that the amino acid sequence of the alamethicin fraction under study was the same as the published amino acid sequence [2,94]. However, the one dimensional proton spectrum (Figure 10) showed that there are three glutamine εNH, which led us to believe that there are three glutamines/asparagines in the fraction being studied instead of two.

Glycine is the simplest spin system among the amino acid residues. The structure of the glycine residue is shown in Figure 11. Glycine residues do not have a β carbon. Both α-protons are coupled to each other and to the NH proton, splitting it into a triplet. A glycine residue is therefore an AMX type of spin system. In a J-correlated spectrum, it should give two NH to α proton cross peaks.

The first spin system identified was the glycine since from the amide region of the one dimensional proton spectrum (Figure 10), it is the only NH peak that is split into a triplet. Knowing the chemical shift of the NH, the two NH to αH cross peaks (ω_1=8.33 ppm, ω_2=3.93 ppm and ω_1=8.33 ppm, ω_2=3.67 ppm) were identified in the TOCSY and DQF-COSY spectra (see Figure 12a).

From the structure of valine in Figure 11b, the spin system consists of the two methyl groups coupled to the same

Figure 10 : One dimensional proton resonance spectrum of 2.39 mM alamethicin fraction pk21.34 in CD_3OH at 11.75 T with solvent presaturation. Acquisition time is 2.125 sec. Number of scans is 256. Internal reference is DSS. No window function was used. Insert shows the expanded amide region with the tentative labels used in the resonance assignments.

Bα
Bb
G11
Bc
L1,2
Bd
Qc
Be
Ab
Qb
Qa
Bf
Yb
Bg
Bh
Aa
Va
QεNH
QεNH
Q2o
QεNH
QεNH
ppm
8.5
8.0
7.5
7.0
6.5
ppm
8
7
6
5
4
3
2
1

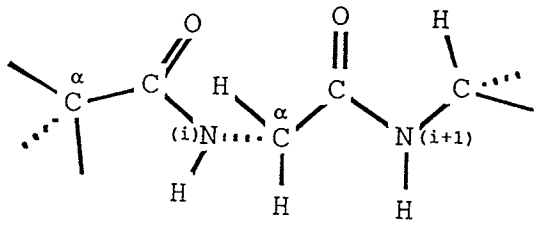

(a) glycyl residue

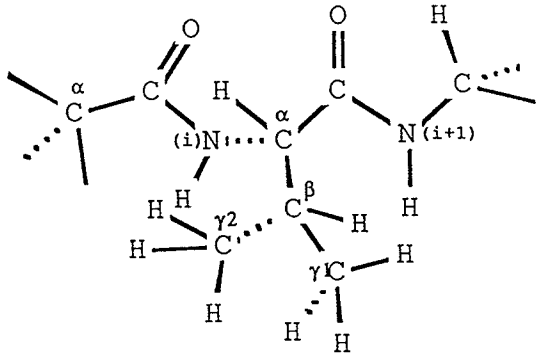

(b) valyl residue

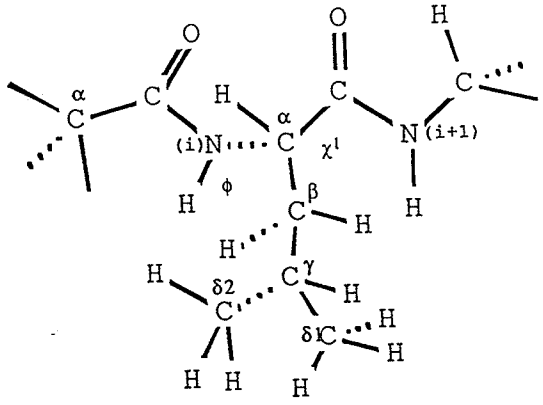

(c) leucyl residue

Figure 11: Structures of the amino acid residues that are found in alamethicin fraction pk21.34. The amide of the residue is indicated by (i) and the amide of the next residue is indicated by (i+1).

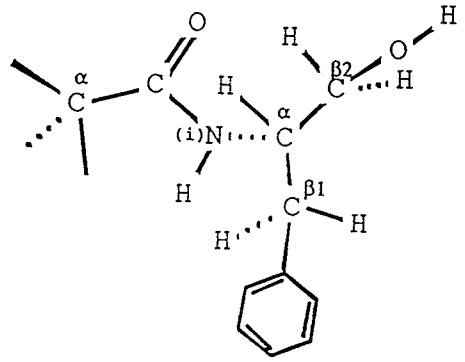

(d) phenylalaninol terminal residue

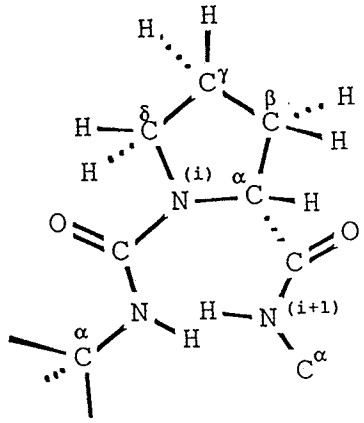

(e) prolyl residue

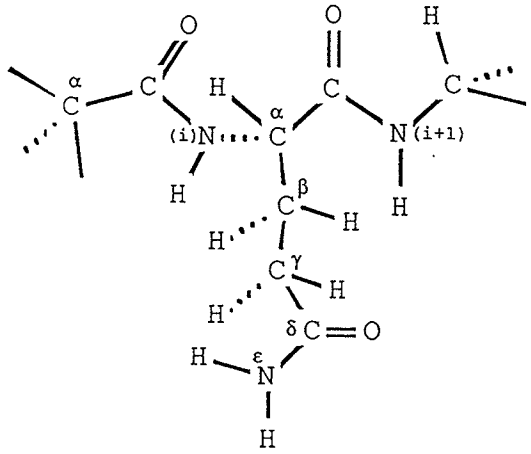

(f) glutaminyl residue

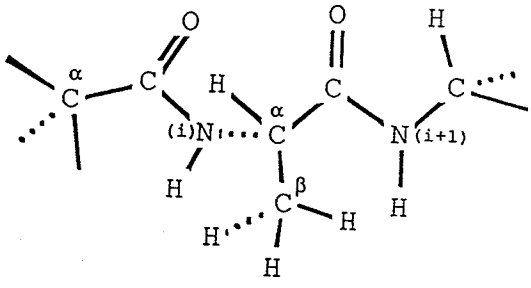

(g) alanyl residue

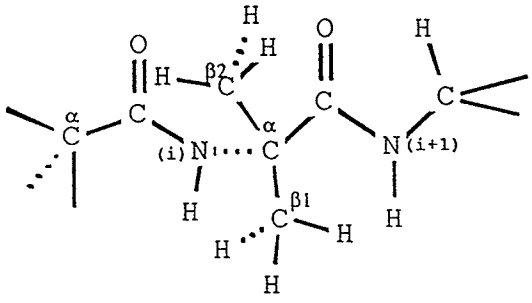

(h) α-aminoisobutyryl residue

β proton which is in turn coupled to the αH. The αH is then coupled to the NH giving an A_3B_3MPX spin system.

The appearance of a group of four cross peaks around (ω_1=1.10 ppm, ω_2=2.30 ppm) was used as a starting point in the identification of the valine spin systems (Figure 12b). From these cross peaks, the two A_3B_3MPX belonging to the two valines in the amino acid sequence were traced.

The leucine spin system, like that of valine, consists of two methyl groups coupled to the same proton. These are the δ methyl groups coupled to the γ proton while in the valine, it is the γ methyl groups coupled to its β proton (compare Figure 11b and 11c). This γ proton is then coupled to a βH_2 which is in turn coupled to the αH. The αH is then coupled to the NH giving an A_3B_3MPQTX spin system.

In the one dimensional proton spectrum in Figure 10, there is a doublet of doublets centered at 0.9 ppm. These peaks are probably from leucine or alanine since both valines have been identified. This doublet of doublets in the 1D spectrum was used as a starting point to trace the spin system for the lone leucine residue in the 2D spectra (see Figure 12b). The difference in chemical shift between the two δ methyl groups is very small so that only one cross peak to the γH was observed in the TOCSY spectrum (Figure 12). The two β protons are well separated but the γH apparently resonates at the same chemical shift as one of the β protons at 1.9 ppm. This assignment is supported by the observation of two cross peaks in the DQF-COSY spectrum (see Figure 13)

Figure 12 : TOCSY spectrum of 2.39 mM alamethicin in CD_3OH at 11.75 T with solvent presaturation. Internal reference used is DSS, with the spin systems for each amino acid residue traced. (a) In the upper half is a trace of a proline residue and in the bottom half is a trace of a AX spin system belonging to glycine and the two A_3X spin systems of the two alanines. (b) In the upper half of the diagonal is traced an A_3B_3MPTX spin system belonging to the lone leucine residue, in the bottom half of the diagonal is traced the two A_3B_3MX spin systems assigned to the two valines. (c) In the upper half is a trace of one of the proline residues and in the bottom half is a trace of the lone phenylalaninol residue. (d) Both halves show the spin systems of the two glutamines. (e) In the upper half is a trace of the third glutamine spin system.

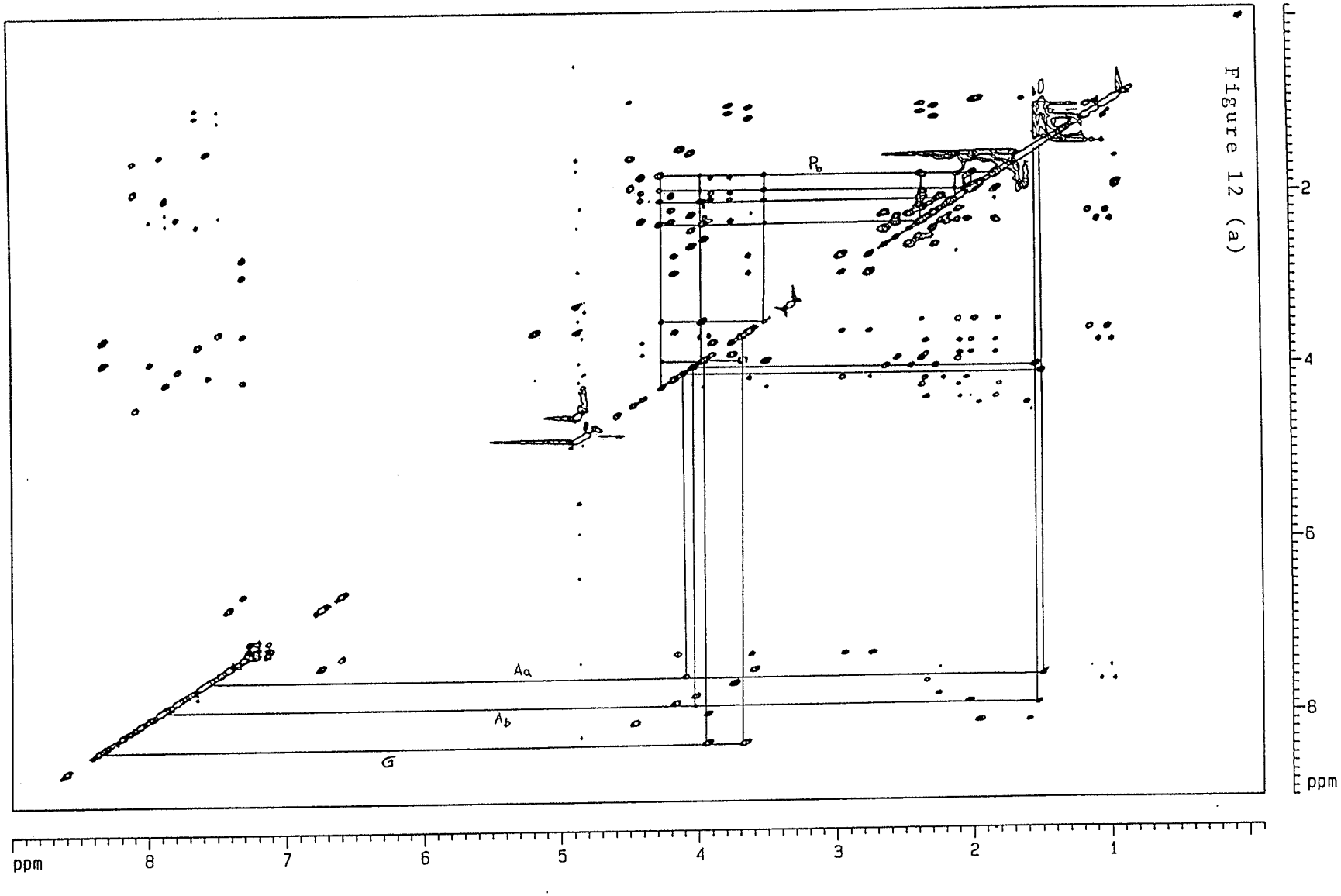

Figure 12 (a)

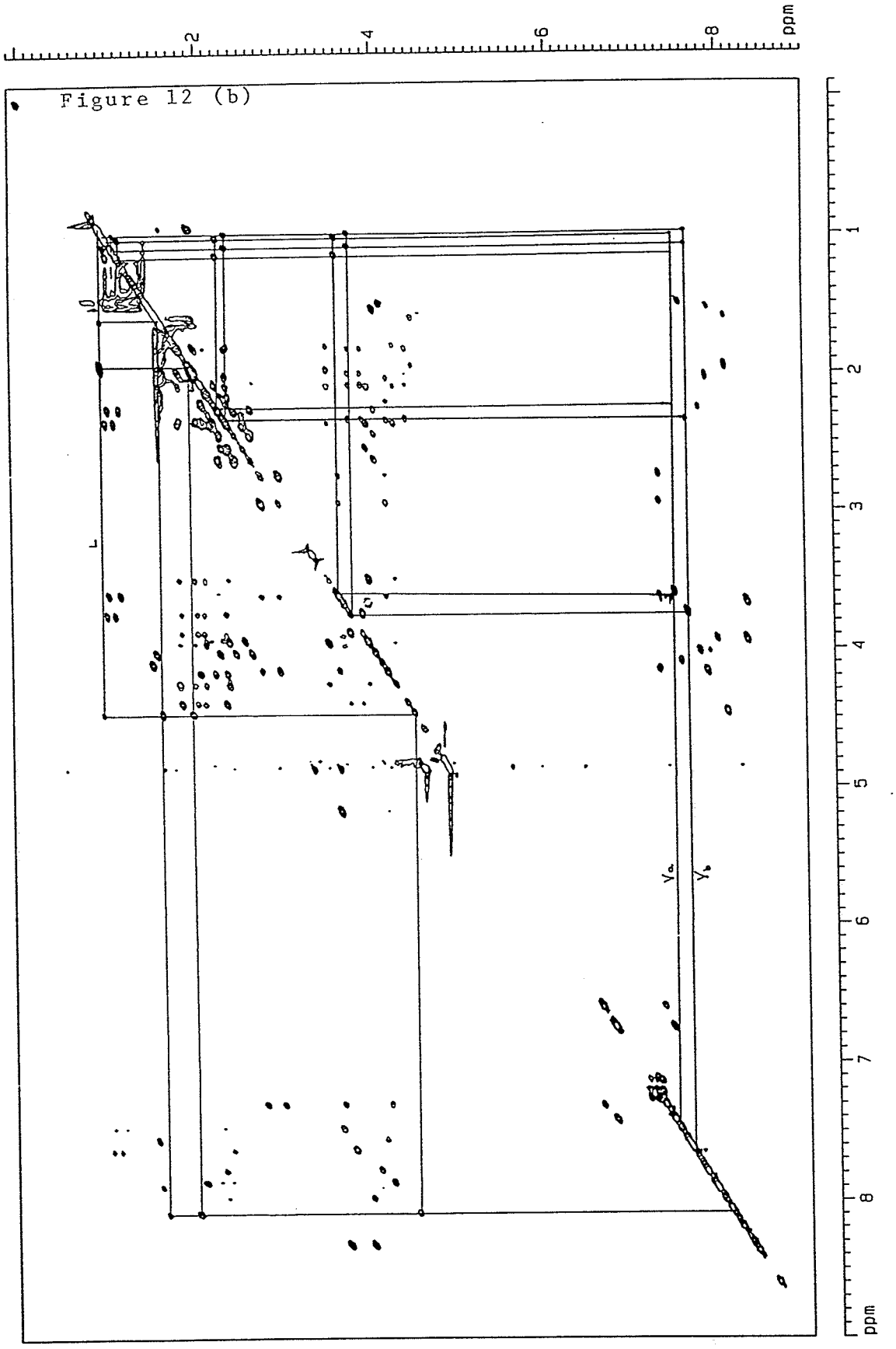

Figure 12 (b)

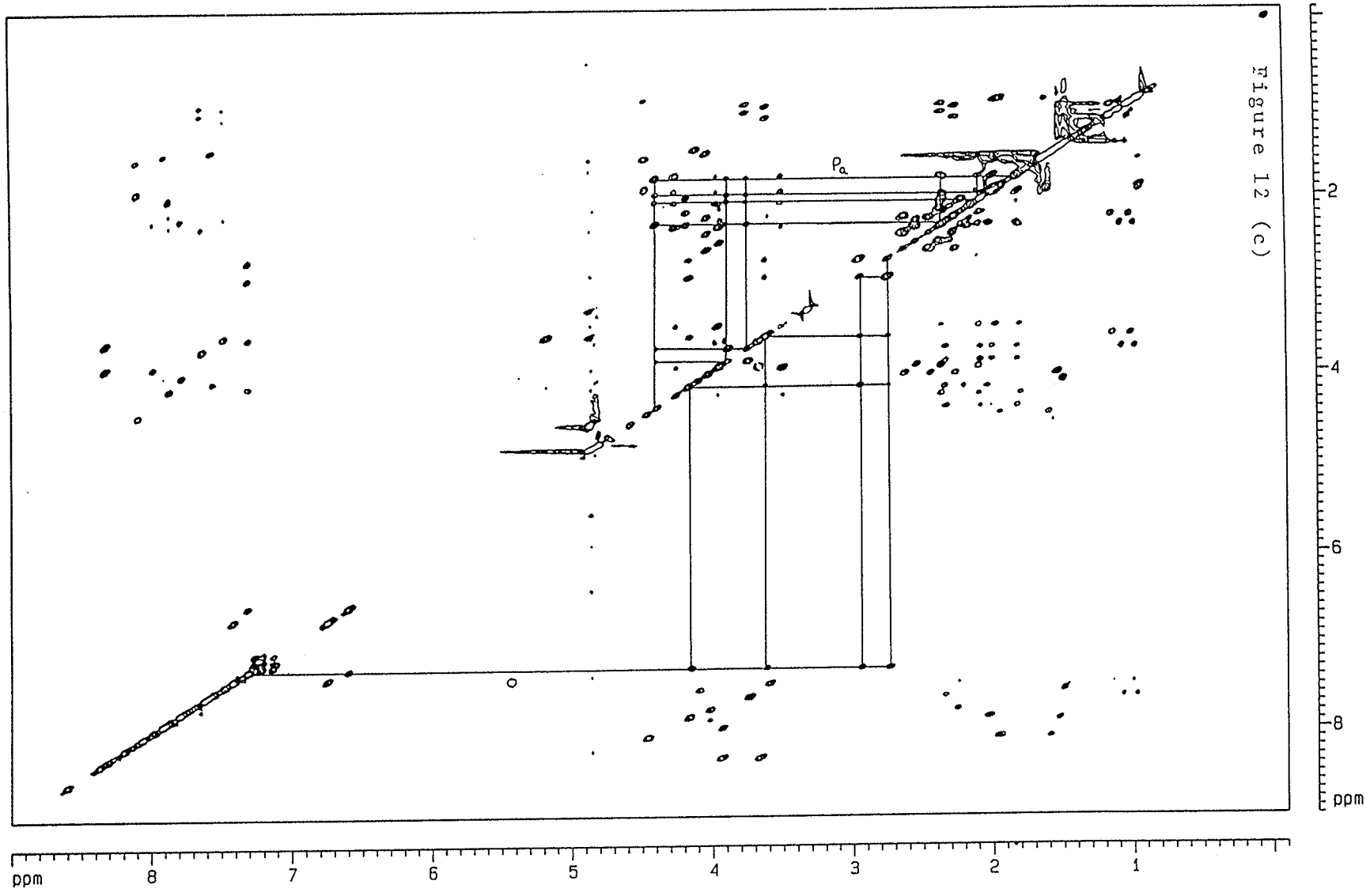

Figure 12 (c)

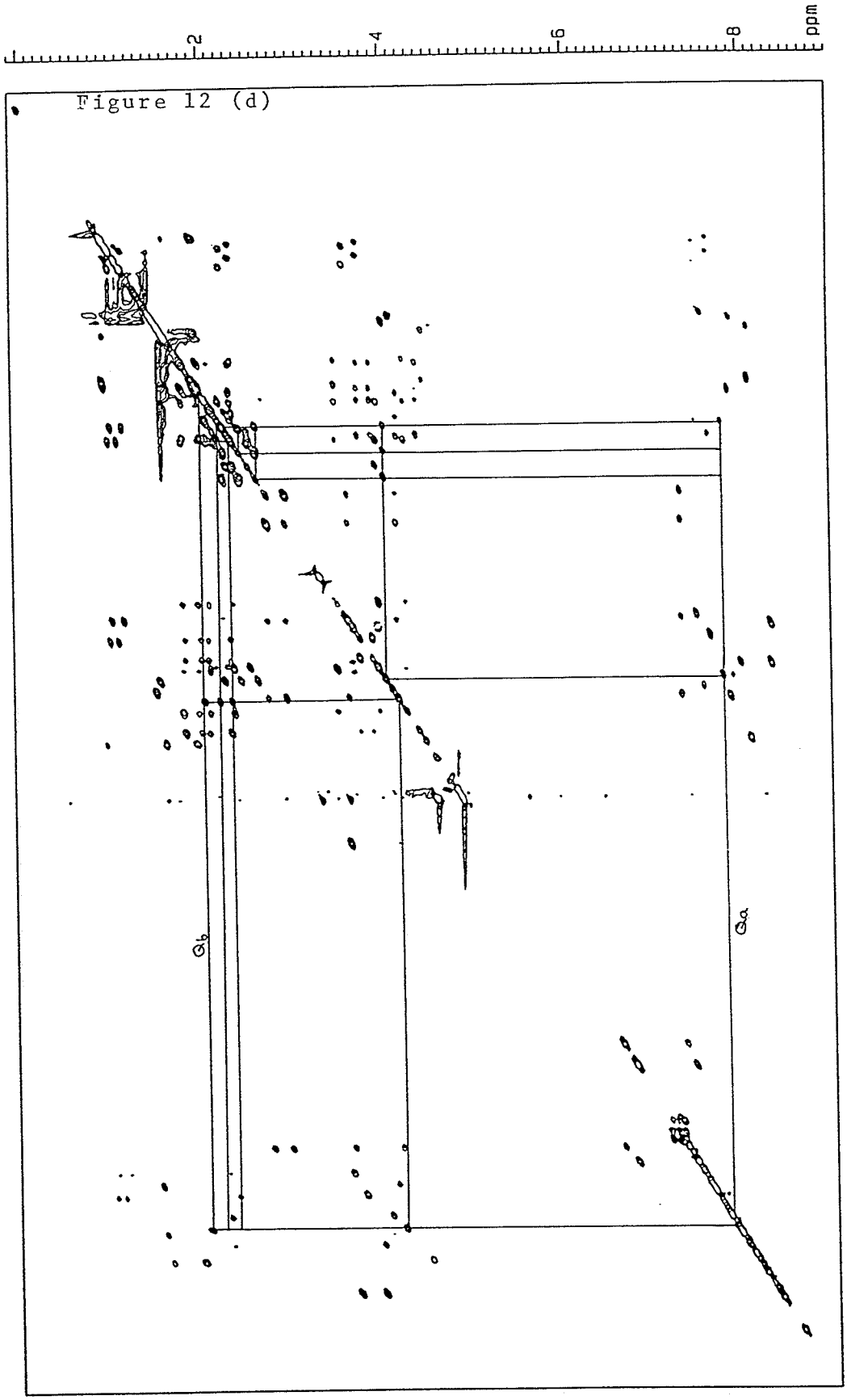

Figure 12 (d)

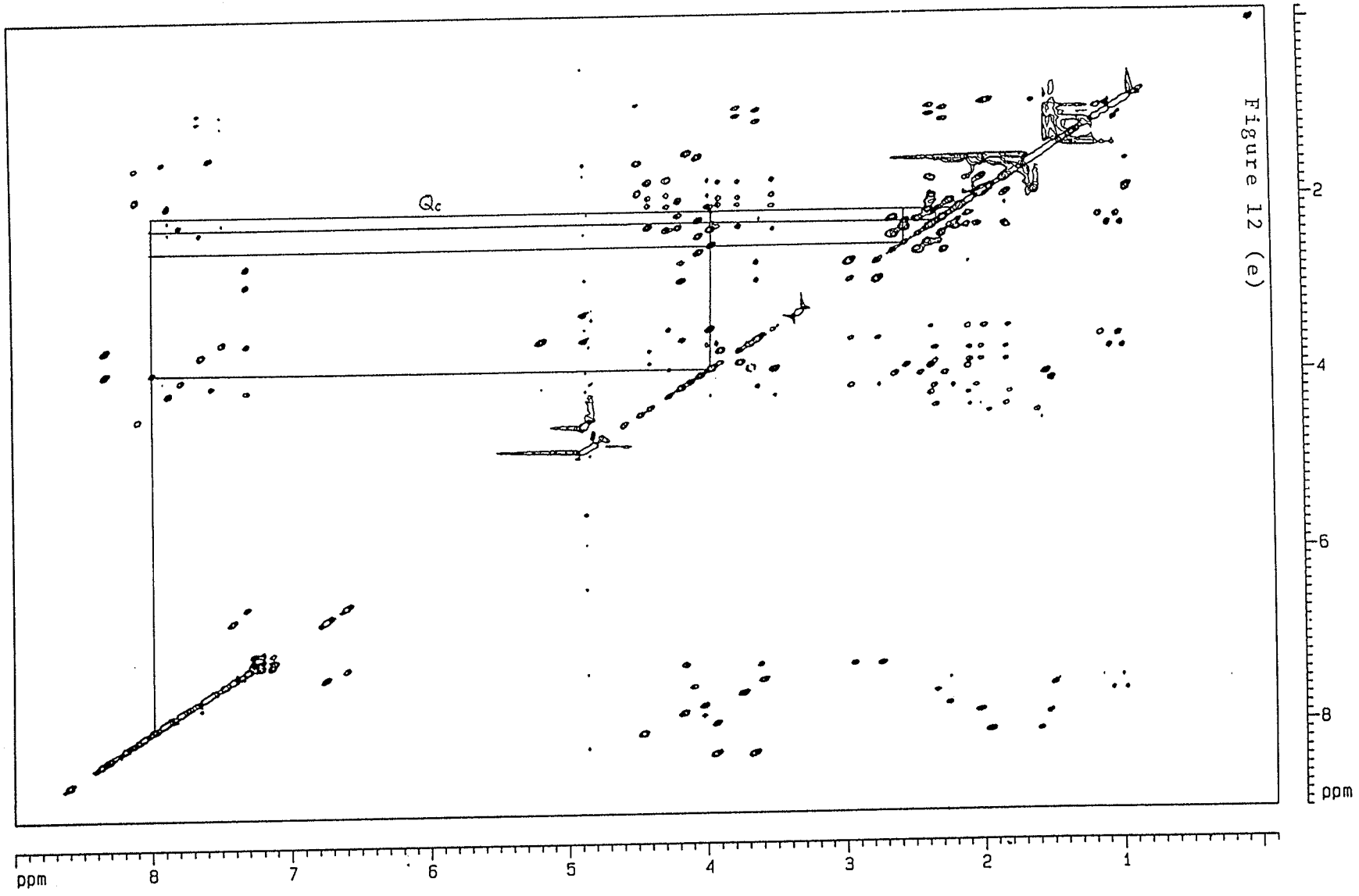

Figure 12 (e)

at ω_1=1.59 ppm, ω_2=1.92 ppm and ω_1=0.92 ppm, ω_2=1.92 ppm; these are the cross peaks of β'H to γH and γH to δH, respectively.

Phenylalaninol is a modification of the common amino acid phenylalanine. It is an amino alcohol (-CH_2OH) rather than an amino acid (-COOH). The phenylalaninol therefore has two β carbons, labeled as β_1 and β_2 in Figure 11d. The αH of the phenylalaninol is coupled to two protons from the β_1 and two protons from β_2. The αH is also coupled to the NH giving an AMP_2TX spin system.

The cross peaks in the TOCSY spectrum (Figure 12c) at (ω_1=2.73, ω_2=4.14 ppm) and (ω_1=2.94, ω_2=4.14 ppm) were used as a starting point to trace the phenylalaninol spin system. Since there is only one aromatic residue in the amino acid sequence, the aromatic ring protons centered at 7.1 ppm therefore belong to this phenylalaninol. The NH of the phenylalaninol is very close to the ring protons. No obvious cross peaks were observed in the TOCSY spectrum between the ring protons and the β protons.

The prolyl residue in a polypeptide does not have an NH (see Figure 11e for structure). The αH is coupled to the β protons which are then coupled to the γ protons which in turn are coupled to the δ protons giving an A_2T_2MPX spin system. The prolines labeled P_a and P_b (see Figures 12a and 12c) were traced from the crowded region from 1.7 ppm up to 2.4 ppm. The two γ protons of both prolines and the two δ protons

Figure 13 : Phase-sensitive DQF-COSY with solvent presaturation of 2.39 mM alamethicin in CD_3OH at 7.05 T with some of the cross peaks assigned.

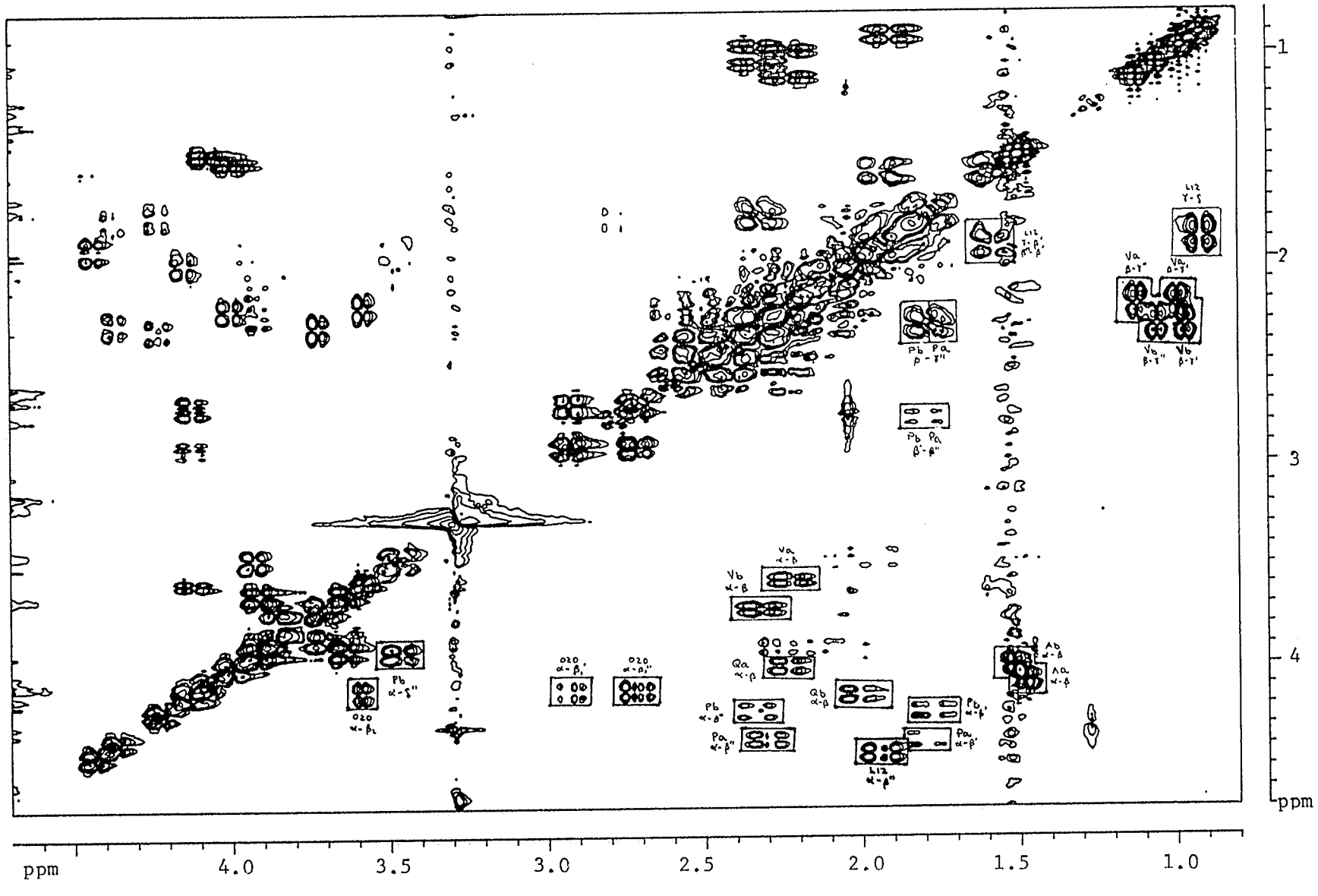
ppm
4.0
3.5
3.0
2.5
2.0
1.5
1.0
ppm
1
2
3
4

resonate at different chemical shifts giving an (AE)(RT)MPX spin system.

Glutamine residues give an AM(PR)TX spin system. No cross peaks between the εNH and the other protons of the same residue are observable in a J-correlated spectrum since those are separated by an amide (-NC=O) bond (see structure, Figure 11f). In the TOCSY spectrum, one would expect four cross peaks from the αH to the two βH and two γH for an AM(PR)TX spin system. In the TOCSY spectrum of alamethicin only three cross peaks (ω_1=4.02 ppm, ω_2=2.23 ppm; ω_1=4.02 ppm,ω_2=2.62 ppm; ω_1=4.02 ppm, ω_2=2.43 ppm) are observed for Q_a (see Figure 12d) and (ω_1=4.16 ppm,ω_2=2.02 ppm; ω_1=4.16 ppm,ω_2=2.19 ppm; ω_1=4.16 ppm, ω_2=2.33 ppm) for Q_b (see Figure 12d). From the DQF-COSY spectrum (Figure 13), only the cross peak at ω_1=4.02 ppm, ω_2=2.23 ppm is observable for Q_a and ω_1=4.16 ppm, ω_2=2.02 ppm for Q_b. The cross peaks observable from the DQF-COSY were assigned to αH to βH since αH to γH will not be observed in DQF-COSY and the remaining two cross peaks were assigned to αH to γH cross peaks. This assignment is also supported by the fact that the γ protons should be downfield of the βH because they are bonded to a carbonyl group. For the case of Q_a and Q_b, the spin system was A_2(PR)TX. Assignment of the third glutamine spin system was a little difficult since some of its cross peaks are very close to the prolines. Nevertheless, four cross peaks to the αH of Q_c were observed and were assigned using methods similar to those used for Q_a and Q_b.

Alanine is an aliphatic amino acid having one β methyl group coupled to an αH which in turn is coupled to the NH. The spin system for the alanine residue is a simple A_3MX (Figure 11g). After all the other amide to aliphatic cross peaks from the crowded region from 1.49 ppm up to 2.43 ppm in Figure 12a had been assigned, the remaining cross peaks at (ω_1=1.49, ω_2=4.09 and ω_1=1.52, ω_2=4.02 ppm) could easily be recognized as belonging to the two alanines.

α-Aminoisobutyric acid is not one of the twenty common amino acids found in proteins. It has two methyl groups attached to the α carbon. An α-aminoisobutyric acid, therefore, does not have an αH (see Figure 11h for structure). The four bonds between the NH and the two β methyls eliminate the possibility of a cross peak between them being observable in a DQF-COSY or a TOCSY spectrum. In the amide region of the one dimensional proton spectrum there are eight singlets corresponding to the eight α-aminoisobutyric acids in the sequence and these are labeled B_a to B_h (see Figure 10).

3.3 Sequence-Specific Assignments

The spin systems assigned to the glycine, leucine and phenylalaninol were assigned to residues 11, 12 and 20, respectively, since these residues are unique in the peptide sequence. Other sequence-specific assignments were made easy using the NH-NH region of the ROESY spectrum (Figure 14a). The presence of a cross peak between the glycine and the

leucine confirms the glycine and leucine assignment. Aib 13 was assigned on the basis of the observed cross peak between leu 12 and B_b. There is an α-aminoisobutyric acid at 8.06 (B_d) and one at 8.20 (B_c) ppm both of which show a cross peak with the same valine (V_a) at 7.48 ppm. This lead to the assignment of V_a to val 9 since it is between two α-aminoisobutyric acids in the amino acid sequence whereas val 15 is between a proline and an α-aminoisobutyric acid. By elimination, the other valine (V_b) belongs to val 15. Gln 19 was assigned on the basis of a strong cross peak between phol 20 and a glutamine (Q_b). A cross peak between two α-aminoisobutyric acids at 7.59 (B_h) and 7.80 (B_f) ppm can be assigned to aibs 16 and 17 since these are the only consecutive α-aminoisobutyric acids in the amino acid sequence; however, which is 16 and which is 17 cannot be assigned at this point. There is a cross peak between an alanine (A_a) and an α-aminoisobutyric acid (B_e) but this cannot be assigned on this basis alone since both alanines have neighboring α-aminoisobutyric acids.

Close to the diagonal are five weak cross peaks which can be assigned to A_b and Q_c at ω_1=7.90 ppm, ω_2=7.98 ppm. There are only two alanines in the sequence and ala 6 is the only one next to a glutamine. Therefore, A_b was assigned to A_6 and Q_c to Q_7. Since Q_b had previously been assigned to Q_{19}, then Q_a is Q_{18}. The other alanine (A_a) is A_4. The cross peak at ω_1=7.92 ppm, ω_2=7.56 ppm can be assigned to A_a (A_4) and an α-aminoisobutyric acid (B_e), this leads to the assignment of

Figure 14 : ROESY spectrum of 2.39 mM alamethicin in CD_3OH at 11.75 T tentatively labelled for use in the resonance assignment, (a) amide (NH-NH) region and (b) fingerprint (αH and βH-NH) region. The mixing time was 300 msec.

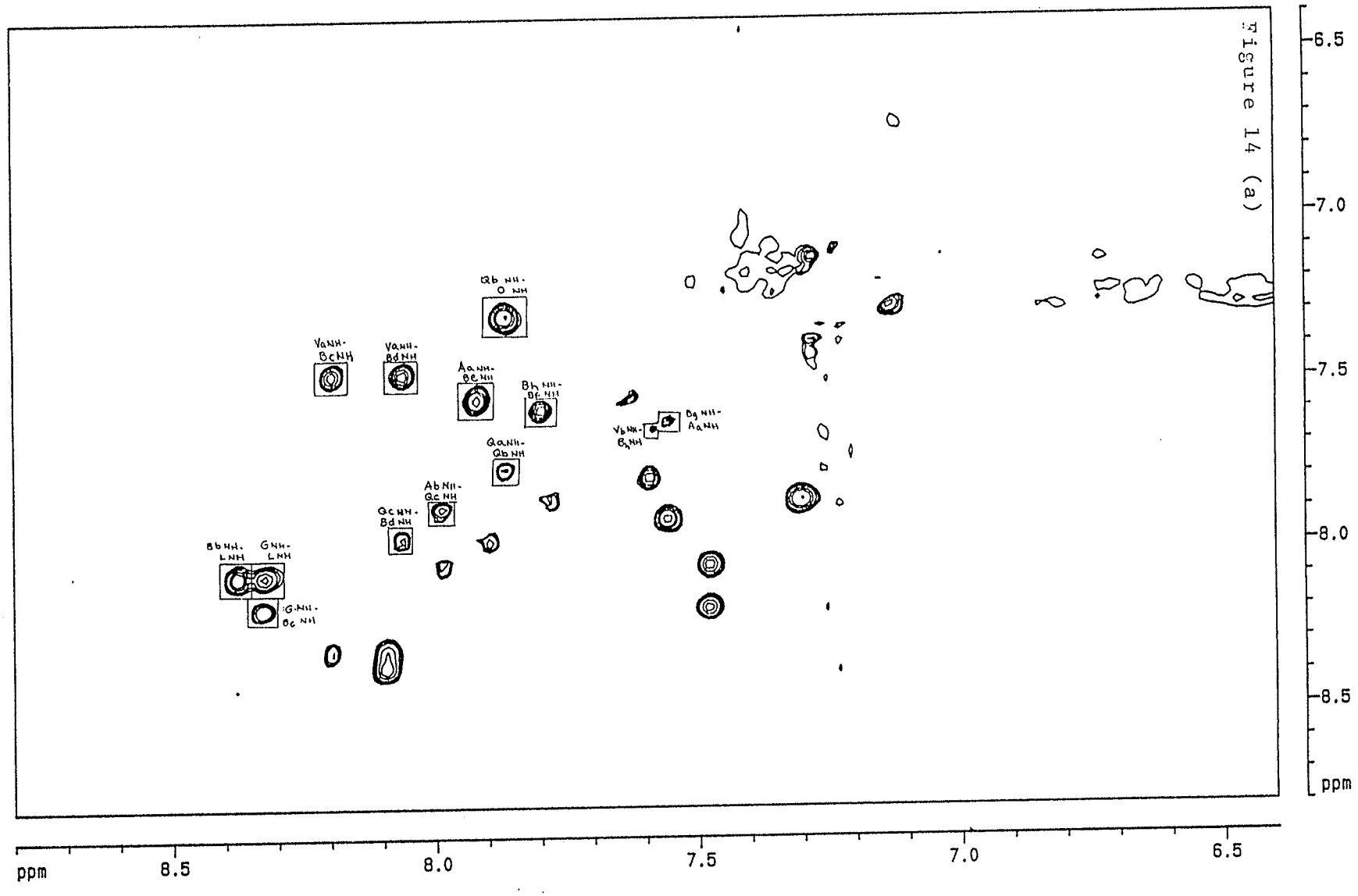
Figure 14 (a)
6.5
7.0
7.5
8.0
8.5
ppm
8.5
8.0
7.5
7.0
6.5
ppm

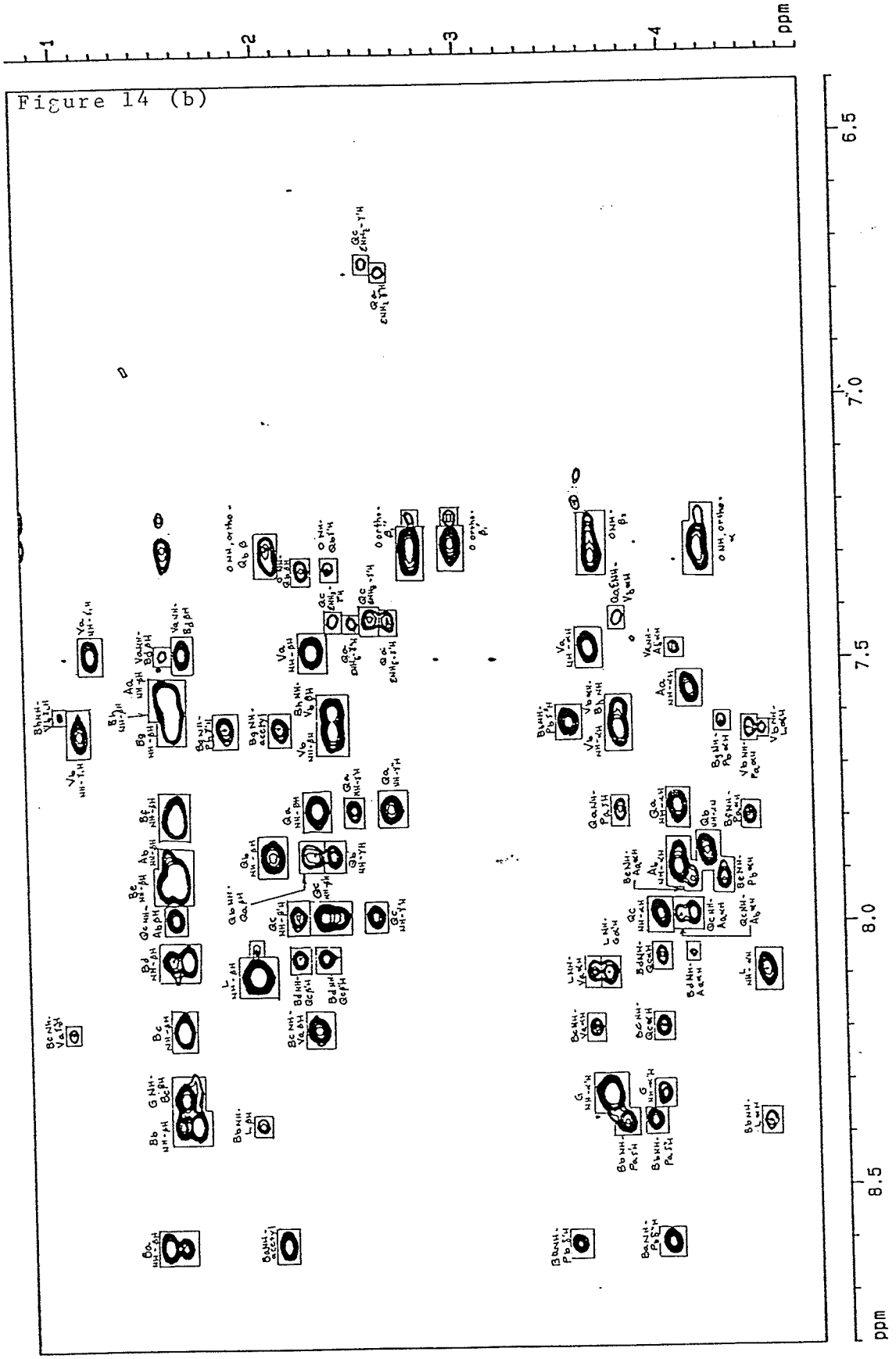

Figure 14 (b)

B_e as B_5 which would also confirm that A_a is A_4. The cross peak at ω_1=7.87 ppm, ω_2=7.78 ppm is between Q_a and Q_b. This confirms the assignment of Q_{18} and Q_{19}. A very weak cross peak is observed between A_4 and B_g. The A_4 is between two α-aminoisobutyric acids, B_5 had already been assigned, therefore, B_g is B_3. A very weak cross peak is also observed between V_b and B_h. Since V_b had previously been assigned to V_{15}, then B_h is B_{16} which leaves B_f as B_{17}.

The two prolines, B_c, B_d and B_a remain unassigned at this point. The prolines can be assigned using the NH to αH or βH region (Figure 14b) and this region can also confirm the assignments done using the NH-NH region. Cross peaks between B_b NH and leu 12 αH and leu 12 βH confirms the previous assignment of B_b to aib 13. Cross peaks between B_b NH (aib 13) and P_a δ'H and P_a δ"H were the basis of the assignment of P_a to residue 14. The cross peak between V_b NH (val 15) and P_a δH and P_a αH (pro 14) confirms the assignment of pro 14 and also the assignment of V_b to val 15 in the first region. This leaves the other proline (P_b) to residue 2. This can be confirmed by the presence of cross peaks between the δ'H and δ"H of P_b (pro 2) and the NH of an α-aminoisobutyric acid (B_a) which in turn is connected to the N-terminal acetyl at 2.04 ppm. Another α-aminoisobutyrid acid (B_g) showed cross peaks between its NH and the N-terminus acetyl at 2.04 ppm and to the pro 2 αH, δ"H and γH. B_g was previously assigned to residue 3. It is closer to the proline αH than B_a which confirms its assignment to B_3. B_a shows a

stronger cross peak with the N-terminus acetyl than B_3, and was assigned to residue 1; this assignment can be further supported by the cross peaks between B_1 NH with both δH of the pro 2.

Aib 10 (B_c) was assigned on the basis of the cross peaks between its NH and the αH and βH of val 9 (V_a). The assignment of Q_b to residue 18 was confirmed by a crosspeak between its βH and the NH of glu 19. The assignment of Q_c to Q_7 can be confirmed by the presence of cross peaks between Q_c-NH (gln 7) and the αH of both alanines. B_d was the only aib left unassigned which was assigned to aib 8 and this is confirmed by the strong cross peaks of its NH to the β'H and β"H of gln 7. Cross peaks between the γCH_2 protons of the glutamines to the εNH_2 protons allows the assignment of the ε protons. The ones resonating downfield were assigned as syn and those upfield are the anti [70].

3.4 ^{15}N-^{1}H 2D Correlation Spectroscopy of Alamethicin

The fully coupled ^{15}N-^{1}H correlation spectrum of alamethicin is shown in Figure 15. Aside from the directly bonded protons correlated to ^{15}N in the NH region, ^{15}N correlations to the methyls of the α-aminoisobutyric acids and alanines are also observable. Twenty two one-bond ^{15}N-to-proton correlations are observed of which 18 are backbone ^{15}N-^{1}H. The two proline ^{15}N's have no directly attached proton and are not observable. Two of the ^{15}N-^{1}H correlations belong to the Q_{19} sidechain ^{15}N to the two ε protons and the other two

Figure 15 : HMQC spectrum of uniformly labelled alamethicin in CD_3OH at 11.75 T. (a) ^{15}N-amide proton region and (b) ^{15}N-methyl proton region. The internal ^{1}H reference is DSS. The external ^{15}N reference is 2.9M $^{15}NH4Cl$ on 1M HCl which resonates at 24.93 ppm with respect to $NH_{3(l)}$ [54]. The number of scans was 128 for each of 512 increments. The vertical scales of (a) and (b) are the same.

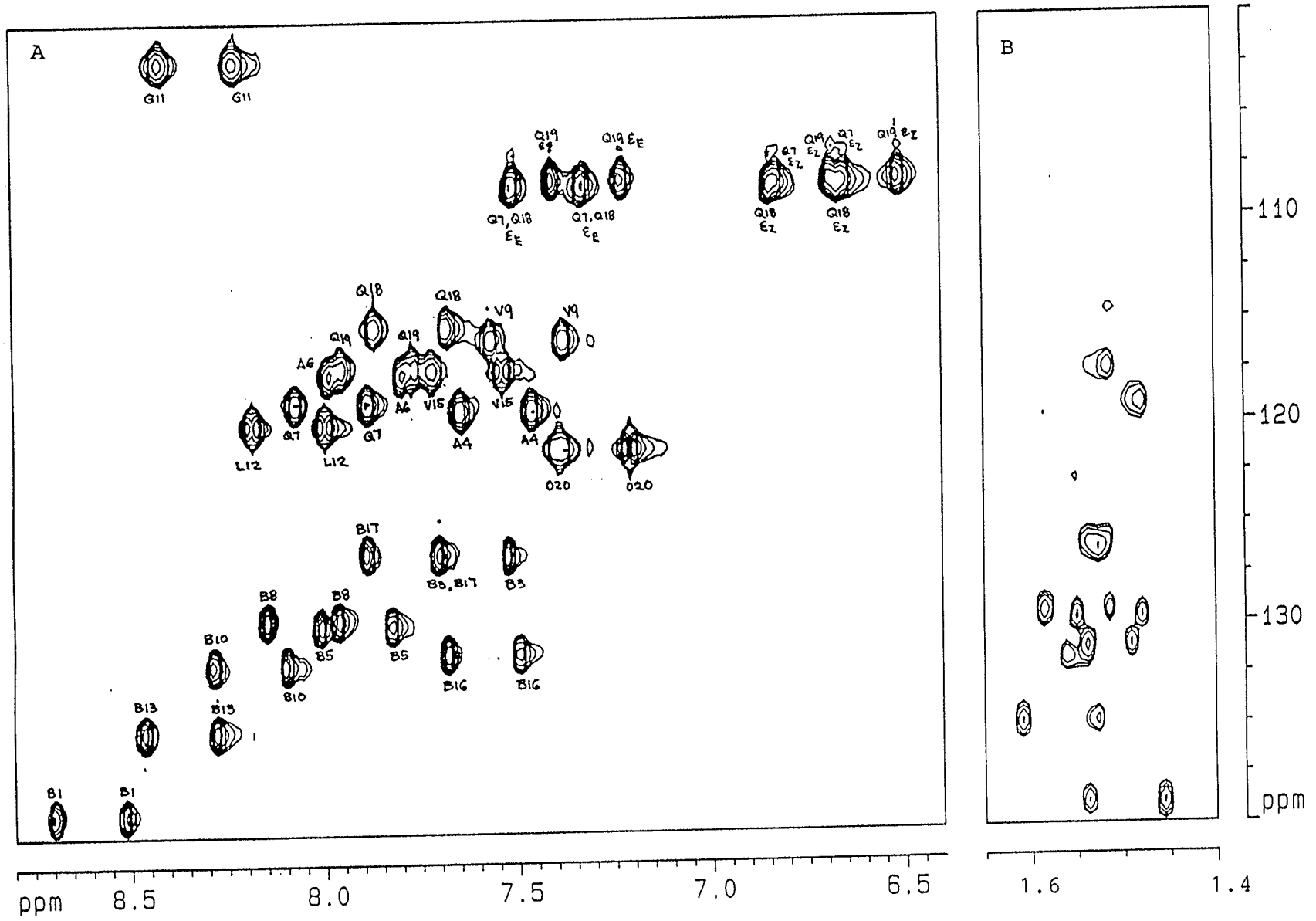
A
B
G11
G11
Q19 εE
Q19 εE
Q7,Q18 εE
Q7,Q18 εE
Q19 εZ
Q7 εZ
Q19 εZ
Q7 εZ
Q18 εZ
Q18 εZ
Q18
Q18
V9
V9
Q19
Q19
A6
A6
V15
V15
Q7
Q7
A4
A4
L12
L12
020
020
B17
B5,B17
B3
B8
B8
B10
B5
B5
B10
B16
B16
B13
B13
B1
B1
ppm
8.5
8.0
7.5
7.0
6.5
1.6
1.4
110
120
130
ppm

crosspeaks belong to the Q_7 and Q_{18} side chains. The ε protons of Q_7 and Q_{18} are partially overlapping; their H_Z have the same chemical shift and their H_E are very close in chemical shift. Since all amide protons of alamethicin have been assigned, assignment of the ^{15}N spectrum was straightforward and their chemical shifts are listed in Table 5.

The assignments of the α-aminoisobutyric acid's methyls were also made using the ^{15}N-^{1}H correlations (Figure 15b and Table 5). The one bond ^{15}N-^{1}H coupling constant ($^{1}J_{NH}$) for phenylalaninol was obtained from this spectrum and it also facilitated the identification of coupled doublets in the one dimensional proton spectrum of ^{15}N-labelled alamethicin (Figure 16) where the $^{1}J_{NH}$ for the other amino acids were obtained and these are listed in Table 6.

3.5 ^{15}N Nmr of Alamethicin

^{15}N nmr has a very poor sensitivity because of its low magnetogyric ratio and, as shown in Figure 17, the signal-to-noise ratio in the ^{15}N coupled spectrum is still very small even after 21,120 scans. Considerable enhancement was obtained by decoupling the protons but this took at least 60 hours to acquire compared with the two dimensional HMQC spectrum, which only took about 12 hours to acquire. The advantage of ^{15}N nmr spectrum over the HMQC spectrum is that it gave the chemical shift of the two prolines although specific assignment is not possible at this point. The ^{15}N spectrum with noe showed that only two signals are positive,

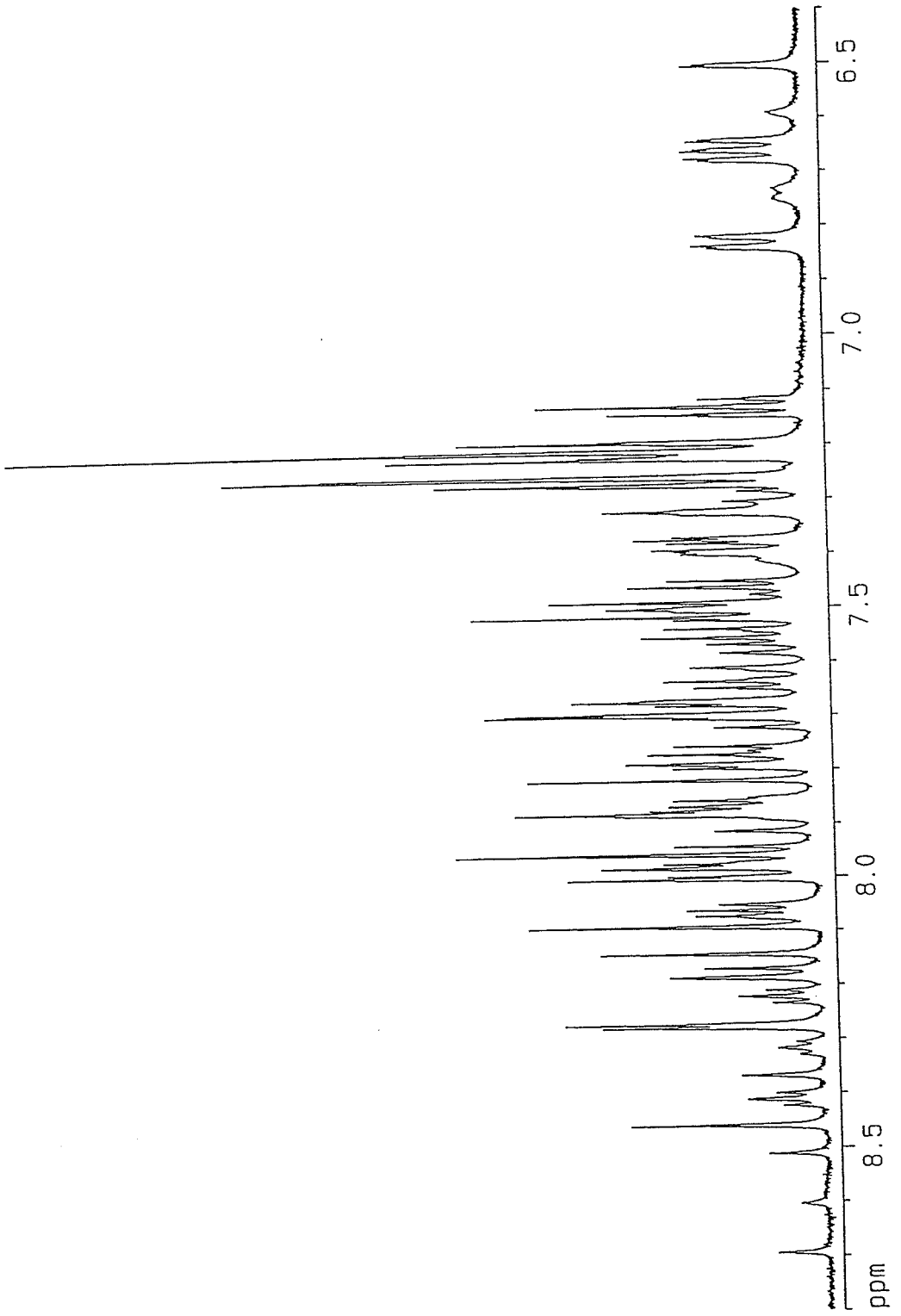

Figure 16: Amide region of the ^{1}H NMR spectrum of uniformly labelled ^{15}N-alamethicin in CD_3OH at 11.75 T with solvent presaturation. The number of scans was 256.

Figure 17 : ^{15}N nmr spectra of uniformly labelled alamethicin in CD_3OH at 11.75 T. (a) without ^{1}H decoupling, (b) ^{1}H decoupled without noe, (c) ^{1}H decoupled with noe. Number of scans was 21,120, acquisition time of 0.8 sec. Protons were decoupled using WALTZ-16. The external reference was 2.9M $^{15}NH_4Cl$ in 1M HCl which resonates at 24.93 ppm relative to $NH_{4(l)}$ [54].

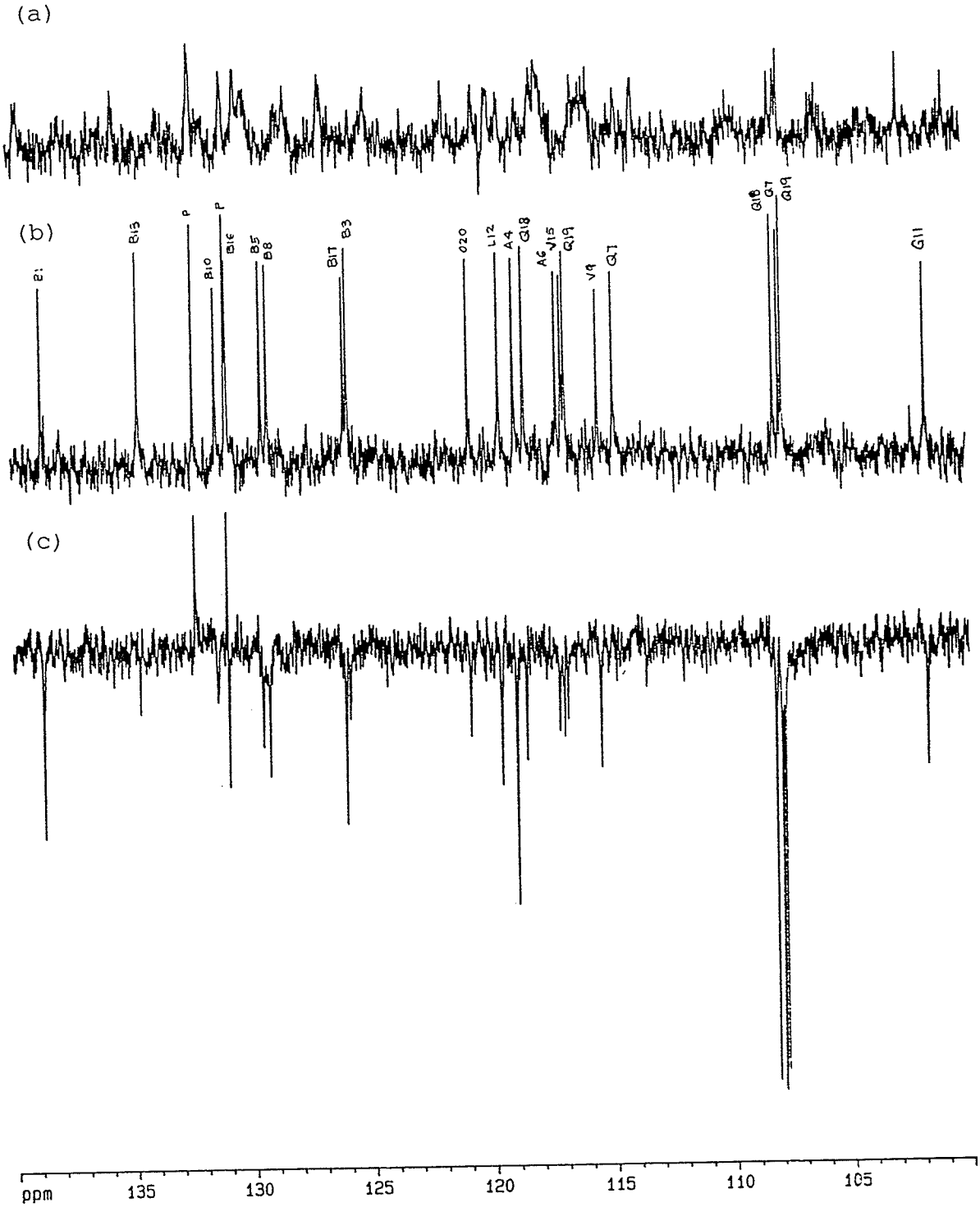
(a)
(b)
(c)
E1
B13
P
P
B10
B16
B5
B8
B17
B3
O20
L12
A4
G18
A6
V15
Q19
V9
Q17
Q16
Q17
Q19
G11
ppm
135
130
125
120
115
110
105

one was nulled and the rest are negative. Since ^{15}N has a negative magnetogyric ratio while proton has positive, all the noe enhancements are negative.

3.6 Summary

The ROESY and TOCSY spectra of alamethicin in methanol with the cross peak assignments are shown in Figures 19 and 20 respectively. Assignments of the ^{1}H and ^{15}N resonances are tabulated in Table 5. Homonuclear and heteronuclear coupling constants are tabulated in Table 6. Homonuclear interresidue noes and heteronuclear (^{15}N-^{1}H) noes are summarized in Figure 21.

3.7 Determination of Percentage Labelling of Alamethicin

The presence of small, broad peaks in the amide region of the one dimensional proton spectrum of the labeled alamethicin (Figure 16) shows that labelling is less than 100%. The most obvious peaks are at 8.61, 8.32, 6.60, and 6.75 ppm which are in between the peaks at 8.70 and 8.51, 8.42 and 8.23, 6.51 and 6.67, 6.66 and 6.84 ppm, respectively. These small broad peaks are the amide protons that are attached to the ^{14}N in unlabeled alamethicin. To determine the percentage of ^{14}N bound, or unlabeled alamethicin, one could integrate all the peaks in Figure 16. The integral of the small broad peaks would give the relative intensity of the ^{14}N bound amide protons and the sum of the integrals of the two peaks beside these small broad peaks

Figure 18 : One dimensional proton resonance spectrum of 2.39 mM alamethicin in CD_3OH at 11.75 T. Internal reference used is DSS. Acquisition time of 2.125 sec with pulse width of 11 μsec and with solvent OH presaturation. The number of scans was 256 and no window function was used. (a) full spectrum (b),(c) & (d) expanded plots with the amino acid residue assignments.

Figure 18 (a)

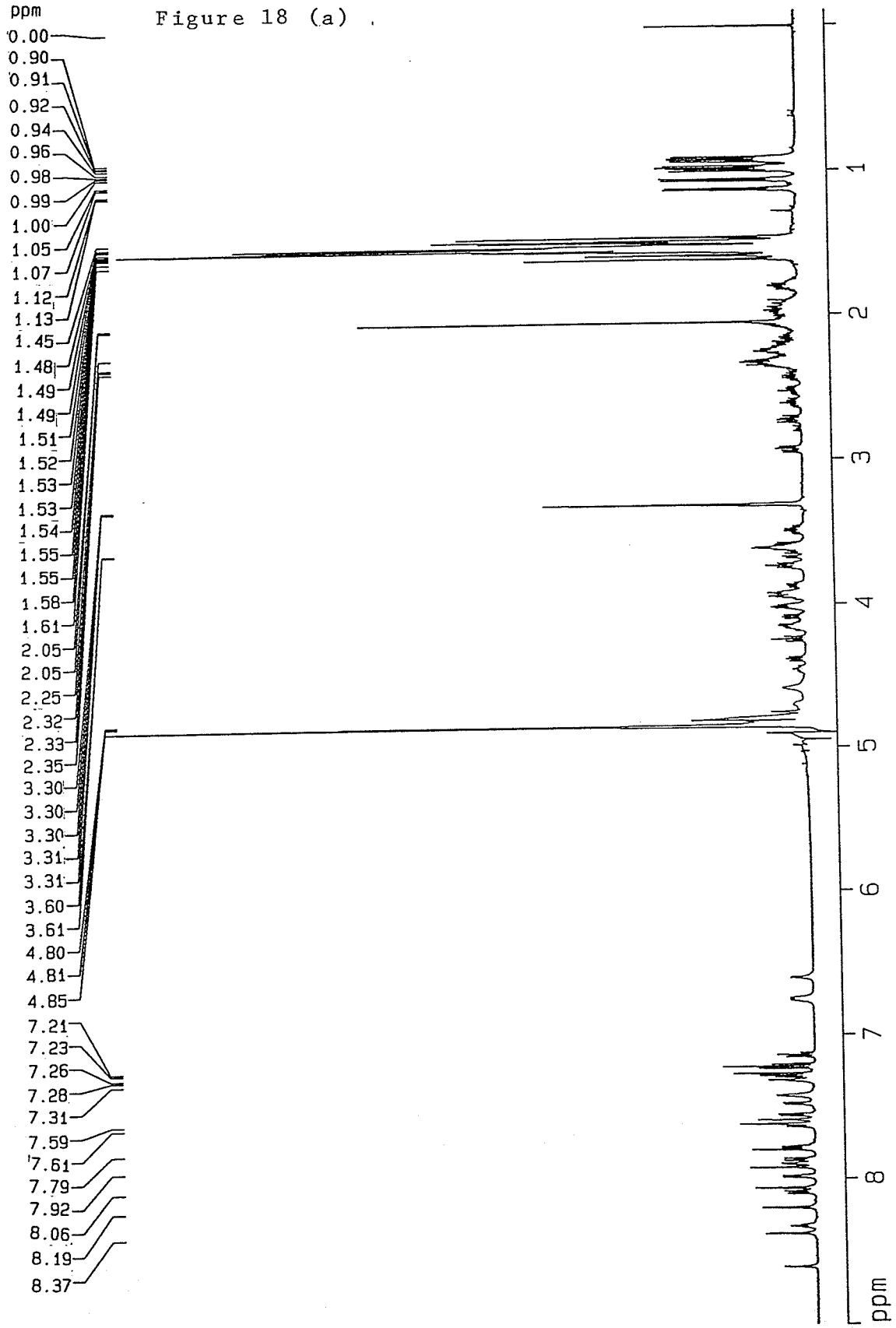
ppm
0.00
0.90
0.91
0.92
0.94
0.96
0.98
0.99
1.00
1.05
1.07
1.12
1.13
1.45
1.48
1.49
1.49
1.51
1.52
1.53
1.53
1.54
1.55
1.55
1.58
1.61
2.05
2.05
2.25
2.32
2.33
2.35
3.30
3.30
3.30
3.31
3.31
3.60
3.61
4.80
4.81
4.85
7.21
7.23
7.26
7.28
7.31
7.59
7.61
7.79
7.92
8.06
8.19
8.37
1
2
3
4
5
6
7
8
ppm

Figure 18 (b)

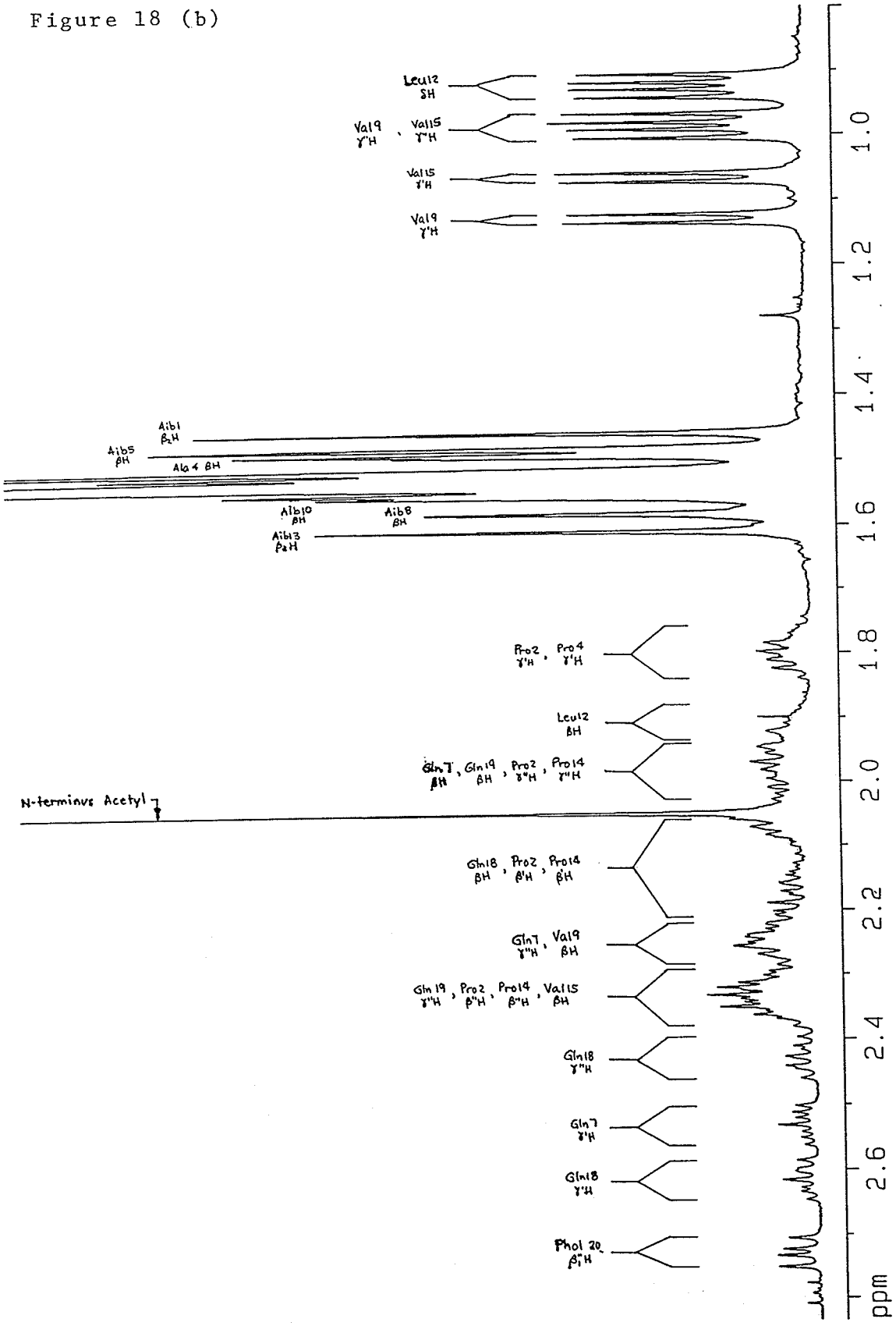
Leu12 δH
Val9 γ'H , Val15 γ''H
Val15 γ'H
Val9 γ'H
Aib1 β₂H
Aib5 βH
Ala 4 βH
Aib10 βH
Aib8 βH
Aib13 β₂H
Pro2 , Pro4 γ'H
Leu12 βH
Gln7 βH , Gln19 βH , Pro2 δ''H , Pro14 γ''H
N-terminus Acetyl
Gln18 βH , Pro2 β'H , Pro14 β'H
Gln7 γ''H , Val9 βH
Gln 19 γ''H , Pro2 β''H , Pro14 β''H , Val15 βH
Gln18 γ''H
Gln7 γ'H
Gln18 γ'H
Phol 20 β'H
1.0
1.2
1.4
1.6
1.8
2.0
2.2
2.4
2.6
ppm

Figure 183(c)

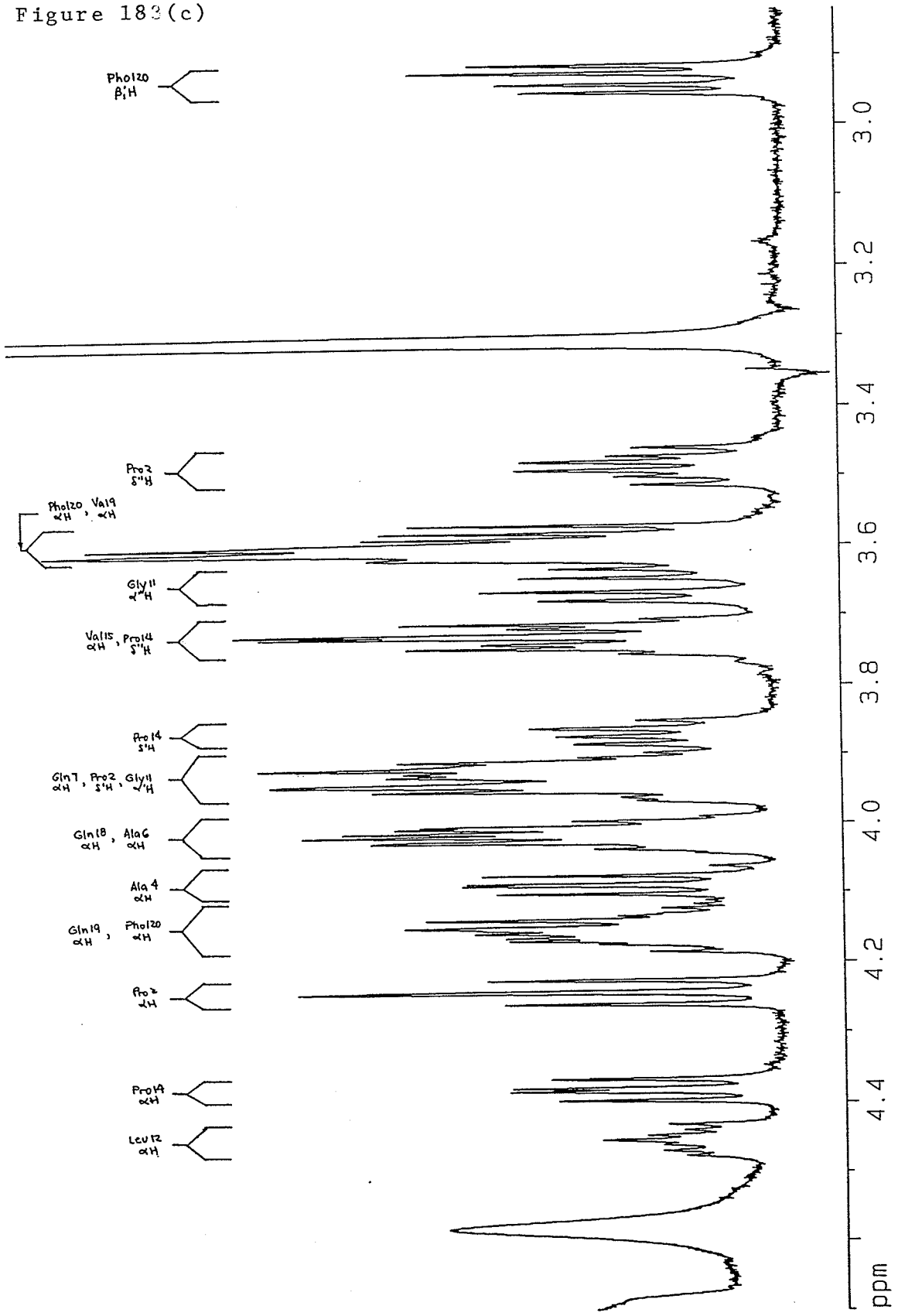
Phol20 βH
Pro2 δ"H
Phol20 αH, Val9 αH
Gly11 α"H
Val15 αH, Pro14 δ"H
Pro14 δ'H
Gln7 αH, Pro2 δ'H, Gly11 α'H
Gln18 αH, Ala6 αH
Ala4 αH
Gln19 αH, Phol20 αH
Pro2 γH
Pro14 αH
Leu12 αH
3.0
3.2
3.4
3.6
3.8
4.0
4.2
4.4
ppm

Figure 18 (d)

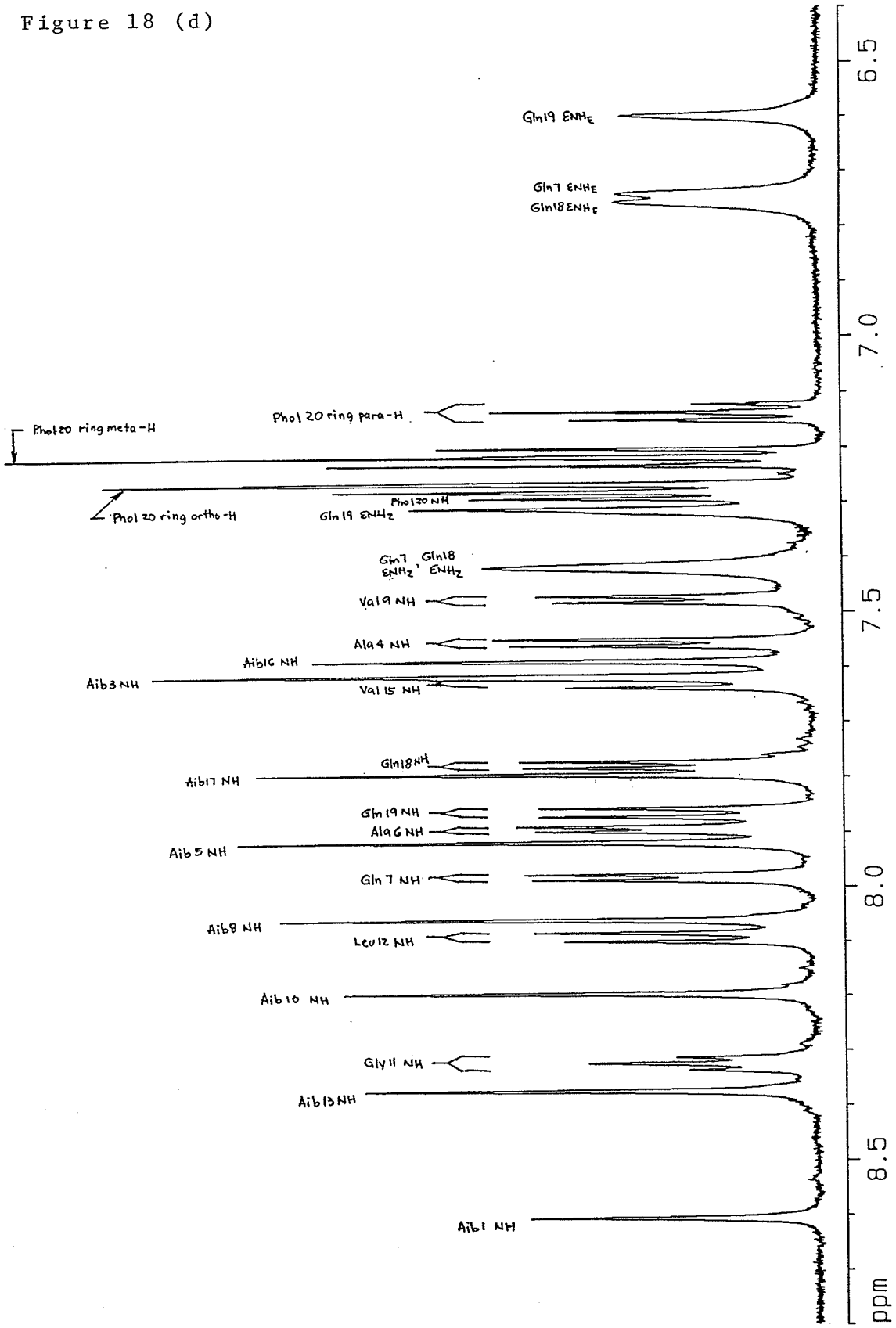
Gln19 ENHε
Gln7 ENHε
Gln18 ENHε
Phol20 ring para-H
Phol20 ring meta-H
Phol20 ring ortho-H
Phol20 NH
Gln19 ENHz
Gln7, Gln18 ENHz, ENHz
Val9 NH
Ala4 NH
Aib16 NH
Aib3 NH
Val15 NH
Gln18 NH
Aib17 NH
Gln19 NH
Ala6 NH
Aib5 NH
Gln7 NH
Aib8 NH
Leu12 NH
Aib10 NH
Gly11 NH
Aib13 NH
Aib1 NH
6.5
7.0
7.5
8.0
8.5
ppm

Figure 19 : TOCSY spectrum of 2.39 mM alamethicin in CD_3OH at 11.75 T with solvent OH presaturation. Internal reference used is DSS. (a),(b), & (c) expanded plots with the amino acid residue assignments of the cross peaks.

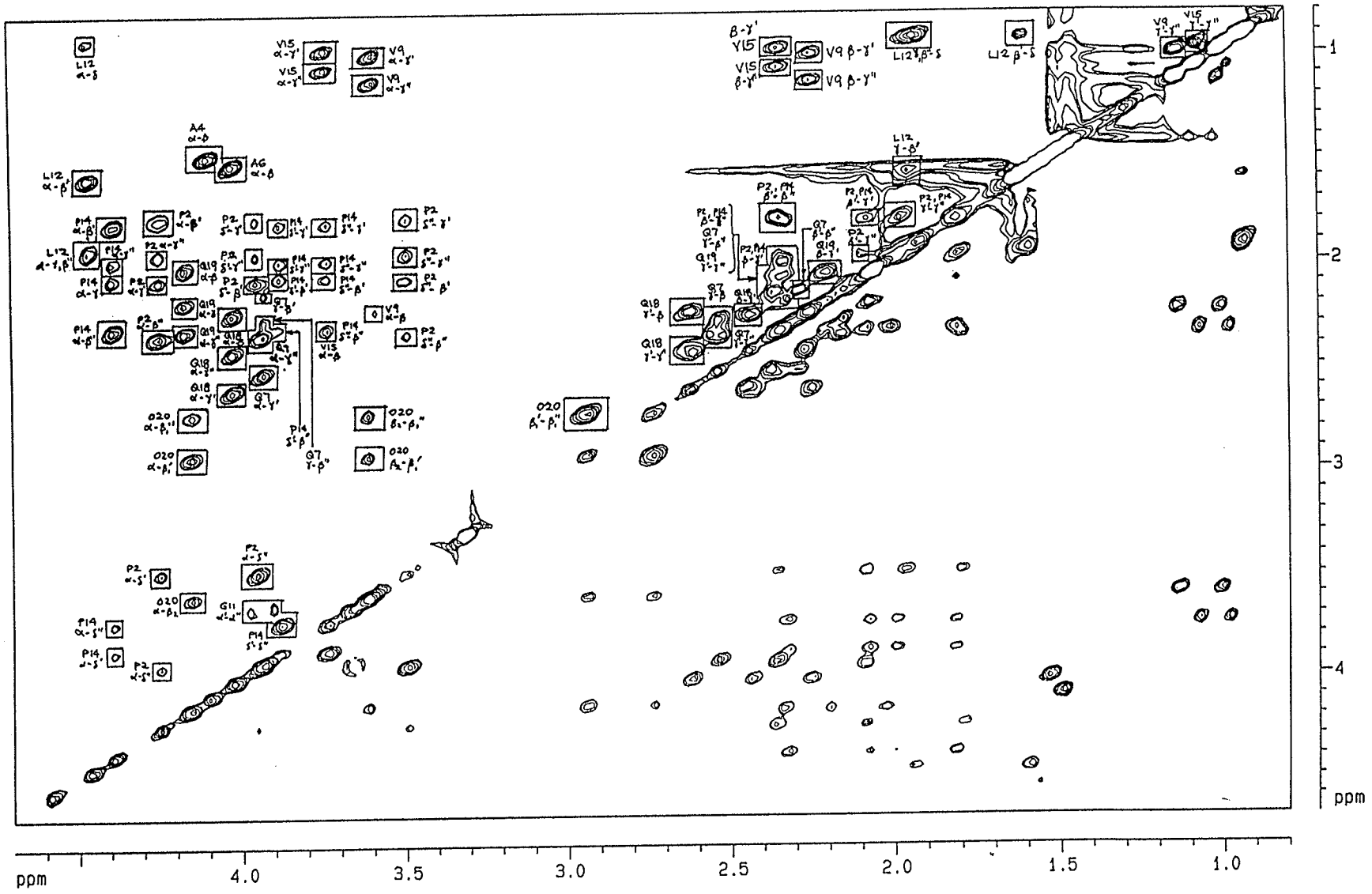
ppm
4.0
3.5
3.0
2.5
2.0
1.5
1.0
ppm
1
2
3
4

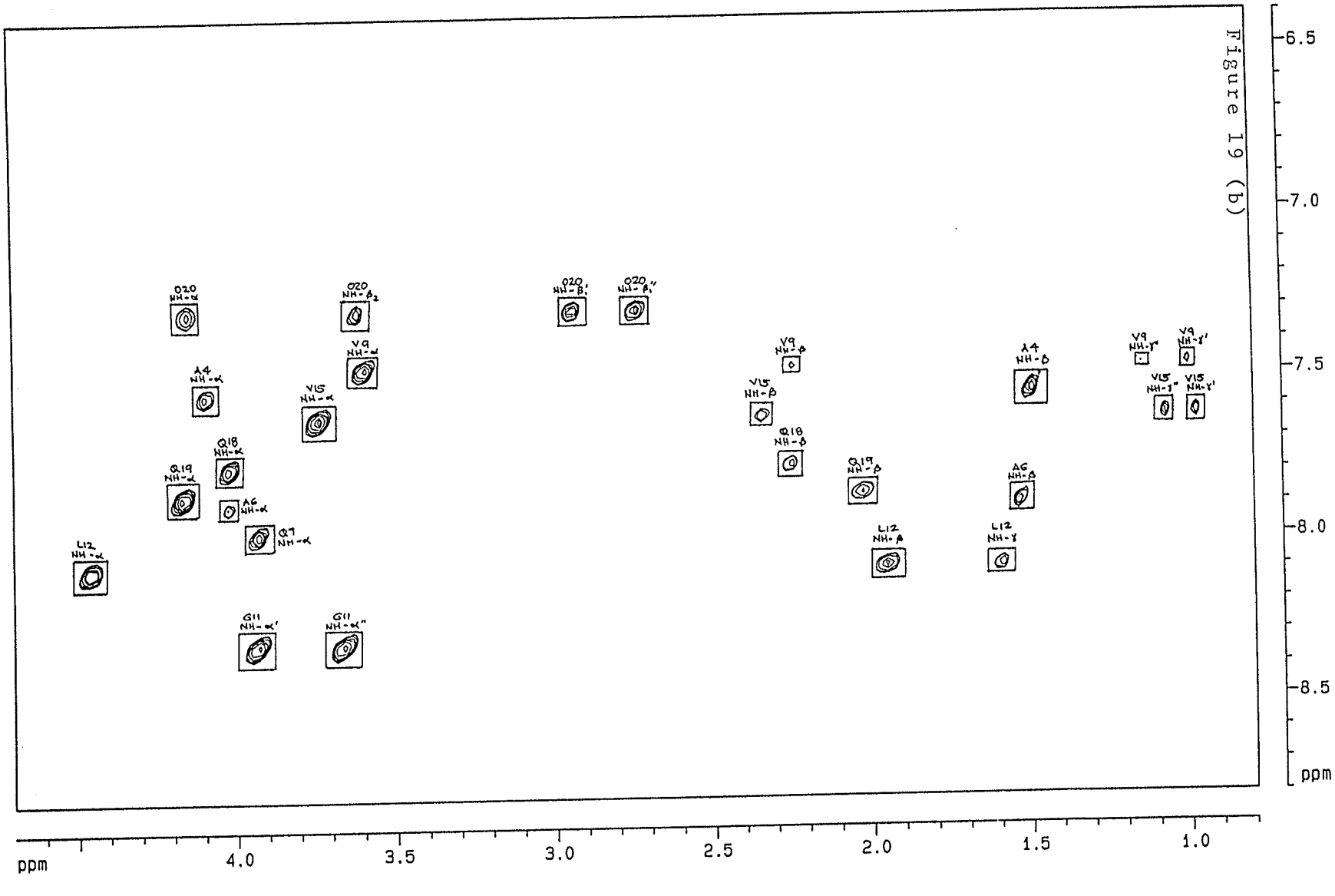
Figure 19 (b)
ppm
4.0
3.5
3.0
2.5
2.0
1.5
1.0
6.5
7.0
7.5
8.0
8.5
ppm

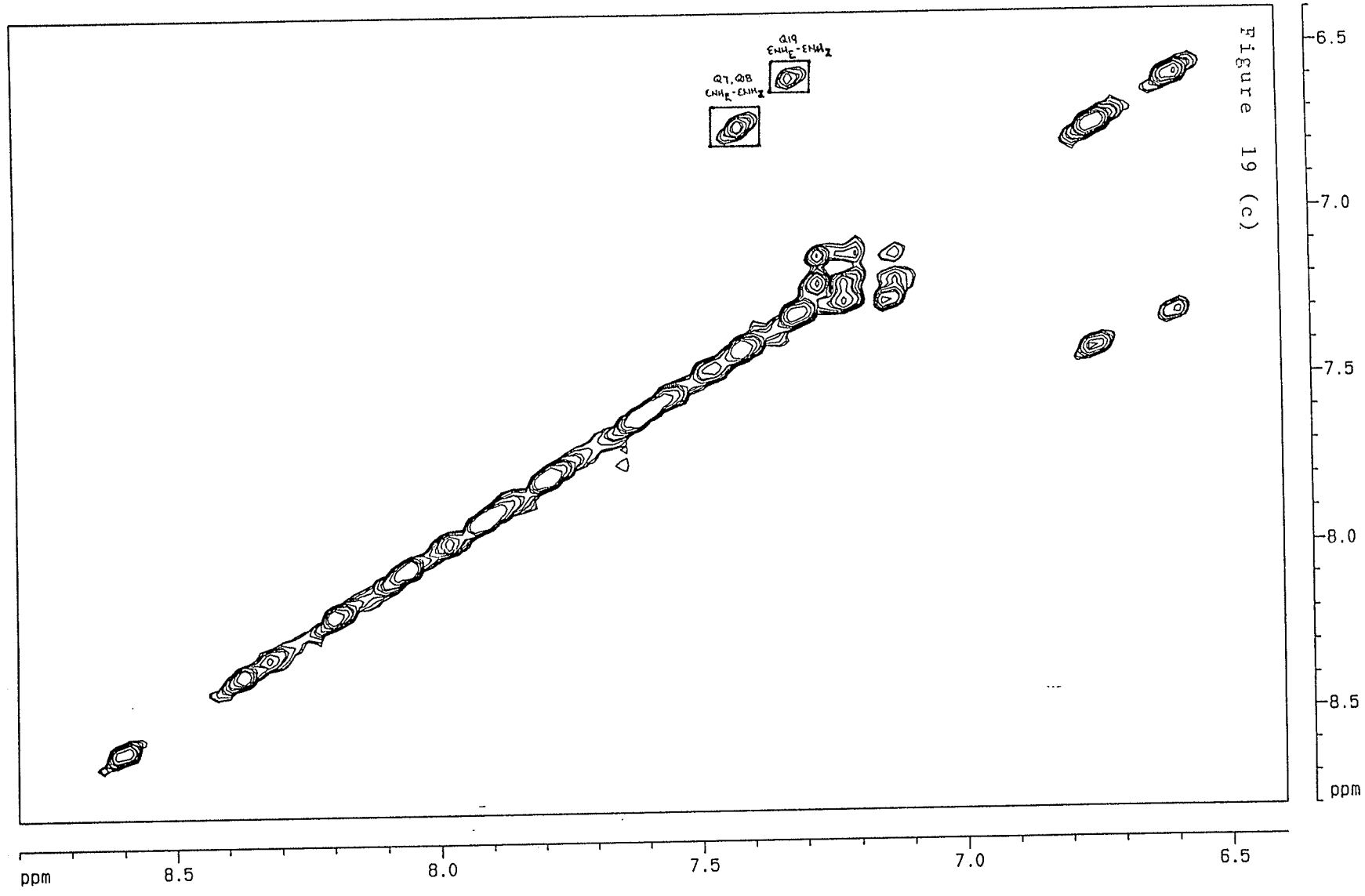

Figure 19 (c)

Figure 20 : ROESY spectrum of 2.39 mM alamethicin in CD_3OH at 11.75 T with solvent OH presaturation. Internal reference used is DSS. Mixing time was 300 msec.(a), (b), (c), and (d) expanded plots with the amino acid residue assignments of the cross peaks.

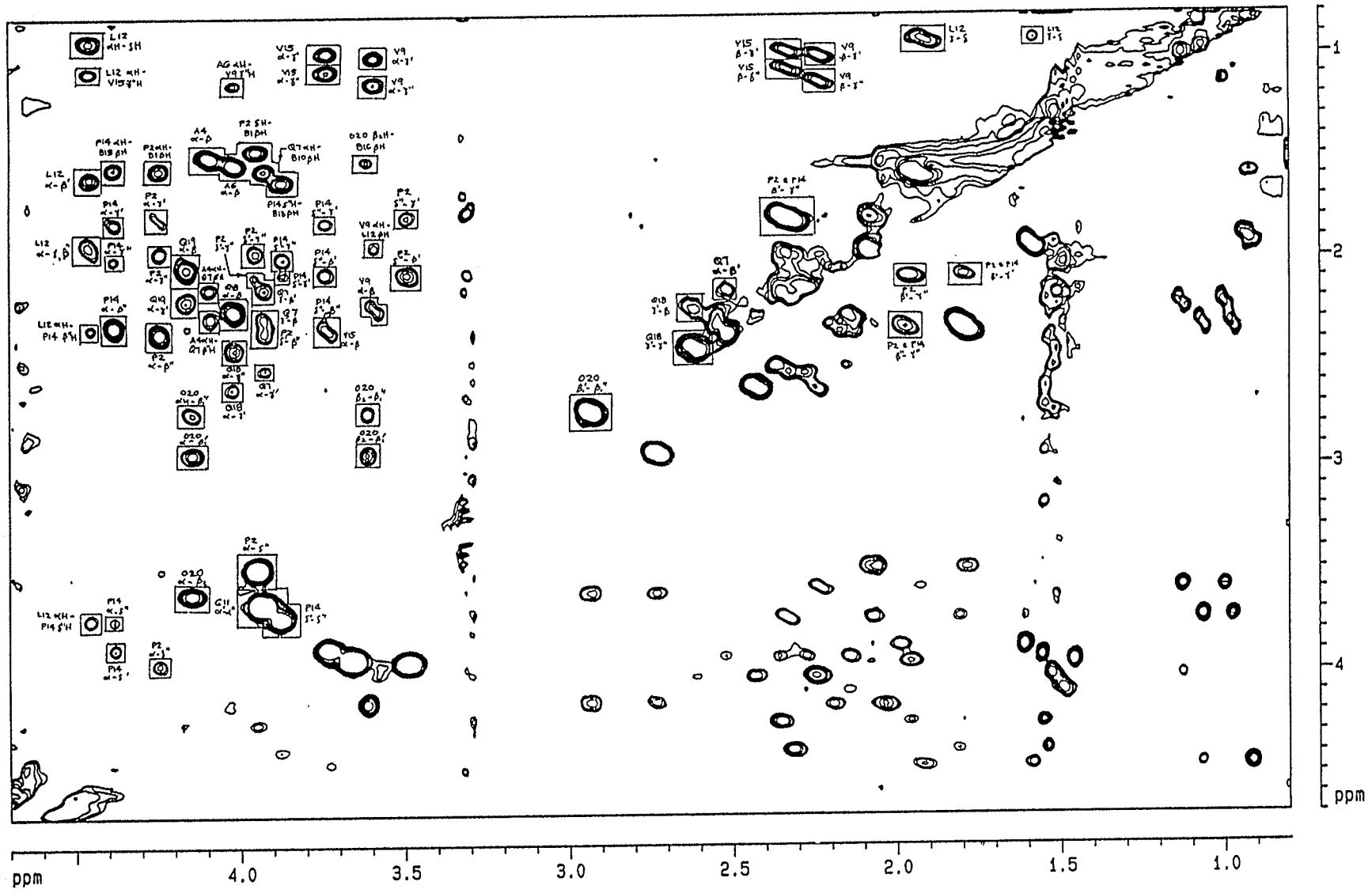
ppm
4.0
3.5
3.0
2.5
2.0
1.5
1.0
ppm
1
2
3
4

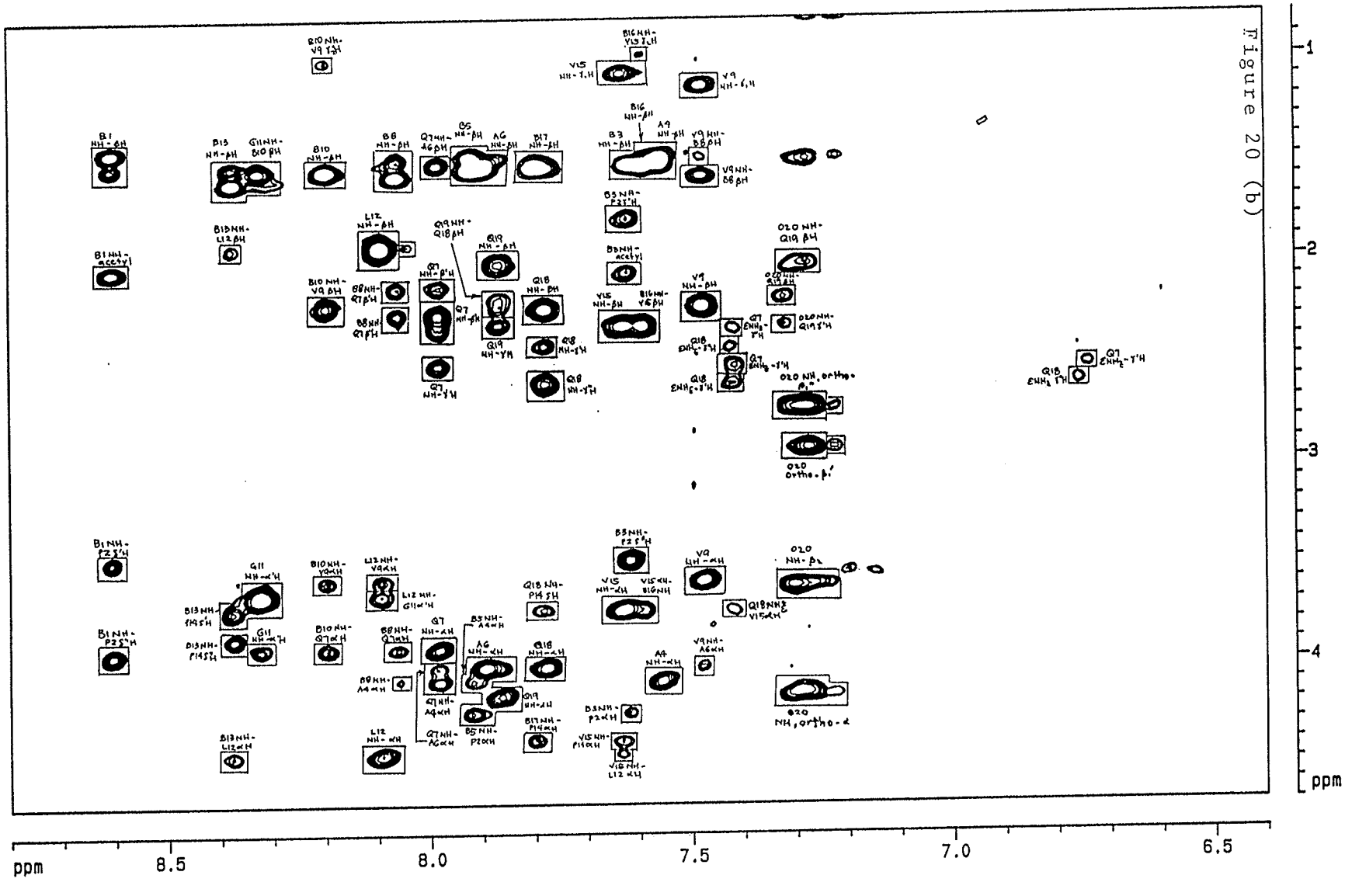

Figure 20 (b)

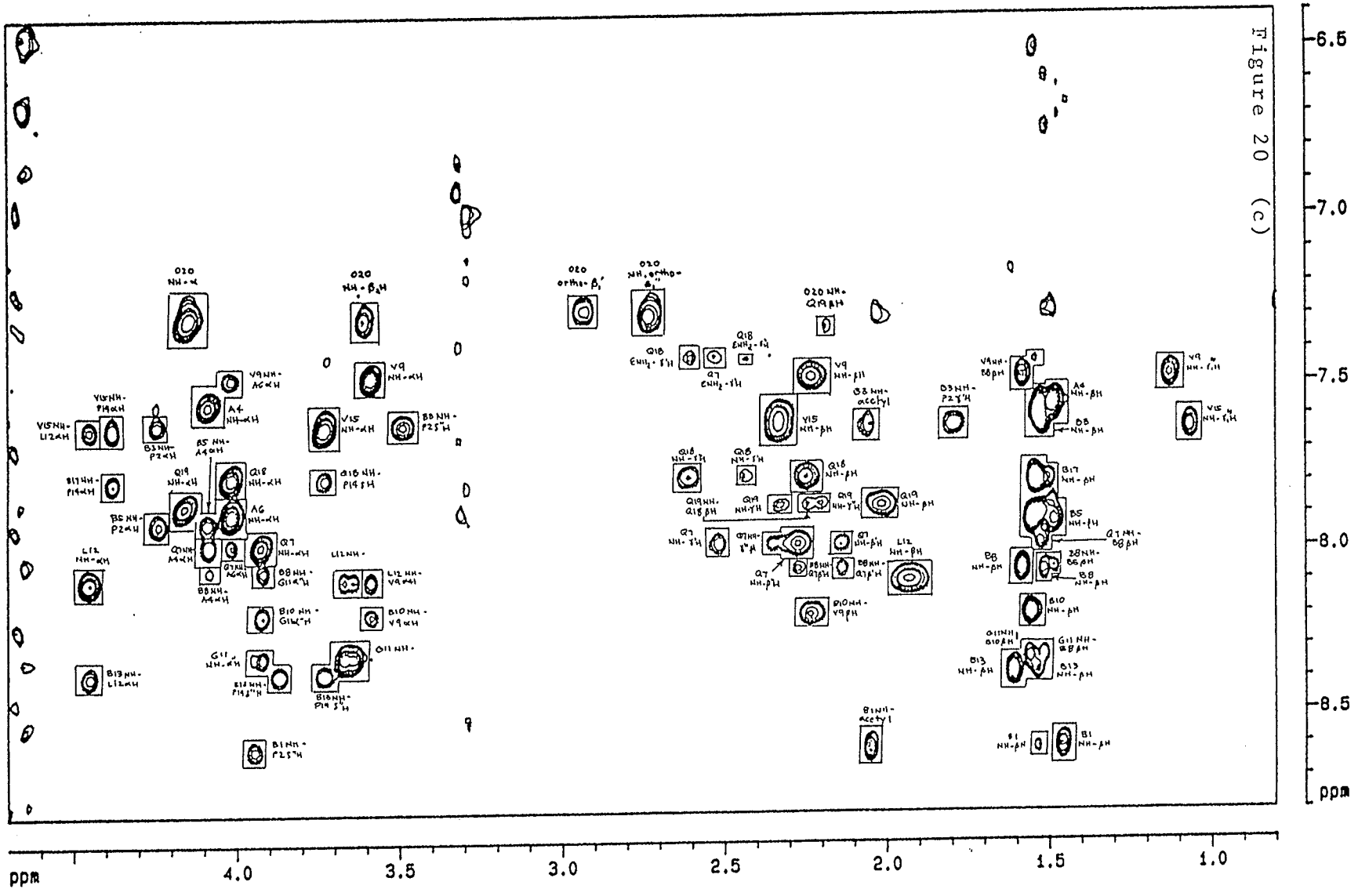

Figure 20 (c)

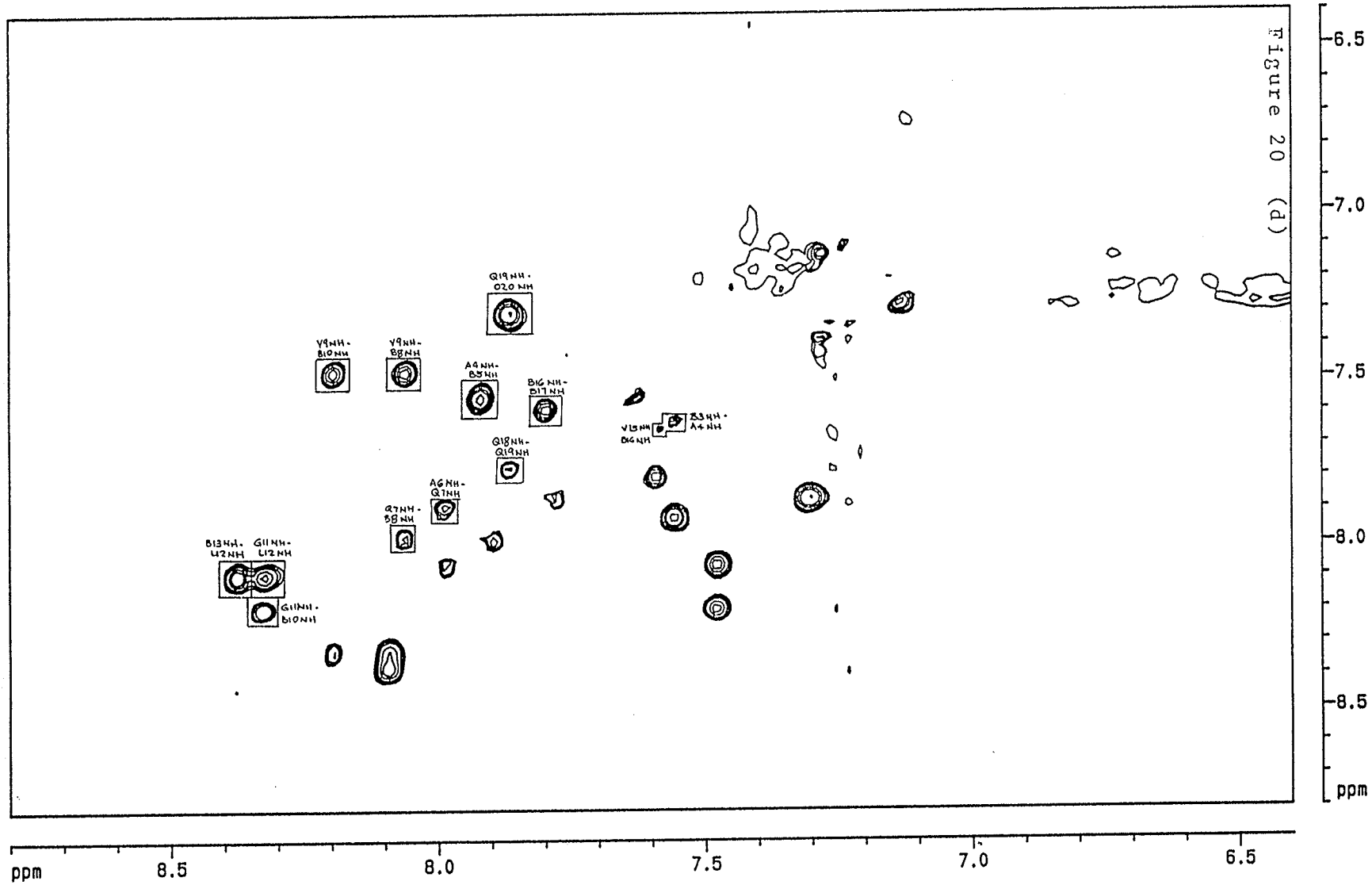
Figure 20 (d)
Q19NH - O20 NH
V9NH - B10NH
V9NH - B8NH
A4NH - B5NH
B16 NH - B17 NH
V15NH - B16NH
B3NH - A4 NH
G18NH - Q19NH
A6NH - Q7NH
Q7NH - B8 NH
B13NH - U2NH
G11NH - U12NH
G11NH - B10NH
6.5
7.0
7.5
8.0
8.5
ppm
ppm
8.5
8.0
7.5
7.0
6.5

Table 5 : ^{15}N and ^{1}H chemical shifts (in ppm) of alamethicin fraction pk21.34 in methanol. Internal ^{1}H resonance is DSS. External ^{15}N reference is 2.9 M $^{15}NH_4Cl$ in 1M HCl which resonates at 24.93 ppm relative to $NH_{3(l)}$.

Residue	^{15}N	NH	$C^{\alpha}H$	$C^{\beta}H$	Others
aib 1	138.7	8.61		1.46, 1.54	N-acetyl CH_3 2.05
pro 2	132.3		4.24	2.34, 1.79	$C^{\gamma'}H$ 2.07; $C^{\gamma''}H$ 1.95
	131.0				$C^{\delta'}H$ 3.49; $C^{\delta''}H$ 3.95
aib 3	126.0	7.62		1.54	
ala 4	118.9	7.56	4.09	1.49	
aib 5	129.5	7.92		1.48, 1.55	
ala 6	117.2	7.90	4.02	1.52	
gln 7	118.6	7.98	3.92	2.28, 2.15	$C^{\gamma'}H$ 2.53; $C^{\gamma''}H$ 2.36;
	N^{ε} 107.9				$N^{\varepsilon}H_E$ 6.74; $N^{\varepsilon}H_Z$ 7.42
aib 8	129.22	8.06		1.59, 1.52	
val 9	115.5	7.48	3.58	2.23	$C^{\gamma'}H$ 1.13; $C^{\gamma''}H$ 0.99
aib 10	131.4	8.20		1.56	
gly 11	101.7	8.33	3.93		
			3.67		
leu 12	119.6	8.09	4.46	1.92, 1.59	$C^{\gamma}H$ 1.92;
					$C^{\delta'}H$ 0.94; $C^{\delta''}H$ 0.91
aib 13	134.7	8.38		1.61, 1.53	
pro 14	132.3		4.38	2.31, 1.80	$C^{\gamma'}H$ 2.07; $C^{\gamma''}H$ 1.98
	131.0				$C^{\delta'}H$ 3.87; $C^{\delta''}H$ 3.73
val 15	117.0	7.63	3.73	2.32	$C^{\gamma'}H$ 1.07; $C^{\gamma''}H$ 0.96
aib 16	131.0	7.59		1.55, 1.50	

aib 17	126.0	7.80		1.53	
gln 18	114.8	7.78	4.02	2.23	$C^{\gamma'}H$ 2.62; $C^{\gamma''}H$ 2.43;
	N^{ε} 108.1				$N^{\varepsilon}H_E$ 6.76; $N^{\varepsilon}H_Z$ 7.42
gln 19	116.9	7.87	4.16	2.02	$C^{\gamma'}H$ 2.33; $C^{\gamma''}H$ 2.19;
	N^{ε} 107.8				$N^{\varepsilon}H_E$ 6.60; $N^{\varepsilon}H_Z$ 7.31
phol 20	120.8	7.29	4.14	2.94, 2.73	$C^{\beta 2}H$ 3.61; $C^{o}H$ 7.28;
					$C^{m}H$ 7.20; $C^{p}H$ 7.14

Table 6 : Summary of the homonuclear and heteronuclear coupling constants found in alamethicin fraction pk21.34 in methanol. [a] Values of the coupling constants (in Hz) were obtained from one dimensional proton spectrum. [b] Values were obtained from DQF-COSY experiment. [c] Values were obtained from 2D $^{1}H-^{15}N$ correlation experiment.

	$^3J_{\alpha-NH}$[a]	$^3J_{\alpha-\beta}$[a]	$^3J_{\beta-\gamma}$[a]	$^3J_{\gamma-\delta}$[a]	$^2J_{\delta-\delta}$[a]	$^1J_{15N-H}$[a]	others[a]
aib 1						91.8	
pro 2		8.5		6.0	10.4		
aib 3						89.6	
ala 4	5.9	7.3				92.8	
aib 5						92.5	
ala 6	4.5	7.9[b]				93.1	
gln 7	5.1					93.7	
aib 8						92.9	
val 9	5.5	10.2[b]	6.5			92.9	
			6.7				
aib 10						92.7	
gly 11	5.8					93.5	$^2J_{\alpha-\alpha}$=16.5
leu 12	7.9	6.1[b]				93.2	
		10.6[b]					
aib 13						92.9	
pro 14		8.8		5.9	11.5		
		6.3					
val 15	8.5	10.0[b]	6.6			91.4	
			6.8				
aib 16						92.0	
aib 17						90.3	
gln 18	5.6	6.3[b]				93.1	
gln 19	7.5	6.9[b]				93.0	
phol 20	9.9	8.8				94.8[c]	$^2J_{\beta-\beta}$=13.7
		5.6					

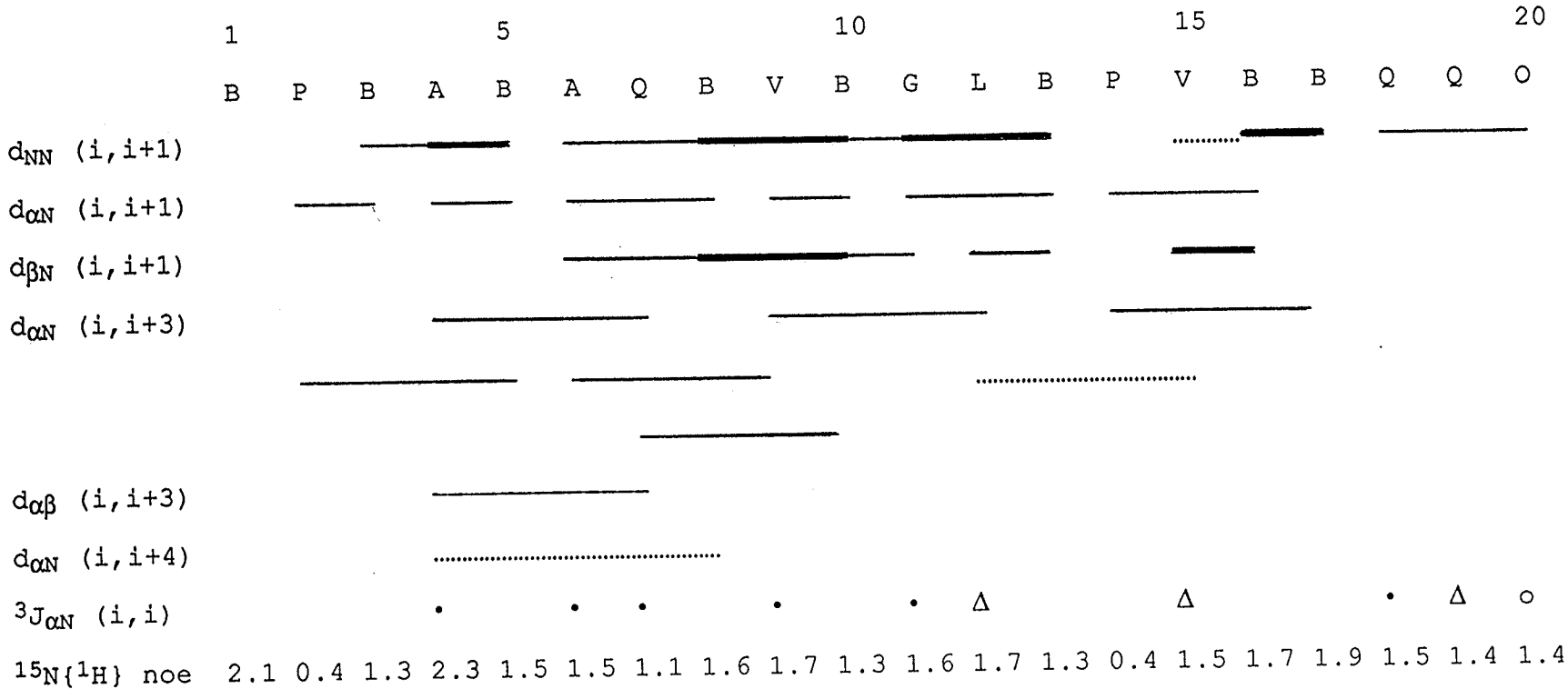

Figure 21 : Summary of the short and medium-range homonuclear transverse noe connectivities, heteronuclear $^{15}N\{^1H\}$ noe and $^3J_{\alpha N}$ coupling constants. The thickness of the lines indicate the intensity of the noe as strong (▬▬), medium (——), or weak (.....). All heteronuclear noes are negative. Coupling constants : < 6 Hz (•); > 9 Hz (o); 6 - 9 Hz (Δ). For exact values of the coupling constants, see Table 6.

would give the relative intensity of the ^{15}N bound amide proton of the same residue. The problem with this method is that many of the peaks overlap so that distinguishing which "sets of three" peaks (i.e. two peaks separated by about 90 Hz and a small broad peak in between) belong to a specific amino acid residue is difficult. And although these peaks can be identified with the aid of the heteronuclear coherence transfer spectrum (Figure 15), integration of each individual peak in the crowded and overlapping amide region would be difficult and the results would be inaccurate.

A better way to determine the percentage labelling would be to use the Spin Echo Difference Spectroscopy (SEDS) experiment as suggested by Griffey *et al.*[33]. The pulse sequence is given in Figure 22. In each SEDS experiment, two spectra are acquired, one in which ^{1}H is pulsed with 90-t-180-t-acq without a 180° pulse on the ^{15}N and the other in which ^{15}N is pulsed with a 180° pulse. In the first spectrum, all the ^{14}N, ^{15}N and carbon bound protons are of the same phase. In the second spectrum, the protons bound to ^{15}N are antiphase to those bound to ^{14}N and carbon because of the 180° flip pulse applied to ^{15}N. The sum of these two spectra gives only ^{14}N and carbon-bound protons while the difference of these spectra gives only those protons bounds to ^{15}N. The ratio of the peak integrals of the sum spectrum to the difference spectrum gives the ratio of the protons bound to ^{14}N to those bound to ^{15}N. See Figure 23.

A summary of the percentage ^{15}N-labelling for all amino acid residues except for the prolines and phol 20, because its NH resonance is buried under the ring proton resonances, is shown in Figure 24.

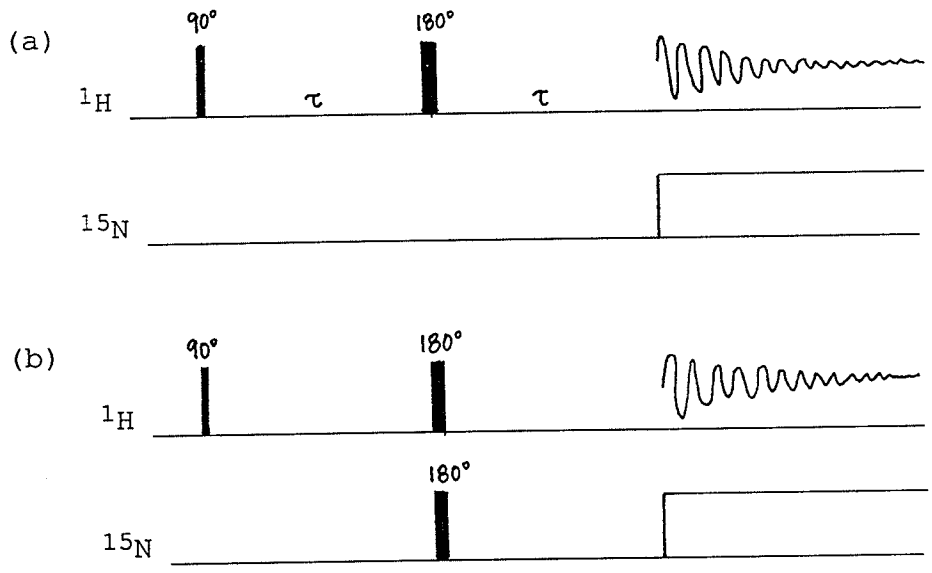

Figure 22: Pulse sequence for Spin Echo Difference Spectroscopy (SEDS) as suggested by Griffey *et al.* [33]. (a) Normal ^{1}H observe sequence with ^{15}N decoupling, (b) SEDS pulse sequence with ^{15}N decoupling.

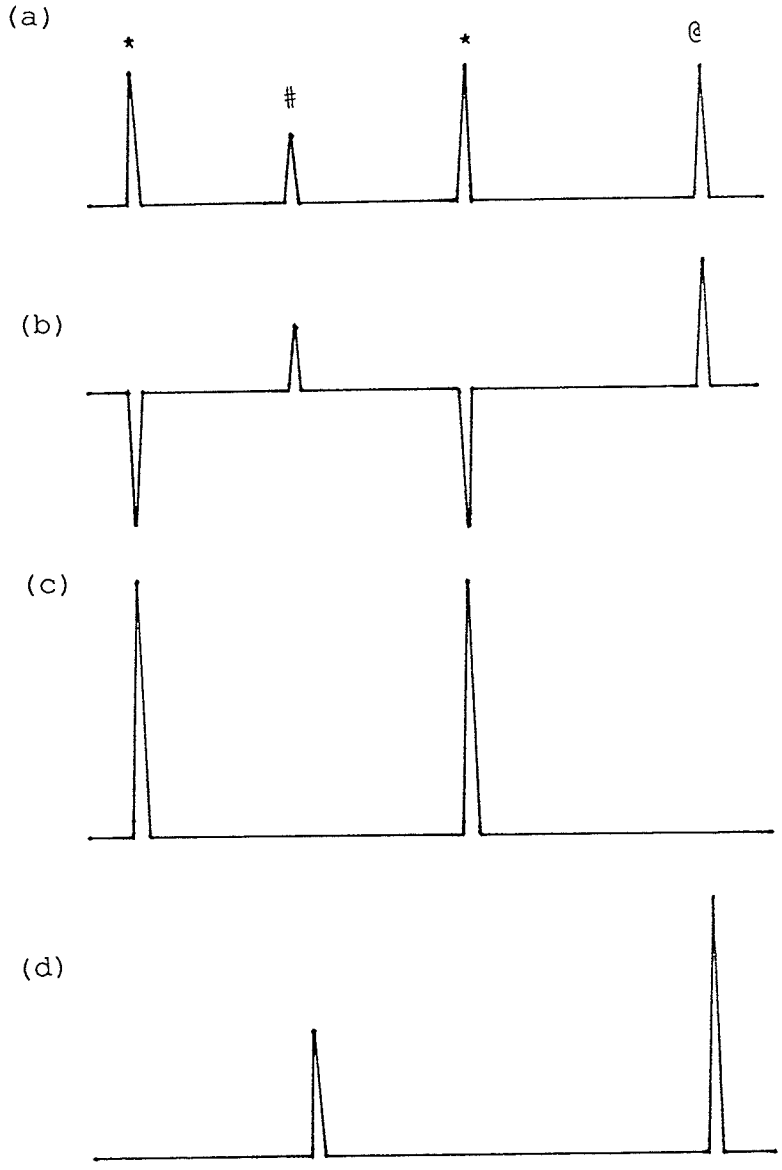

Figure 23: Schematic representation of a ^{1}H spectrum without ^{15}N decoupling. (a) Normal ^{1}H observe spectra, (b) ^{1}H spectrum from SEDS pulse sequence, (c) difference spectrum of (a) and (b), (d) sum spectrum of (a) and (b). * signal from ^{15}N-bound proton, # signal from ^{14}N-bound proton, @ signal from carbon-bound proton.

Figure 24 : Amide region of the SEDS proton spectrum of uniformly labelled alamethicin in CD_3OH with ^{15}N decoupling. (a) Normal observe spectrum with ^{15}N decoupling, (b) SEDS spectrum with application of 180° pulse to the ^{15}N with the peak assignments shown, (c) sum of spectra (a) and (b), (d) difference of spectra (a) and (b) with percentage enrichment for each nitrogen shown.

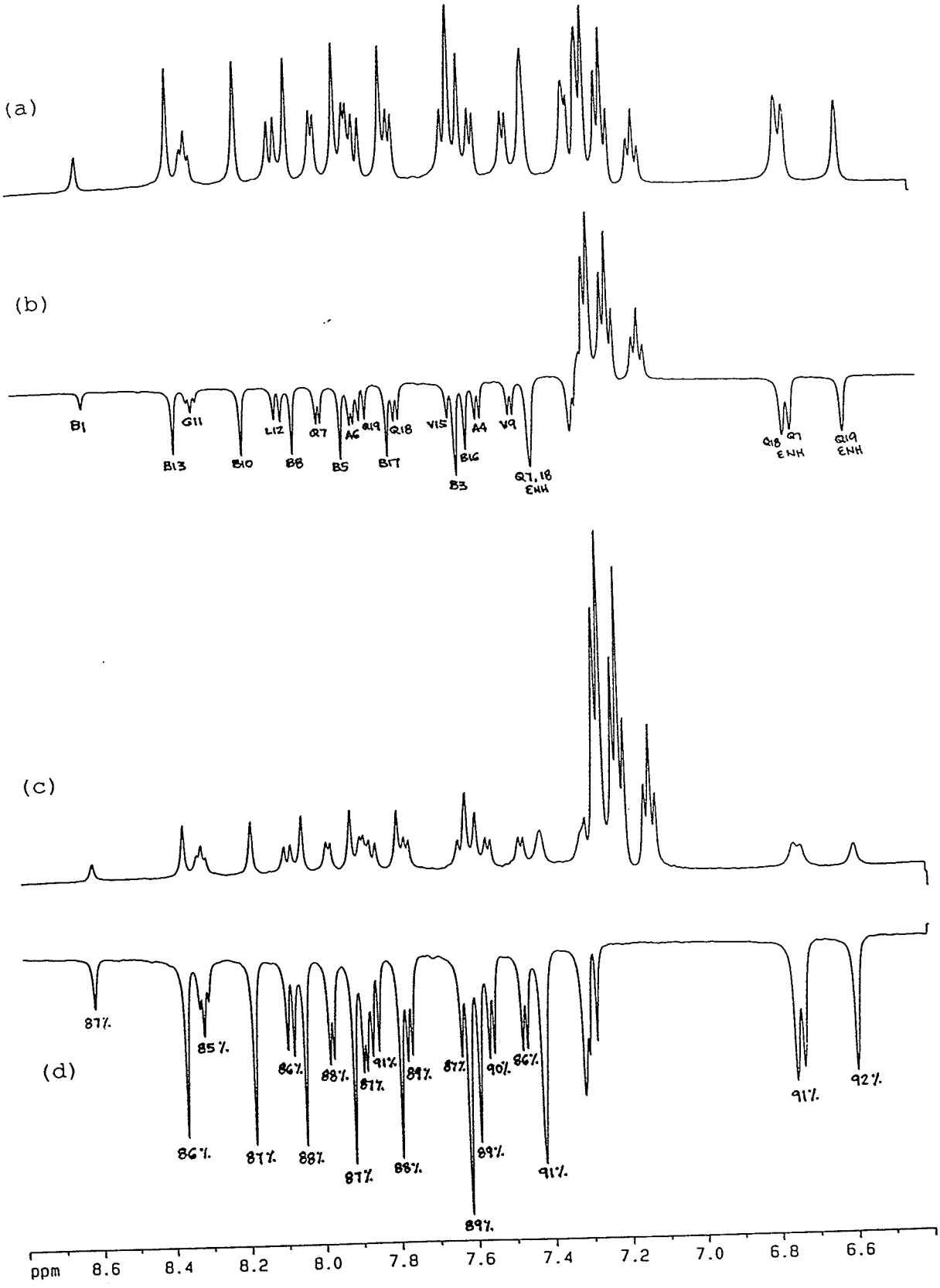
(a)
(b)
B1
G11
B13
B10
L12
B8
Q7
B5
A6
Q19
Q18
B17
V15
B16
B3
A4
V9
Q7,18 ENH
Q18 ENH
Q7
Q19 ENH
(c)
(d)
87%
85%
86%
88%
91%
87%
89%
87%
90%
86%
86%
87%
88%
87%
88%
89%
89%
91%
91%
92%
ppm
8.6
8.4
8.2
8.0
7.8
7.6
7.4
7.2
7.0
6.8
6.6

Chapter 4
Discussion

4.1 Microheterogeneity of Alamethicins

Puromycin is an analog of the 3' end of an aminoacyl tRNA and will bind to the ribosome in place of an incoming aminoacyl tRNA with the result that the growing peptide chain is transferred to the puromycin and protein synthesis is arrested. Rindfleisch and Kleinkauf [78] showed that puromycin failed to influence the synthesis of alamethicin. Reuser [77] also showed that cycloheximide, an antibiotic which inhibits peptidyl transferase, failed to inhibit the formation of alamethicin. These experiments suggest that alamethicin is produced by a non-ribosomal mechanism.

The non-ribosomal system of polypeptide synthesis, also known as the protein thiotemplate mechanism [31], involves multienzyme complexes. The amino acids are first activated through the formation of aminoacyl adenylates and they are bound as thioesters to specific cysteine-thiol groups on the multienzyme complex. The first activated amino acid in the sequence is transferred to the thiol group of an enzyme-bound phosphopantotheine which brings it to the position of the next activated amino acid where peptide bond formation occurs. The dipeptide formed is transferred to the phosphopantetheine which brings it to the third activated amino acid and so on until the peptide is completed. The protein sequence of the amino acid is determined by a protein

template and not by mRNA. In the thiotemplate mechanism, there are differing molecular specificities of insertion of particular amino acid residues in the chain [15].

The alamethicin produced by *T. viride* is microheterogenous, as the HPLC chromatograms (Figure 8) showed at least five different major peaks and several smaller minor peaks. As pointed out by Brewer *et al.*[15], the components of natural alamethicin, and other similar polypeptide metabolites of the fungal species, differ by one or more amino acid residues with some amino acids in certain positions conserved. The proton nmr spectrum of the alamethicin fraction which we have studied showed that this fraction has glutamine in position 18 in place of glutamic acid. The 19 amino acid peptaibols excreted by the fungus *T. harzanium*, trichozianines TA IIIc and TB IIIc, differ only by the substitution of glutamine in place of glutamic acid at the 18th residue [66].

Changes in the medium, from complex to semi-basal, resulted in changes in the relative amounts of each HPLC peak. This result agrees with Brewer's suggestion [15] that, because of the non-specific insertion of some amino acid residues in a thiotemplate mechanism of protein synthesis, alteration of the fermentation medium and growth conditions could result in a change in the number of metabolites and the relative amounts of each fraction. The major peak produced here is not the same as the major peak in the Upjohn alamethicin. This could be due to differing compositions of

the fish meal, pharmamedia and molasses which would vary considerably from batch to batch and from source to source.

4.2 Secondary Structure of Alamethicin Based on ^1H Nmr Data

Studies of a number of protein crystal structures showed that common secondary structures (e.g., α-helix and β-sheet) contain medium and long range ^1H-^1H distances whose noes may be observable. For example, a helix is characterized by intrachain H-bonding between the H atom attached to the electronegative nitrogen of one amino acid and the carbonyl oxygen of the third amino acid beyond it. Thus, the distance between the α-proton of the i^{th} residue and the NH of the $(i+3)^{th}$ residue is close enough for an noe to be observed between them. The distance between the NH of the i^{th} residue to the NH of the $(i+1)^{th}$ residue in an α-helix is shorter than in a β-sheet. From the summary of the interresidue noes of alamethicin (Figure 21), a series of $d_{\alpha N}(i,i+3)$ noes are observed from pro 2 to leu 12 and a very weak noe from leu 12 to val 15 is observed. An noe between pro 14 αH to aib 17 NH is also observed. This would suggest the presence of an α-helix from pro 2 to leu 12 which may even extend to aib 17. The sequential NH(i) to NH(i+1) between val 15 and aib 16 is very weak. The i to i+3 noe connecting val 15 with the rest of the helix is also very weak. These would cast doubt as to whether val 15 is in the helical conformation .

4.2.1 Backbone Conformation of Alamethicin Based on $^3J_{NH\alpha CH}$

In the present study, the amide region of the one dimensional proton spectrum at 11.75 T (see Figure 18d) is well resolved except for val 15 where half of the doublet overlaps with the aib 3 NH, and for phol 20, where half of the NH overlaps with the phol ortho ring protons. The $^3J_{NH\alpha}$ for val 15 was measured from the ^{15}N decoupled proton spectrum of the ^{15}N-labeled alamethicin applying a line broadening of zero. The $^3J_{NH\alpha}$ for phol 20 was measured from Figure 24d. The other half of the doublet of phol 20 NH became visible when the ring protons were subtracted out. All other $^3J_{NH\alpha}$ values were measured from Figure 18d.

All the α-aminoisobutyric acid amides are singlets because of the absence of an α-proton and therefore no $^3J_{NH\alpha}$ can be measured. $^3J_{NH\alpha}$ measured from ala 4 to gly 11 are all less than 6 Hz, indicating the presence of an α-helix in this region. This is in good agreement with the observed noes, $d_{\alpha N}(i,i+3)$ and $d_{NN}(i,i+1)$. The start of the helix cannot be unambigously set since no $^3J_{NH\alpha}$ or $d_{NN}(i,i+1)$ can be measured from aib 1, pro 2, or aib 3. This is because pro 2 does not have an amide proton and the α-aminoisobutyric acids lack αCH's. The $d_{\alpha N}(i,i+3)$ showed an noe from the pro 2 αH to the aib 5 NH but this alone cannot support the presence of a helix at residues 2 and 3.

The $^3J_{NH\alpha}$ of leu 12, val 15 and gln 18 are 7.9 Hz, 8.5 Hz and 7.5 Hz respectively which fall outside the range of coupling constants usually associated with α-helix or β-

sheet. This suggests that the conformation is neither of these or may point to conformational averaging at one or more of these positions. The $^3J_{NH\alpha}$ of glu 18 is 5.6 Hz indicating that the backbone adopts a helical conformation here while the $^3J_{NH\alpha}$ of phol 20 is 9.9 Hz indicating that the backbone adopts an extended conformation.

4.2.2 Sidechain conformations:

In our study, some of the coupling constants for the α-to-β protons were measured from the one dimensional spectrum and others were obtained from the DQF-COSY spectrum. Since the $^3J_{\alpha\beta}$ measured from the DQF-COSY are not as accurate for the reasons mentioned previously, therefore, the numerical value of χ^1 was not calculated but the conformations of the sidechains were classified as to case one, two or three (Figure 5). As shown in Figure 5, coupling constants and noe information are required to classify the sidechain conformation. Caution should be applied in interpreting the intensity of the crosspeaks in a ROESY spectrum as pointed out by Newhaus and Williamson [70] because in a ROESY experiment, it is possible to get HOHAHA transfer, aside from the transverse noe.

Alanine has three magnetically equivalent β-protons. The $^3J_{\alpha\beta}$ of 7.3 Hz and 7.9 Hz for ala 4 and ala 6, respectively, represent the average coupling constant for the three equally populated rotameric conformations. For valine, which has only one βH, Hβ', in Figure 5 is replaced by one of

the γ methyl groups. The $^3J_{\alpha\beta}$" for val 9 and val 15 are 10.2 Hz and 10.0 Hz, respectively. The large value of $^3J_{\alpha\beta}$" suggests conformation 2. The TOCSY spectrum (Figure 19) showed that no interresidue HOHAHA is possible. As for intraresidue transfer, the TOCSY spectrum showed an almost equal HOHAHA intensity of NH to the 2 γCH_3s of both val 9 and 15 but in the ROESY spectrum (Figure 20), only the γCH_3 at 1.07 ppm and 1.13 ppm showed a crosspeak with the NH. This result supports conformation 2 in which the β-proton is *trans* to the α. The α-to-γ methyl noes are both strong and almost of the same intensity which further supports the classification to case 2. For leu 12, $^3J_{\alpha\beta}$ is 6.1 Hz for the β-proton at 1.59 ppm and 10.6 Hz for the one at 1.92 ppm. The large coupling constant suggests that the 1.92 ppm β-proton is *trans* to the α-proton. The other β-proton could be either 60° (case 2) or -60° (case 3) relative to the α-proton. The α-to-β noe cross peaks cannot be used to confirm this since one of the β-protons at 1.92 ppm overlaps with the γ-proton. The noe is likely to be between α and γ because in both cases 2 and 3, the γ is *gauche* to the α. The NH showed a very strong noe to the 1.92 ppm proton and no noe to the proton at 1.59 ppm which suggests that the β at 1.59 ppm is *trans* to the NH. This would classify the conformation to case 3. The strong NH noe at 1.92 ppm could be a combined noe to both the β and γ protons since both would be *gauche* to the NH in a case 3 conformation.

For phol 20, the $^3J_{\alpha\beta}$ measured were 5.6 Hz and 8.8 Hz for the two β-methylene protons. This suggests either case 2 or 3. The β-proton with the larger $^3J_{\alpha\beta}$ of 8.8 Hz (δ=2.73 ppm) was assigned as *trans* to the α. Inspection of Figure 20a showed that the α gave a stronger noe cross peak to the β at 2.94 ppm than to the 2.73 ppm β-proton which confirms that the latter is the β further away from the α-proton. The NH-to-β noe should distinguish between cases 2 and 3 but unfortunately, for phol 20 the NH resonance overlaps with the ortho of the phenyl ring. The two $^3J_{\alpha\beta}$ were measured from the one dimensional spectrum, hence, the reliability is better than those obtained from the DQF-COSY. The three rotameric populations corresponding to the conformations in the three cases were calculated using ^3J_g and ^3J_t derived from the Karplus relationship described in the Introduction (page 18). The calculation is shown in the appendix. The result shows that case 3 (57%) is more populated than 2 (23%).

The sidechain conformation of the other residues was not assigned because the $^3J_{\alpha\beta}$ cannot be accurately measured from the present experiments. The assignment of the sidechain conformations to a particular case does not mean that the conformation is fixed, but rather that it stays more often in the assigned conformation than in the other two.

The absence of some cross peaks from the ROESY spectrum which are present in the TOCSY suggests that the intraresidue HOHAHA transfer is negligible compared with the noe in this particular experiment and hence, that the ROESY

(a) valine 9

Case 2

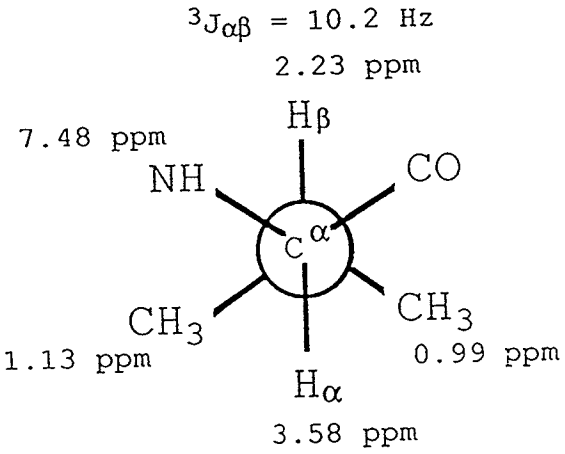

(b) valine 15

Case 2

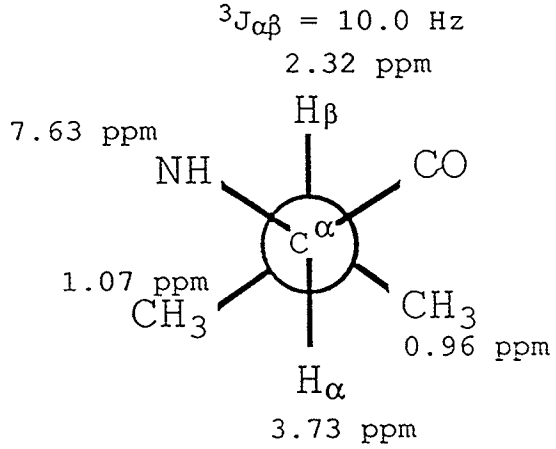

(c) leucine 12

Case 3

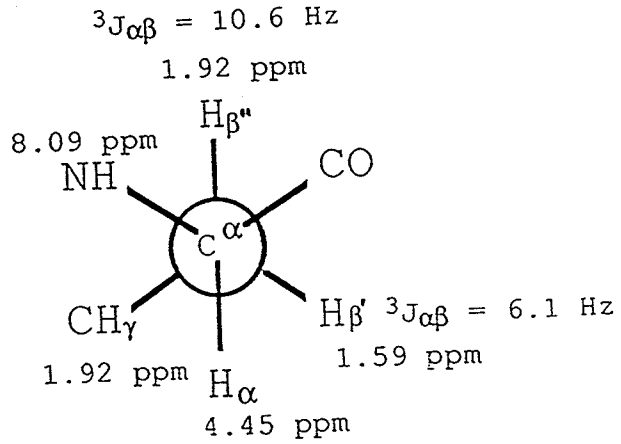

Figure 25 : Preferred sidechain conformations of valine 9, 15 and leucine 12.

crosspeaks in this experiment may be evaluated or translated into distances just like a NOESY crosspeak.

4.3 ^{15}N Chemical Shifts

The ^{15}N chemical shift, like ^{13}C, is affected by structural and electronic influences, but the ^{15}N shifts are more sensitive to environmental changes than ^{13}C because of the unshared pair of electrons. In an amide bond, the nitrogen lone-pair can delocalize to the π system of the adjacent carbonyl group and this deshields the nitrogen. The chemical shifts of amide nitrogens are more downfield than amine nitrogens [54]. In alamethicin, all the nitrogens present are in the amide form, including the side chains, except for the prolines which are imides. The nitrogens resonate between 102 ppm and 139 ppm relative to $NH_{3(l)}$. All the α-aminoisobutyric acid and proline nitrogens resonate downfield of the others (126 to 139 ppm) and glycine is upfield at 101.73 ppm. This grouping of chemical shifts may be explained by substituent effects on the nitrogens. The amide nitrogens in alamethicin can be classified into: primary (1°), the glutamine sidechains where two protons are attached to the nitrogen; secondary (2°), the residues where only one proton is attached to the nitrogen; tertiary (3°), the proline residues where no proton is attached to the nitrogen (see Figure 11e for structures). The effect of the substituent directly attached to the nitrogen on its chemical shift is known as the α effect. The chemical shifts of the

glutamine sidechains are upfield of all the secondary amides except glycine. The prolines resonate downfield of the secondary amides except for some α-aminoisobutyric acids, so the trend in chemical shift is 3°>2°>1°. The chemical shift of neat primary, secondary and tertiary formamide showed the trend 1°>2°>3° [54] which is the reverse of the trend observed in alamethicin but ^{15}N shifts, unlike ^{13}C, do not show a consistent deshielding α effect [54]. For example, the chemical shift of N-methyl acetamide is downfield from that of acetamide (2°>1°) [92] which is the reverse of the trend found in formamide.

Among the secondary amides of alamethicin, there is a certain trend observed, that is, glycine, having two protons attached to the α carbon is the most upfield followed by residues with only one proton attached to the α carbon then followed by the α-aminoisobutyric acids with no proton attached to the α carbon. The effect of the substituent attached to the α carbon on the amide ^{15}N chemical shift is known as the β effect. The β effect has been studied on acetamide [92] and the trend observed is that the more alkyl substituted the α carbon, the more downfield the ^{15}N resonance. This is the same trend observed in the ^{15}N spectrum of alamethicin. The β deshielding effect in ^{13}C was attributed to the small steric crowding by the β carbons which causes a small contraction of electron orbitals in the α carbon [87] and the same analogy may be extended to nitrogen. The differences in the chemical shifts among the α-

aminoisobutyric acids could be due to the differing adjacent amino acids [92] or local environment.

4.4 ^{15}N Noe

As mentioned in the previous section, assignment of a particular conformation to alamethicin does not mean that the molecule is fixed in that conformation but rather, as shown by the rotameric population calculations for the phenylalaninol sidechain, the molecule populates one conformation more than others. Because the molecule is mobile, different parts of the molecule can experience a different rotational correlation time. This is referred to in Noggle and Schirmer [71] as the effective rotational correlation time. The steady-state enhancement equations clearly show that for a mobile molecule like alamethicin, the noe depends on the effective correlation time. The steady state noe is not a function of the internuclear distance so that even the ^{15}N without any protons attached (e.g., proline) may have noe. For $^{15}N\{^{1}H\}$, like in $^{13}C\{^{1}H\}$, dipole-dipole relaxation is assumed to predominate [11,85]. The noe for ^{13}C with directly bonded hydrogens is the same regardless of the number of hydrogens attached to the carbon whenever dipole-dipole relaxation predominates [51], and this may be extended to $^{15}N\{^{1}H\}$. Therefore, the large difference in noe observed between the glutamine sidechain NH_2 and the backbone amide NH is likely to be due to differences in relative motion or the effective rotational correlation time. The glutamine

sidechain nitrogens have a much larger noe (-2.63 to -2.96) compared with the backbone amide nitrogens in the same residue (-1.10 to -1.54). This suggests that the sidechain nitrogens have lower effective correlation times (i.e., more conformational freedom) than the backbone nitrogens. The noes of the two prolines are quite small (-0.45) compared with the rest of the backbone. These difference could suggest a very large difference in effective correlation times or the possibility that other relaxation pathways may be significant. Although the steady state noe equation is not a function of the internuclear distance, the spin-lattice relaxation rate ($1/T_1^{dd}$) is strongly dependent on the internuclear distance [22]. The dipole-dipole relaxation rate decreases with increasing internuclear distance. Proline does not have a directly bonded proton to its nitrogen so the dipole-dipole relaxation will be with the neighboring protons. Therefore, other relaxation mechanisms *via* different paths may not be negligible compared to dipole-dipole relaxation. This may reduce the noe of the proline ^{15}N because R_I will have to include ρ_I^*.

Based on the noes of aib 1 and ala 4, it appears that they have a higher effective correlation time than the rest of the backbones. However this does not correspond to the ^1H exchange rate pattern reported by Davis and Gisin [20].

4.5 ^{15}N-^{1}H One-bond Coupling Constant

$^{1}J_{NH}$ for trigonal bonded nitrogens (amides) fall within the region ~90 Hz. The more linear the bond to nitrogen is, the larger is the $^{1}J_{NH}$, e.g. linear bonding to nitrogen gives a $^{1}J_{NH}$ of ~135 Hz while pyramidal bonding gives only ~75 Hz [54]. This value is based on the percentage of s character of the nitrogen in a trigonal bond. All the $^{1}J_{NH}$ in alamethicin fall within 90 ± 5 Hz.

4.6 Summary

The alamethicin studied here has a glutamine in position 18 rather than a glutamic acid. This alamethicin can be a good model to check the role of the negatively charged sidechain of glutamic acid, if it plays a role at all, in the voltage-gated channel. Hall *et al.*[35] reported that blocking the negative charge of glu 18 by esterification with a methyl or phenyl group alters the current-voltage curve (see Introduction, page 8). The methyl or phenyl is a bulky substituent and its presence could alter the conformation of the entire monomer. Menstrina *et al.*[62] and Molle *et al.*[67] synthesized an alamethicin analogue without the glutamic acid to study its role in the channel. Removing glu 18 altogether may also alter the conformation of the monomer (i.e., the glu 18 backbone NH or C=O might be hydrogen bonded to another residue's backbone). The NH_2 of the glutamine is not as bulky as a methyl or a phenyl group and is therefore a better model

to study the role of a formal negative charge on a monomer in the voltage-gated channel.

From the ^1H homonuclear noe data and coupling constants, ala 4 to gly 11 adopts a helical conformation. This agrees with the structure proposed by Fraternali [30] based on molecular dynamics simulations. The conformation of the other residues can not be assigned with certainty at this point because of the lack of $^3J_{backbone}$ information from the α-aminoisobutyric acids and prolines. The $^3J_{NH\alpha}$ of leu 12, val 15, and gln 18 suggest that these backbones adopt a conformation that is not distinctly helical nor extended. A better picture of alamethicin might be obtained from distance geometry calculation since the ^1H noes are translated into distances and the energy of the conformation is taken into account. Unfortunately, no such software is available in the department at present. Therefore, the interpretation of the ^1H noes were limited to a qualitative interpretation.

No evidence (intermolecular noe) of dimers was observed from this experiment. The non-exponential decay of magnetization of the N-terminal methyl group observed by Banerjee *et al.* [3,4] may be due to hindered rotations of the 3 protons in the methyl group. Calculations [41,91] have been done on methyl groups in small and large molecules and the results indicate that for a methyl group undergoing hindered rotations about a fixed axis with respect to a molecule undergoing Brownian rotational motion, the relaxation decay is the sum of three decaying exponentials and reduces to the

sum of two decaying exponentials if the rotational diffusion of the molecule is rapid compared to the Larmor frequency. Hence, the non-exponential decay of CH_3 magnetization can not be used as an evidence for dimerization.

We have shown that alamethicin was uniformly labeled with ^{15}N using the method described in Chapter 2. The $^{15}N\{^1H\}$ noe provided independent information on the dynamics of alamethicin. The ^{15}N-labeled alamethicin could also provide additional information on the backbone conformation (ψ torsion angle) through measurements of $^3J_{\alpha i-N(i+1)}$. The torsion angle ψ cannot be determined using ^{13}C or ^1H coupling constants. Likewise, it could provide information on the χ_1 torsion angle through measurements of $^3J_{\alpha i-Ni}$. Another advantage of using ^{15}N-labeled alamethicin is the increased resolution of ^1H resonances which can be obtained by utilizing the ^{15}N chemical shift in a three-dimensional experiment [23,42]. This will be particularly helpful since further studies will be carried out on alamethicin in an aqueous, detergent, or other environment that would broaden the ^1H nmr signals.

4.7 Suggested Experiments for Further Research

Heteronuclear vicinal coupling constants (e.g., ^{15}N with ^1H, ^{15}N with ^{13}C, or ^{13}C with ^1H) can provide independent information about conformations. Likewise, the T_1's of ^{13}C can provide information on the dynamics at different parts of the molecule. ^{13}C has a higher natural abundance (1.11%) and

sensitivity (γ=6.73x10^7 $s^{-1}T^{-1}$) than ^{15}N. Natural abundance ^{13}C nmr of alamethicin is possible [46]. A ^{13}C-^{1}H correlation experiment for alamethicin has recently been carried out but the data are not included in this thesis. Natural abundance ^{13}C nmr at the present concentration being studied could be very time consuming and increasing the protein concentration could result in aggregation or micellization since alamethicin is amphipathic. Besides, if vicinal coupling constants are to be determined, one needs to have as much sensitivity (and subsequently, resolution) as possible.

T. viride uses insoluble starch (dextrin) and sucrose as sources of carbon. One possible way of introducing ^{13}C to alamethicin is through labeled sucrose but a study by Brewer *et al.* [15] showed that a soluble carbon source supported the growth of *T. viride* but not the production of alamethicin. Another way would be to substitute labeled carbohydrates in place of dextrin. Synthetic ^{13}C-labeled carbohydrates would be very expensive to synthesize chemically but there are some microorganisms that can produce complex carbohydrates from a simpler carbon source. Some species of the algae *Chlamydomonas* can produce starch from simpler carbon sources. Example, *C. pseudococcum* can use glucose as the sole carbon source and *C. reinhardtii* can use acetate as carbon source [36]. Both the acetate and glucose are commercially available in ^{13}C-labelled form. However, starch granules that are produced by the *Chlamydomonas* during the dark cycle are not excreted but stored in the chloroplast and these are degraded

during the light cycle. This may pose some difficulties in harvesting the starch for fungus utilization. Another insoluble carbon source that could be tried is the polysaccharide carrageenan from the red algae *Chondrus crispus*. This species has been shown to incorporate ^{14}C into the carrageenan from $NaH^{14}CO_3$ [59] and the carrageenan is easily extracted from the cells.

Comparing the one dimensional proton spectrum of the alamethicin with the ^{15}N enriched alamethicin, the only couplings observable, aside from the amide region, are of the aib 1 and aib 13 βCH_3's. 1D ^1H nmr alone can not determine whether these splittings are due to coupling with ^{15}N of the same residue or with the adjacent residue. A TOCSY spectrum of the enriched alamethicin at high digital resolution may be able to resolve these and perhaps determine other couplings [69,72].

The structure of alamethicin in its native state in a membrane may differ from that in methanol. CD spectroscopy showed that the α helix content of alamethicin in methanol/acetonitrile mixture differs from that in lipid vesicles [18,61,89]. The native structure of alamethicin may be best represented if it is incorporated into a phospholipid vesicle or an SDS micelle to mimic the membrane environment and hence a channel model derived from this structure would be a better representative of the actual voltage-gated membrane channel. A one-dimensional proton spectrum of alamethicin in SDS micelles is shown in Figure 26. The

spectrum suggests that a full structural determination of alamethicin in this environment is quite feasible.

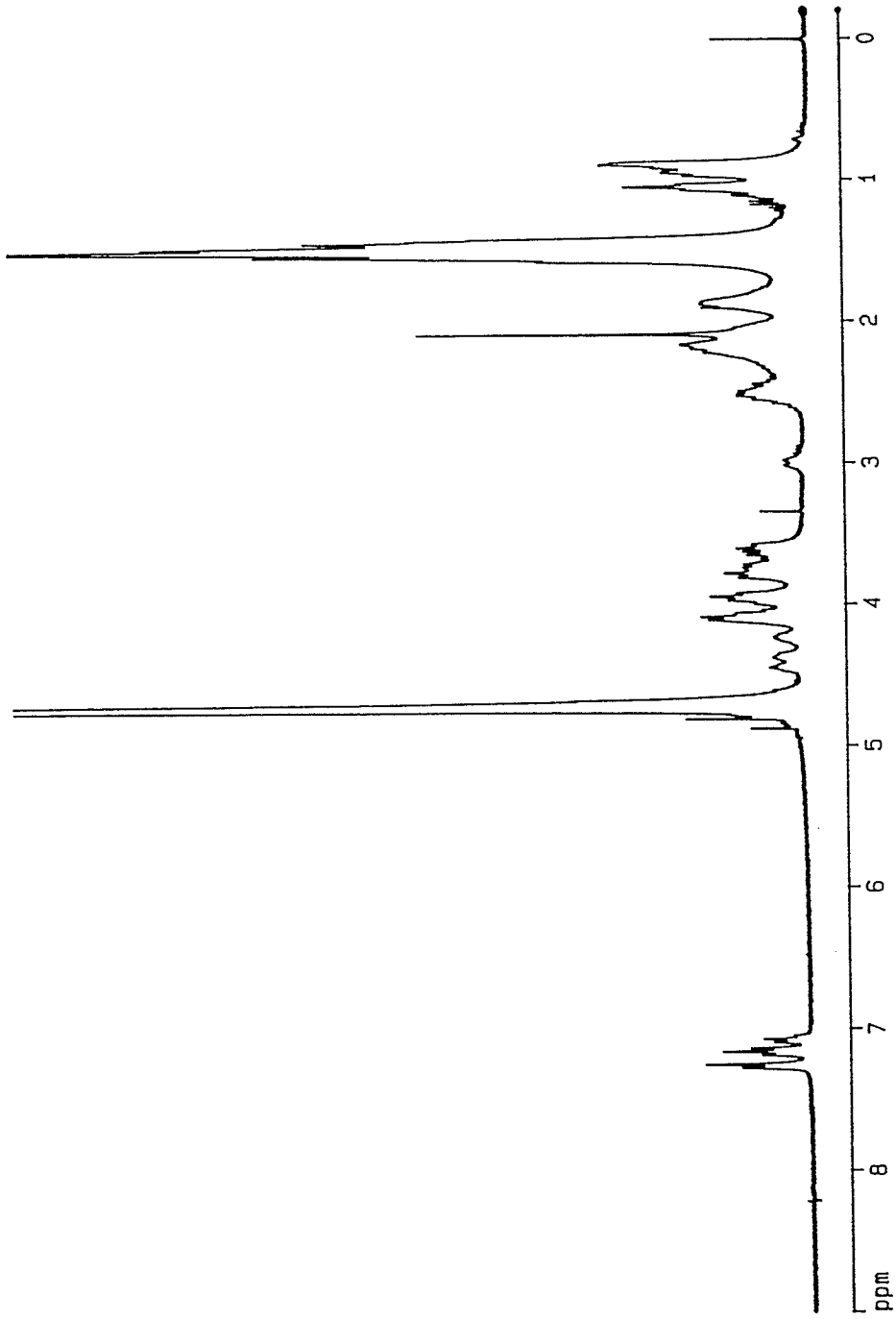

Figure 26 : Proton resonance spectrum at 7.05 T of 3.35 mM alamethicin fraction 21.34 in 15mM SDS-D_{25}, 20 mM phosphate buffer in D_2O, pH=6.93. The number of scans is 256, acquisition time of 2.05 secs, exponential window function was applied with line broadening of 0.3.

Appendix A : Calculation of fractional populations in the sidechain conformation of phol 20 of alamethicin.

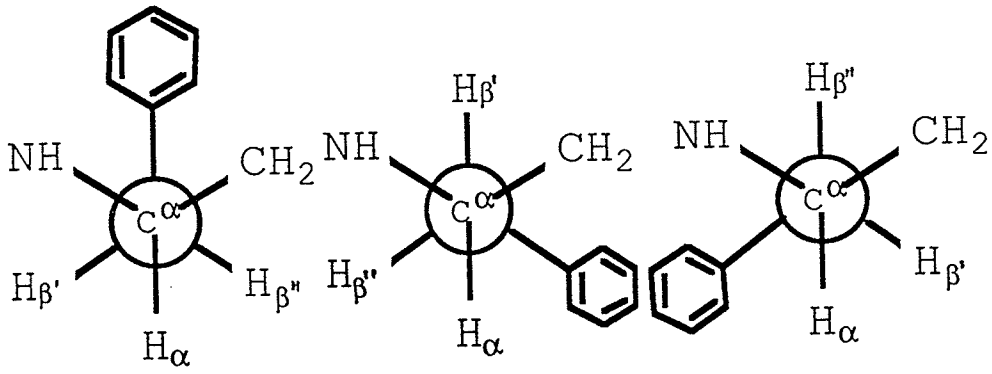

P_1 P_2 P_3

$^3J_{\alpha\beta'} = P_1{}^3J_g + P_2{}^3J_t + P_3{}^3J_g$

$5.6 = P_1(3.4) + P_2(12.9) + P_3(3.4)$

$^3J_{\alpha\beta''} = P_1{}^3J_g + P_2{}^3J_g + P_3{}^3J_t$

$8.8 = P_1(3.4) + P_2(3.4) + P_3(12.9)$

$P_1 + P_2 + P_3 = 1$

$P_1 = 0.20$

$P_2 = 0.23$

$P_3 = 0.57$

Appendix B : Pulse programs copied from the standard Bruker manual and used in Bruker AMX500 and Bruker AM300 NMR spectrometers. Values in square brackets [] were used in the experiment.

B.1. Pulse program used to acquire the 2D ^{15}N-^{1}H correlation spectra (Figure 15, page 63).

```
;inv4ndprtp.sm
;2D H-1/X correlation via heteronuclear zero and double
quantum coherence
;phase sensitive using TPPI
;A. Bax, R.H. Griffey & B.L. Hawkins, J. Magn. Reson. 55, 301
(1983)

1 ze
2 d11 do
3 d12 h12
  p18 ph29
  d13
  d12 hl1
  p1 ph1
  d2
  p3:d ph3
  d0
  p2 ph2
  d0
  p3:d ph4
  d13
  d2
  go=2 ph31
  d11 do wr #0 if #0 id0 ip3 zd
  lo to 3 times td1
exit

ph1=0
ph2=0
ph3=0 2
ph4=0 0 2 2
ph29=0
ph31=0 2 2 0

;hl1: ecoupler high power level                    [4 dB]
;h12: ecoupler power level for presaturation       [55 dB]
```

```
;dl0: power level for dlo mode                                    [15 dB]
;p1 : 90 degree transmitter high power pulse                      [10 µsec]
;p2 : 180 degree transmitter high power pulse                     [20 µsec]
;p3 : 90 degree decoupler high power pulse                        [22 µsec]
;p18: presaturation during relaxation delay                       [1 sec]
;p31: 90 degree pulse for slave timer (cpd-sequence)             [79 µsec]
;d0 : incremented delay                                           [3 µsec]
;d2 : 1/(2J)XH                                                    [5.5msec]
;d11: delay for disk I/O                                          [30 msec]
;d12: delay for power switching                                   [20 µsec]
;d13: short delay (e.g. to compensate delay line)                 [3 µsec]
;in0: 1/(4*SW(X)) = (1/2)DW(X)                                    [40 µsec]
;nd0: 4
;NS : 4*n                                                         [128]
;DS : 2 or 4                                                      [8]
;td1: number of experiments                                       [256]
;MC2: TPPI
;cpd: cpd-decoupling according to sequence defined by cpdprg
```

B.2 Pulse program used to acquire the 2D rotating frame noe experiment (Figure 19, page 66).

```
;roesyprtp
;2D ROESY with cw spinlock for mixing
;phase sensitive using TPPI
;A. Bax & D.G. Davis, J. Magn. Reson. 63, 207-213 (1985)

1 ze
2 d11
3 d12 h12
  p18 ph29
  d13
  d12 hl1
  p1 ph1
  d13
  d0
  d12 hl4
  p15 ph2
  go=2 ph31
  d11 wr#0 if #0 id0 ip1 zd
  lo to 3 times td1
exit

ph1=0 2 2 0 1 3 3 1
ph2=0 2 0 2 1 3 1 3
ph29=0
ph31=0 2 2 0 1 3 3 1

;hl1: ecoupler high power                                         [4 dB]
;hl2: ecoupler power level for presaturation                      [55 dB]
;hl4: ecoupler low power level for ROESY spinlock                 [30 dB]
```

```
;p1 : 90 degree transmitter high power pulse        [11 µsec]
;p15: cw pulse for ROESY spinlock                   [300 msec]
;p18: presaturation during relaxation delay         [1 sec]
;d0 : incremented delay (2D)                        [3 µsec]
;d11: delay for disk I/O                            [30 msec]
;d12: delay for power switching                     [20 µsec]
;d13: short delay (e.g. to compensate delay line)  [3 µsec]
;in0: 1/(2*SW) = DW                                 [85 µsec]
;nd0: 2
;NS : 8*n                                           [64]
;DS : 2 or 4                                        [4]
;td1: number of experiments                         [512]
;MC2: TPPI
```

B.3 Pulse program used to acquire the TOCSY spectrum (Figure 18, page 66).

```
;mlevprtp
;homonuclear Hartman-Hahn transfer using MLEV17 sequence for
mixing
;using two power levels for excitation and spinlock
;phase sensitive using TPPI
;A. Bax & D.G. Davis, J. Magn. Reson. 65, 355-360 (1985)

1 ze
2 d11
3 d12 hl2
  p18 ph29
  d13
  d12 hl1
  p1 ph1
  d13
  d0
  d12 hl3
  (p17 ph26)
4 (p6 ph22 p7 ph23 p6 ph22)
  (p6 ph24 p7 ph25 p6 ph24)
  (p6 ph24 p7 ph25 p6 ph24)
  (p6 ph22 p7 ph23 p6 ph22)
  (p6 ph22 p7 ph25 p6 ph24)
  (p6 ph24 p7 ph25 p6 ph24)
  (p6 ph22 p7 ph23 p6 ph22)
  (p6 ph22 p7 ph23 p6 ph22)
  (p6 ph24 p7 ph25 p6 ph24)
  (p6 ph22 p7 ph23 p6 ph22)
  (p6 ph22 p7 ph23 p6 ph22)
  (p6 ph24 p7 ph25 p6 ph24)
  (p6 ph22 p7 ph23 p6 ph22)
  (p6 ph22 p7 ph23 p6 ph22)
  (p6 ph24 p7 ph25 p6 ph24)
  (p6 ph24 p7 ph25 p6 ph24)
```

```
  (p5 ph23)
  lo to 4 times l1
  (p17 ph26)
  go=2 ph31
  d11 wr #0 if #0 id0 ip1 zd
  lo to 3 times td1
exit

ph1=0 2 2 0 1 3 3 1
ph22=3 1 3 1 0 2 0 2
ph23=0 2 0 2 1 3 1 3
ph24=1 3 1 3 2 0 2 0
ph25=2 0 2 0 3 1 3 1
ph26=0 2 0 2 1 3 1 3
ph29=0
ph31=0 2 2 0 1 3 3 1

;hl1: ecoupler high power level                              [4 dB]
;hl2: ecoupler power level for presaturation                 [55 dB]
;hl3: ecoupler low power level for MLEV spinlock             [13 dB]
;p1 : 90 degree transmitter high power pulse                 [11 µsec]
;p5 : 60 degree transmitter low power pulse                  [19 µsec]
;p6 : 90 degree transmitter low power pulse                  [28 µsec]
;p7 : 180 degree transmitter low power pulse                 [56 µsec]
;p17: trim pulse                                            [5 µsec]
;p18: presaturation during relaxation delay                  [1 sec]
;d0 : incremented delay (2D)                                [3 µsec]
;d1 : relaxation delay; 1-5 * T1                            [10 msec]
;d11: delay for disk I/O                                    [30 msec]
;d12: delay for power switching                             [20 µsec]
;d13: short delay (e.g. to compensate delay line)           [3 µsec]
;L1 : loop for MLEV cycle: (((p6*64)+p5)*l1)+(p17*2) = mixing
time                                                        [25]
;in0: 1/(2*SW) = DW                                         [80 µsec]
;nd0: 2                                                     [2]
;NS : 8 * n                                                 [64]
;DS : 2 or 4                                                [4]
;td1: number of experiments                                 [512]
;MC2: TPPI
```

B.4 Pulse program used to acquire the SEDS spectrum (Figure 24, page 88).

```
;sedpr1
;spin-echo difference spectroscopy part 1
;with decoupling during acquisition
;and presaturation to reduce intense solvent peaks

1 ze
2 d1 do dhi hl2
  p18 ph29
```

```
  d13
  d12 hl1
3 p1 ph1
  d2
  (p2 ph2)(p4 ph3):d
  d2 dlo
  go=2 ph31 cpd
  wra #0
  d2 do
exit

;sedpr2
;spin-echo difference spectroscopy part 2
;with decoupling during acquisition and presaturation

1 ze
2 d12 hl2 do dhi
  p18 ph29
  d13
  d12 hl1
3 p1 ph1
  d2
  (p2 ph2)(d4) ; d4 is dummy c pulse
  d2 dlo
  go=2 ph31 cpd
  wra #0
  d2 do
exit
ph1=0 0 2 2 1 1 3 3
ph2=1 3 3 1 2 0 0 2
ph3=0
ph29=0
ph31=0 0 2 2 1 1 3 3

;hl1: ecoupler high power level                          [4 dB]
;hl2: ecoupler power level for presaturation             [55 dB]
;dl0: power level for dlo mode                           [18 dB]
;p1 : 90 degree transmitter high power pulse             [13.5 µsec]
;p2 : 180 degree transmitter high power pulse            [27 µsec]
;p4 : 180 degree decoupler high power pulse              [48 µsec]
;p18: presaturation during relaxation delay              [1 sec]
;p31: 90 degree pulse for slave timer (cpd-sequence)
                                                         [170 µsec]
;d1 : relaxation delay; 1-5 * T1                         [4 sec]
;d2 : 1/(2J)XH                                          [5555.6 µsec]
;d4 : =p4 (dummy pulse for part 2)                       [48 µsec]
;d12: delay for power switching                          [20 µsec]
;d13: short delay (e.g. to compensate delay line)       [3 µsec]
;NS : 8 * n                                             [8]
;DS : 2 or 4                                            [4]
;cpd: cpd-decoupling according to sequence defined by cpdprg
```

B.5 Pulse program used to acquire the DQF-COSY spectrum (Figure 17, page 66).

```
; COSYDQF.AUR
; COSY-90 with double quantum filter
;Wokaun & Ernst, Chem. Phys. Lett. 52, 407(77)
;Piantini et al., JACS 104, 6800(82)
;Shaka & Freeman, J. Magn. Resn. 51, 169(83)

; D1-90-D0-D2-90-D3-90-d2-FID

1 ze
2 D1              ;relaxation
3 p1 ph1          ;90 deg excitation
4 D0              ;evolution
  D2              ;fixed delay to enhance MQC
5 p1 ph2          ;generate multiple quantum coherence
6 D3              ;3 usec for phase switching
7 p1 ph3          ;selection pulse
  D2
8 go=2 ph4        ;acquire
9 wr #1
10 IF #1
11 IN=1
   exit

ph1=A0 A2 A1 A3 A1 A3 A0 A2
    A1 A3 A2 A0 A2 A0 A1 A3
ph2=A0 A2 A1 A3 A2 A0 A1 A3
    A1 A3 A2 A0 A3 A1 A2 A0
ph3=A0 A0 A0 A0 A1 A1 A1 A1
    A1 A1 A1 A1 A2 A2 A2 A2
ph4=R0 R0 R2 R2 R0 R0 R2 R2
    R1 R1 R3 R3 R1 R1 R3 R3
;phase programs select for quanta of order 2,6,10,...(scans
1-4), with n-type selection (scans 5-8)
;NB: NS=8*n, minimum of 8 trans.                    [48]

;RD=PW=0                                            [0]
;D1=1-5*T1                                          [2.4 sec]
;p1=90 deg pulse                                    [9.9 µsec]
;D0=5E-6                                            [3 µsec]
;D3=3E-6                                            [3 µsec]
;D2=0.05-0.3 sec to enhance intensity of MQC        [71 msec]

;requires twice as many transients for same S/N as for normal
COSY.
```

REFERENCES

[1] Artalejo, A.R., Monteil, C., Garcia, P.S., Uceda, C., Guantes, J.M., & Garcia, A.G. (1990) *Biochemical and Biophysical Research Communications 169*, 1204-1210.

[2] Balasubramanian, T.M., Kendrick, N.C.E., Taylor,M., Marshall, G.R., Hall, J.E., Vodyanoy, I., & Reusser, F. (1981) *Journal of American Chemical Society 103*, 6127-6132.

[3] Banerjee, U., & Chan, S.I. (1983) *Biochemistry 22*, 3709-3713.

[4] Banerjee, U., Tsui, F.P., Balasubramanian, T.N., Marshall, G.R., & Chan, S.I. (1983) *Journal of Molecular Biology 165*, 757-775.

[5] Bax, A., & Davis, D. G. (1985) *Journal of Magnetic Resonance 63*, 207-213.

[6] Bax, A., & Davis, D. G. (1985) *Journal of Magnetic Resonance 65*, 355-360.

[7] Bax, A., & Freeman, R. (1981) *Journal of Magnetic Resonance 44*, 542-545.

[8] Bax, A., Griffey, R.H., & Hawkins, B.L. (1983) *Journal of the American Chemical Society 105*, 7188-7190.

[9] Bax, A., Griffey, R.H., Hawkins, B.L. (1983) *Journal of Magnetic Resonance 55*, 301-315.

[10] Bodenhausen, G., & Ruben, D.J. (1980) *Chemical Physics Letters 69*, 185-189.

[11] Bugosky, M.J., Leighton, P., Schiksnis, R.A., Khoury, A., Lu, P., & Opella, S.J. (1990) *Journal of Magnetic Resonance 86*, 11-29.

[12] Boheim, G., Hanke, W., & Jung, G. (1983) *Biophysics of Structure and Mechanism 9*, 181-191.

[13] Bothner-By, A.A., Stephens, R.L., Lee, J., Warre, C.D., & Jeanloz, R.W. (1984) *Journal of American Chemical Society 106*, 811-813.

[14] Brewer, D., Feicht, A., Taylor, A., Keeping, J.W., Taha, A.A., & Thaller, V. (1982) *Canadian Journal of Microbiology 28*, 1252-1260.

[15] Brewer, D., Mason, F.G., & Taylor, A. (1987) *Canadian Journal of Microbiology 33*, 619-625.

[16] Brewer, D., Jerram, W.A., Meiler, D., & Taylor, A. (1970) *Canadian Journal of Microbiology 16*, 433-440.

[17] Brumfeld, V., & Miller, I.R. (1990) *Biochimica et Biophysica Acta 1024*, 49-53.

[18] Cascio, M., & Wallace, B.A. *Annals of the New York Academy of Sciences*, 527-529.

[19] Clore, M.G., & Gronenborn, A.M. (1987) *Protein Engineering 1*, 275-288.

[20] Davis, D.G., & Gisin, B.F. (1981) *Federation of European Biochemical Societies Letters 133*, 247-251.

[21] Demarco, A., Llinas, M., Wuthrich, K., (1978) *Biopolymers 17*, 617-650.

[22] Doddrell, D., Glushko, V., Allerhand, A. (1972) *Journal of Chemical Physics 56*, 3683-3689.

[23] Driscoll, P.C., Gronenborn, A.M., Wingfield, P.T., & Clore, G.M. (1990) *Biochemistry 29*, 4668-4682.

[24] Eisenberg, M., Hall, J.E., & Mead, C.A. (1973) *Journal of Membrane Biology 14*, 143-176.

[25] Ernst, R.R., Bodenhausen, G., & Wokaun, A. (1987) *Principles of Nuclear Magnetic Resonance in One and Two Dimensions*, Clarendon Press, Oxford.

[26] Esposito, G., Carver, J.A., Boyd, J., Campbell, I.D. (1987) *Biochemistry 26*, 1043-1050.

[27] Feeney, J. (1976) *Journal of Magnetic Resonance 21*, 473-478.

[28] Fonteriz, R.I., Lopez, M.G., Sancho, J.G., & Garcia, A.G. (1991) *FEBS Letters 283*, 89-92.

[29] Fox, R,O., & Richards, F.M. (1982) *Nature 300*, 325-330.

[30] Fraternali, F. (1990) *Biopolymers 30*, 1083-1099.

[31] Froyshov, F., Zimmer, T.L., & Laland, S.G. (1978) in *International Review of Biochemistry* (Arnstein, H.R.V., Ed.) Vol. 18, pp 49-77, University Park Press, Baltimore.

[32] Gisin, B.F., Davis, D.G., Borowski, Z.K., Hall, J.E., & Kobayashi, S. (1981) *Journal of American Chemical Society 103*, 6373-6377.

[33] Griffey, R.H., Redfield, A.G., Loomis, R.E., & Dahlquist, F.W. (1985) *Biochemistry 24*, 817-822.

[34] Gust, D., Moon, R.B., & Roberts, J.D. (1975) *Proceedings of National Academy of Sciences, USA 72*, 4696-4700.

[35] Hall, J.E., Vodyanoy, I., Balasubramanian, T.M., & Marshall, G.R. (1984) *Biophysical Journal 45*, 233-247.

[36] Harris, E.H. (1989) *The Chlamydomonas Sourcebook - A Comprehensive Guide to Biology and Laboratory Use*, Academic Press Inc., San Diego.

[37] Harris, R.K. (1983) *Nuclear Magnetic Resonance Spectroscopy - A Physicochemical View*, Pitman Books Ltd., London.

[38] Hauser, H., Finer, E.G., & Chapman, D. (1970) *Journal of Molecular Biology 53*, 419-433.

[39] Hille, B. (1970) *Progress in Biophysics and Molecular Biology 21*, 1-32.

[40] Homans, S.W. (1989) *A Dictionary of Concepts of NMR*, Clarendon Press, Oxford.

[41] Hubbard, P.S. (1970) *Journal of Chemical Physics 52*, 563-568.

[42] Ikura, M., Kay, L.E., Bax, A. (1990) *Biochemistry 29*, 4659-4667.

[43] Irmscher, G., & Jung, G. (1977) *European Journal of Biochemistry 80*, 165-174.

[44] Jeener, J. (1971) *Ampere International Summer School*, Basko Polje, Yugoslavia.

[45] Jen, W.C., Jones, G.A., Brewer, D., Parkinson, V.O., & Taylor, A. (1987) *Journal of Applied Bacteriology 63*, 293-298.

[46] Jung, G., Dubischar, N., & Leibfritz, D. (1975) *European Journal of Biochemistry 54*, 395-409.

[47] Kaptein, R., Boelens, R., Scheek, R.M., & van Gunsteren, W.F. (1988) *Biochemistry 27*, 5389-5395.

[48] Karle, I.L., & Balaram, P. (1990) *Biochemistry 29*, 6747-6756.

[49] Katz, E., Schmitt, H., Aydin, M., Konig, W.A., & Jung, G. (1985) *Leibigs Annals of Chemistry*, 365-377.

[50] Kucherenko, M. E., & Rybalchenko, V. K. (1990) *Byulleten' Eksperimental'noi Biologii i Meditsiny 109*, 111-113.

[51] Kuhlmann, K.F., Grant, D.M., & Harris, R.K. (1970) *Journal of Chemical Physics 52*, 3439-3448.

[52] Latorre, R., Miller, C., & Quay, S. (1981) *Biophysical Journal 36*, 803-809.

[53] Leggett, B. J. (1967) *Techniques in Protein Chemistry, 2nd Ed.*, Elsevier Publishing Company, New York, 31-37.

[54] Levy, G.C., & Lichter, R.L. (1979) *Nitrogen-15 Nuclear Magnetic Resonance Spectroscopy*, John-Wiley & Sons, New York.

[55] Marion, D., & Wuthrich, K. (1983) *Biochemical and Biophysical Research Communications 113*, 967-974.

[56] Mason, J. (1987) *Multinuclear NMR*, Plenum Press, New York.

[57] Mathew, M.K., & Balaram, P. (1983) *Federation of European Biochemical Societies Letters 157*, 1-5.

[58] Maudsley, A.A. & Ernst, R.R. (1977) *Chemical Physics Letters 50*, 368-372.

[59] McCandless, E.L. and Richer, S. (1972) *Proceedings of the Seventh International Seaweed Symposium*, John Wiley & Sons, New York, 477-484.

[60] McIntosh, T.J., Ting-Beall, H.P., & Zampighi, G. (1982) *Biochimica et Biophysica Acta 685*, 51-60.

[61] McMullen, A.I., Marlborough, D.I., & Bayley, P.M. (1971) *FEBS Letters 16*, 278-280.

[62] Menestrina, G., Voges, K.P., Jung, G., & Boheim, G. (1986) *Journal of Membrane Biology 93*, 111-132.

[63] Meyer, C.E., & Reusser, F. (1967) *Specialia 15*, 85-86.

[64] Miller, I.R., & Doll, I. (1990) *Bioelectrochemistry and Bioenergetics 24*, 129-142.

[65] Miller, I.R., & Doll, I. (1990) *Bioelectrochemistry and Bioenergetics 24*, 323-333.

[66] Molle, G., Duclohier, H., & Spach, G. (1987) *FEBS Letters 224*, 208-212.

[67] Molle, G., Duclohier, H., Julien, S., & Spach, G. (1991) *Biochimica et Biophysica Acta 1064*, 365-369.

[68] Molle, G., Dugast, J.Y., Ducloheir, H., Daumas, P., Heitz, F., & Spach, G. (1988) *Biophysical Journal 53*, 193-203.

[69] Montelione, G., Winkler, M.E., Rauenbuehler, P., & Wagner, G. (1989) *Journal of Magnetic Resonance 82*, 198-204.

[70] Neuhaus, D., & Williamson, M.P. (1989) *The Nuclear Overhauser Effect - Structural and Conformational Analysis*, VCH Publishers, Inc., New York.

[71] Noggle, J.H., & Schirmer, R.E. (1971) *The Nuclear Overhauser Effect - Chemical Applications*, Academic Press, New York.

[72] Norwood, T.J., Boyd, J., & Campbell, I.D. (1989) *FEBS Letters 255*, 369-371.

[73] Pardi, A., Wagner, G., & Wuthrich, K. (1983) *European Journal of Biochemistry 137*, 445-454.

[74] Payne, J.W., Jakes, R., & Hartley, B.S. (1970) *Biochemistry Journal 117*, 757-766.

[75] Perrin, C.L., Johnston, E.R., & Ramirez, J.L. (1980) *Journal of American Chemical Society 102*, 6299-6304.

[76] Portlock, S.H., Clague, M.J., & Cherry, R.J. (1990) *Biochimica et Biophysica Acta 1030*, 1-10.

[77] Reusser, f. (1966) *Journal of Biological Chemistry 242*, 243-247.

[78] Rindfleisch, H., & Klienkauf, H. (1976) *FEBS Letters 62*, 276-280.

[79] Rizzo, V., Stankowski, S., Schwarz, G. (1987) *Biochemistry 26*, 2751-2759.

[80] Schmitt, H., & Jung, G. (1985) *Liebigs Annals of Chemistry*, 321-344.

[81] Schmitt, H., & Jung, G. (1985) *Liebigs annals of Chemistry*, 345-364.

[82] Schwarz, G., Stankowski, S., & Rizzo, V. (1986) *Biochimica et Biophysica Acta 861*, 141-151.

[83] Seppet, E.K., & Dhalla, N.S. (1989) *Molecular and Cellular Biology 91*, 137-147.

[84] Shon, K., & Opella, S.J. (1989) *Journal of Magnetic Resonance 82*, 193-197.

[85] Smith, G.M., Yu, L.P., & Domingues, D.J. (1987) *Biochemistry 26,* 2202-2207.

[86] Sogn, J.A., Gibbons, W.A., Randall, E.W. (1973) *Biochemistry 12,* 2100-2105.

[87] Stothers. J.B. (1972) *Carbon-13 NMR Spectroscopy Vol. 24,* Academic Press, New York.

[88] Taylor, R.J., & Levie, R. (1991) *Biophysical Journal 59,* 873-879.

[89] Vogel, H. (1987) *Biochemistry 26,* 4562-4572.

[90] Wagner, G., Braun, W., Havel, T.F., Schaumann, T., Go, N., Wuthrich, K. (1987) *Journal of Molecular Biology 196,* 611-639.

[91] Werbelow, L.G., & Marshall, A.G. (1973) *Journal of Magnetic Resonance 11,* 299-313.

[92] Westerman, P.W., & Roberts, J.D. (1978) *Journal of Organic Chemistry 43,* 1177-1179.

[93] Wille, B., Franz, B., Jung, G. (1989) *Biochimica et Biophysica Acta 986,* 47-60.

[94] Wipf, P., & Heimgartner, H. (1990) *Helvetica Chimica Acta 73,* 13-24.

[95] Witanowski, M., & Webb, G. A. (1973) *Nitrogen NMR,* Plenum Press, London.

[96] Wuthrich, K. (1986) *NMR of Proteins and Nucleic Acids,* John-Wiley and Sons, New York.